UNIVERSITY OF NAPLES FEDERICO II
DEPARTMENT OF PHARMACY

PhD THESIS
IN

PHARMACEUTICAL SCIENCE

Phytochemical investigation of food and medicinal plants from the Saudi Arabia flora

Supervisors

Prof. Orazio Taglialatela-Scafati

Prof. Shagufta Perveen

PhD Coordinator

Prof. Maria Valeria D'Auria

Candidate

Jawaher H. AlQahtani

XXXIII cycle
2017-2020

Table of Contents

ABSTRACT

In the context of the efforts for building up a comprehensive inventory of Saudi medicinal plants, my PhD thesis came to contribute in these efforts to 'unearth' Saudi plants treasure. The Kingdom of Saudi Arabia (KSA) is a giant arid area covering about 2,250,000 km^2 of the Arabian Peninsula among which, KSA possesses the richest flora biodiversity. Great advancements in Saudi health care systems experienced in last decades did not substitute the use of plants as folk medicine among Saudi population. A considerable number of these medicinal plants were subjected to phytochemical and biological studies and these studies have revealed astonishing biological activities and have uncovered novel phytochemicals among Saudi flora. In my PhD, two Saudi plants were selected: *Cissus rotundifolia* (Forssk.) *Vahl* and *Anvillea garcinii* subsp. *radiata* (Coss & Durieu) Anderb, on the basis of their traditional use by Saudi population in folk medicine and/or as food. *C. rotundifolia* is an edible plant traditionally used as antihyperglycemic agent. The ethanolic extract of this plant was subjected to a bio-guided fractionation which led to the isolation of a new sucrose diester of truxinic acid (cissuxinoside), an unprecedented glycosylated and extensively conjugated dicarboxylic acid (cissoic acid), three flavones *C*-glycosides (one of which was fully characterized for the first time), and two coumaric acid derivatives. One of these latter compounds (namely, 1-*O*-*p*-coumaroyl-*β*-*D*-glucopyranose) was found to be the main responsible for the anti-diabetic activity of the extract. The second plant investigated in my project was *A. garcinii*, which is traditionally used to treat dysentery, gastric ulcers, and pulmonary infections. In this project *A. garcinii* was subjected to comprehensive phytochemical investigation which revealed the presence of four new sesquiterpenoids, five known germacranolides in addition to flavonoids and polypenolics. The isolated compounds were tested for their antimicrobial activities against pathogenic fungi and bacteria and *Anvillea* sesquiterpenoids have shown remarkable activity against some of the tested pathogens.

This work has been carried out under the auspices of University of Naples Federico II (Italy) and External Joint Supervision Program in King Saud University, Riyadh (Kingdom of Saudi Arabia).

Publications of the candidate during the PhD period:

1. Perveen, S., **Alqahtani, J.,** Orfali, R., Aati, H. Y., Al-Taweel, A. M., Ibrahim, T. A., Khan, A., Yusufoglu, H. S., Abdel-Kader, M. S., & Taglialatela-Scafati, O. **(2020)**. Antibacterial and Antifungal Sesquiterpenoids from Aerial Parts of *Anvillea garcinii*. *Molecules*, 25(7), 1730. https://doi.org/10.3390/molecules25071730.

2. Perveen, S., **Alqahtani, J.,** Orfali, R., Al-Taweel, A. M., Yusufoglu, H. S., Abdel-Kader, M. S., & Taglialatela-Scafati, O. **(2019).** Antimicrobial guaianolide sesquiterpenoids from leaves of the Saudi Arabian plant *Anvillea garcinii*. *Fitoterapia*, 134:129-134. doi:10.1016/j.fitote.2019.02.017.

3. **Alqahtani, J.,** Formisano, C., Chianese, G., Luciano, P., Stornaiuolo, M., Perveen S., Taglialatela-Scafati, O. **(2020).** Glycosylated phenols and an unprecedented diacid from the Saudi plant *Cissus rotundifolia*. *Journal of Natural Products*, 83:3298-3304. doi: 10.1021/acs.jnatprod.0c00597.

CHAPTR 1: MEDICINAL PLANTS IN SAUDI ARABIA

1.1. Overview:

Our planet is gifted with tremendous number of plant families which have been discovered through the history of humankind as a natural renewable source of food and medicines. Early humans have developed their knowledge about plants therapy by trial and error which led to cumulative awareness about useful plants with beneficial effects in contrast to toxic or inactive plants. Ever since ancient times and up to now, natural products derived from higher plants and microorganisms have been providing novel and clinically active drugs. A significant number of modern drugs have been isolated from natural sources, particularly plants, or derived from semi-synthetic work on natural compounds. Medicine systems based on plants are still representing cornerstones in health care, given the fact that 80% of the world populations have faith and rely on traditional medicines for their primary health care. This is chiefly factual in developing countries, where traditional medicine has an extended and uninterrupted history of use. Worldwide, it is estimated that there are 21,000 medicinal plants (Sivakrishnan, 2018) and, according to the study by Kate and Laird, 1998, drugs derived from plant sources constitute 18% of the world top 150 prescriptions. At least 25% drugs listed in the modern pharmacopoeias are derived from plants, while many synthetic analogues were designed according to prototype compounds isolated from plants (Kate & Laird, 1999).

According to the World Health Organization (WHO), a medicinal plant is any plant, in which one or more of its organs contain substances that can be used for the therapeutic purposes or which are precursors for the synthesis of useful drugs". This definition differentiates between plants with scientifically established therapeutic properties and plants with observed therapeutic effects, but which have not yet been subjected to thorough investigation (Sivakrishnan, 2018). Re-evolving interest in plants as sources of medicinal agents has been empowered by the rising costs of prescribing drugs with a greater number of people seeking remedies and health approaches free from side effects caused by synthetic drugs. Industry of plants-based medicine is moving from fringe to mainstream. Medicinal herbs, shrubs and trees are broadly utilized in the world including

both developed and developing countries with wide domestic and commercial acceptance.

Despite the advances in the medical field, many of acute and chronic diseases including diabetes, hypertension, hyperlipidemia, malaria, infectious diseases, etc.. are still resulting in high mortality and morbidity rates and the introduction of novel drugs with new mechanisms of activities is crucial. Solutions from natural sources (including plants, microorganisms, marine invertebrates, and animals) should be extensively examined to ensure providing valid options to manage, if not cure, these diseases.

1.2. Saudi Arabia, an`unearthing plant treasure`:

Saudi Arabia is a huge arid country covering an area of about 900,000 square miles (2,250,000 km^2) which constitutes about two thirds of the Arabian Peninsula. It is the largest desert area on Asia and the second largest on Earth, surpassed in size only by the Sahara, in northern Africa. Saudi Arabia is occupying a large area of natural spots including great biodiversity and synergistic framework of associated ecosystems with different plant species (Ahmad and Ghazanfar, 1991; Ghazanfar, 2007; Abdel Khalik *et al.* 2013). A major part of the country comprises dry land territories with species-poor plant assemblage. The climate of the Saudi Arabia is hot and dry with rare rainfall except for the southern region. Due to its arid climate, the flora of Saudi Arabia (like the other countries in the peninsula) has been abandoned for a long time. The scientific investigation about the flora of Saudi Arabia dates back to 1974 (Alfarhan *et al.*, 1998). According to reviews by Mossa *et al*, 1987, Saudi Arabia is gifted with a wide range of flora, consisting of a large number of medicinal herbs, shrubs and trees. It is estimated that the flora of Saudi Arabia has a great medicinal species diversity, which is expected to be more than 1200 (over 50%) out of its 2250 species (Atiqur Rahman *et al*., 2004).

Saudi Arabia flora is composed of large number of endemic species in addition to the admixture of the elements of Asia, Africa and Mediterranean region. Indeed, flora of Saudi Arabia comprises very important genetic resources of crop and medicinal plants (Atiqur Rahman *et al*., 2004). According to Collenette *et al*. (1998), the flora of the Kingdom of Saudi Arabia is represented by a total of 142 families comprising 2250 species (including pteridophytes and gymnosperms). Among these, there are 242 endemic

and 600 rare endangered species in the wild (Atiqur Rahman *et al*., 2004). The western mountainous area of the Kingdom on the boarders of the Red Sea, including Asir and Hijaz, shows the greatest species diversity in the country. This is due to heavier rainfall and range of altitude from sea level to 9300 ft at Jabal Sawdah, near Abha (Collenette, 1998).

Plants in Saudi Arabia which can adapt to natural stressful conditions of drought and heat are believed to possess valuable medicinal properties as suggested by several researchers including Atiqur Rahman *et al*.; 2004, El-Ghazali *et al*.; 2010, Daur, 2012.

The use of traditional folk medicine in Saudi Arabia has begun since immemorial times. Medicinal healers (Hakim) have been part of Saudi Arabia tradition. Hakims were prescribing medicinal plants such as herbs for prevention and treatment of acute and chronic diseases (Al-Daihan *et al*., 2013). Although there are many reports on medicinal and wild plants of Saudi Arabia, many medicinal plants among the flora are still to be phytochemically examined. In the present PhD project, efforts have been made to document the phytochemical and pharmacological activities of two medicinal plants (*C. rotundifolia* and *A. garcinii*) selected within the Saudi flora. The selection was based on the evidence that these two plants are traditionally used by Saudi population but need verification to rationalize their use.

References

Abdel Khalik, K., El-Sheikh, M., El-Aidarous, A. **(2013)**. Floristic diversity and vegetation analysis of Wadi Al-Noman, Holy Mecca, Saudi Arabia. *Turk. J Botany.* 37, 894–907.

Ahmad, H.A., Ghazanfar, S.A. **(1991)**. Conservation of medicinal plants on the Arabian Peninsula. Two case studies. *Med. Plant Conserv.*, 3, 15-16.

Al-Daihan, S., Al-Faham, M., Al-shawi, N., Almayman, R., Brnawi, A., zargar, S., Bhat, R.S. **(2013)**. Antibacterial activity and phytochemical screening of some medicinal plants commonly used in Saudi Arabia against selected pathogenic microorganisms, *Journal of King Saud University - Science*, 25 (2), 115-120.

Alfarhan, A.H., Chaudhary, S.A., Thomas, J. **(1998)**. Notes on the flora of Saudi Arabia (Third edition). *J. King Saud Univ.*, 10(1):31-40.

Atiqur Rahman, M., Mossa, J.S., Al-Said, M. S., Al-Yahya, M. A. **(2004).** Medicinal plant diversity in the flora of Saudi Arabia 1: a report on seven plant families Fitoterapia 75, 149–161.

Collenette S. **(1998).** Checklist of botanical species in Saudi Arabia. West Sussex (UK): International Asclepiad Society, p. 78.

Daur. **(2012).** Plant flora in the rangeland of western Saudi Arabia. *Pak. J. Bot.*, 44 , 23-26.

El-Ghazali, G.E., Al-Khalifa, K.S., Saleem, G.A., Abdallah, E.M. **(2010)**. Traditional medicinal plants indigenous to Al-Rass province, Saudi Arabia. *J. Med. Plants Res.*, 4 (24), 2680-2683.

Ghazanfar, S.A. **(2007)**. Saline and alkaline vegetation of NE Africa and the Arabian peninsula: an overview. In: Öztürk, M., Waisel, Y., Khan M.J., Görk, G. (eds.), Biosaline Agriculture and Salinity Tolerance in Plants, Springer Verlag, Birkhauser Basel, 108-109, ISBN: 978-3-7643-7609-3.

Kate, K.T., Laird, S.A. **(1999)**. Natural products and the pharmaceutical industry. In: Kate, K.T., Laird, S.A. (Orgs), The Commercial Use of Biodiversity: Access to Genetic Resources and Benefit-Sharing. Royal Botanic Gardens, Kew.,; 34–77.

Mossa JS, Al-Yahya MA, Al-Meshal IA. **(1987)**. Medicinal plants of Saudi Arabia. Riyadh: King Saud University Press.

Sivakrishnan, S. **(2018).** Traditional herbal medicines – a review. *International Journal of Research and Analytical Reviews*, 5, Issue 4

CHAPTER 2

TECHNIQUES AND METHODS EMPLOYED IN THIS STUDY

2.1. Plant preparation, extraction, and compounds isolation

Extraction is the crucial first step in the analysis of medicinal plants, because it is necessary to extract the desired chemical components from the plant materials for further separation and characterization. The basic operation included steps such as pre-washing, drying and grinding the plant materials to obtain a homogenous sample and to improve the kinetics of analytic extraction by increasing the contact of sample surface with the solvent system (Sasidharan *et al*., 2011). Plant extracts are commonly prepared by maceration or percolation of fresh green plants or dried powdered plant material in water and/or organic solvent systems. The selection of solvent system largely depends on the specific nature of the bioactive compound being targeted. Different solvent systems are available to extract the bioactive compound from natural products. The extraction of hydrophilic compounds uses polar solvents such as methanol, ethanol, or ethyl-acetate (EtOAc). For extraction of more lipophilic compounds, dichloromethane or a mixture of dichloromethane/methanol in ratio of 1:1 are used. In some cases, pre-treatment with hexane is used to remove chlorophyll. In the approach followed for the present work, we started with powdering the plant material and the obtained powder was defatted in *n*-hexane (2 × 3 L, 8 h each) and then extracted with 80% ethanol (5 × 2 L, 8 h each) at room temperature. The EtOH extract was filtered and evaporated to obtain a dried material that was partitioned between H_2O and EtOAc, and then between H_2O and n-BuOH, to afford the EtOAc and *n*-BuOH fractions. These extracts are subjected to bioassay guided fractionation using Sephadex LH-20 and silica gel column chromatography and HPLC to isolate the active compounds.

High Performance Liquid Chromatography (HPLC) is an advanced column chromatography in which the analyte is pumped with solvent (mobile phase) at high pressure through a column with chromatographic packing material (stationary phase) which is usually normal or reverse phase silica gel. HPLC is usually employed as last step of purification process of plant fractions and precede the spectroscopical analysis of the isolated compounds. For structural elucidation of the isolated compounds, we used

different NMR and Mass spectrometry using advanced equipment available in King Saud University Pharmacy college labs and University of Naples Federico II.

2.2. Mass spectrometry

Mass spectrometry is an analytical technique that can provide both qualitative (structure) and quantitative (molecular mass or concentration) information on analyte molecules after their conversion to ions. The molecules of interest are first introduced into the ionisation source of the mass spectrometer, where they are ionised to acquire positive or negative charges. The ions then travel through the mass analyser and arrive at different parts of the detector according to their mass/charge (*m/z*) ratio. After the ions contact the detector, useable signals are generated and recorded by a computer system. The computer displays the signals graphically as a mass spectrum showing the relative abundance of the signals according to their *m/z* ratio (Ho *et al*., 2003).

Over the last decade, electrospray ionisation mass spectrometry (ESI-MS) has emerged as the most important technique in chemical laboratories. Coupled with HPLC for molecular fractionation prior to mass spectrometric analysis, HPLC/ESI-MS has become a very powerful technique capable of analysing both small and large molecules of various polarities in a complex biological sample.

Mass spectrometer consists of three essential components:

1- Ionization source
2- Mass analyzer
3- Detector

Ionization can be carried out by hard or soft techniques. In hard ionization techniques the molecules are not only ionized but they will be also fragmented into smaller pieces. The array of ionized fragments produced is considered as a fingerprint for each compound and helps in the identification of compounds by the resultant mass spectrum.

In soft ionization techniques (including ESI-MS), a fine mist of droplets is created through spraying the compound solution of interest through a nebulizer. Large potential difference between the end of the nebulizer needle and the entrance of the capillary will allow droplets to be charged. Meanwhile, the droplets will be dried by the drying gas

(nitrogen) inside the capillary. As the droplet sizes decrease with drying, the electrostatic repulsion movement between the charged particles pushes some of them to pass into the gas phase. By the help of high vacuum in the analyzer, the gas-phase ions are drawn through the capillary. By this procedure, the molecules in solution are ionized but not fragmented and each molecule in the solution can adsorb different number of charges. As a result, mass spectrum of differently charged particles will be created (Hofstadter & Smith, 1996).

In ESI-MS, a modified quadrupole is used as mass analyzer. The quadrupole detector consists of four parallel rods kept at equal distance, two of them are positively charged while the other two are negatively charged. In such system, each pair of opposite rods is connected electrically. An equal but opposite DC voltage superimposed with a radio frequency (RF) AC voltage is applied to the diagonally placed pair of rods. The resulting electrical field causes the ions to travel forward in the z direction with oscillatory motion in the x-y plane. The amplitude of oscillation bears a unique relationship with the *m/z* ratio and can be controlled by changing the DC and RF voltages simultaneously in a pre-fixed ratio. These DC and RF voltages help to sort the molecules so that ions having oscillations of desirable *m/z* ratios will be "stable" and will travel along the z-axis without hitting the quadrupole rods, and success to reach the detector. The oscillatory amplitudes of undesirable ions are large and "unstable", they hit the metal rods, get neutralized, and fail to reach the detector. Quadrupole mass analysers are robust, economical, physically small, and more readily interfaced with a wide variety of inlet systems when compared with other conventional mass analysers like the magnetic sector (Ho *et al*., 2003). Due to the rapidity of data acquisition, the quadrupole detector is perfect for the analysis of HPLC output.

In a typical tandem quadrupole system, there are three quadrupoles set up in a linear style, often called "triplequad" (Figure 2.2). In first quadrupole (Q1), the sample ion (called the precursor ion) is selected according to its mass to charge ratio (*m/z*). The precursor ions are activated by colliding with a “collision gas” (usually argon) and undergo further fragmentation (this process is known as collision-induced dissociation, CID) in the second quadrupole collision cell (Q2). The daughter ions resulting from CID

are related to the molecular structure of the ions and can be monitored by a third quadrupole mass analyser (Q3) providing structural information of the molecular ions. It can be said that triple quadrupole mass spectrometers utilize the first and third quadrupoles as mass filters while the second quadrupole is the place for the fragmentation by collision with gas. This tandem system is commonly denoted as MS/MS in the literature. Since Q1 is set to select only one specific *m/z* ratio, it can filter out other undesirable molecular ions. This is a "purification" step takes place inside the MS system and substitutes complicated and time-consuming sample purification procedures prior to MS analysis (Ho *et al*., 2003).

The mass spectrum is a plot display of the intensity (relative a bundance) against the *m/z* ratios. The highest signal is taken as 100% abundance while all the other signals are expressed as a percentage of this signal. In ESI, mass spectra are relatively simple and fragmentation of the protonated or de-protonated molecular ions generated is generally limited.

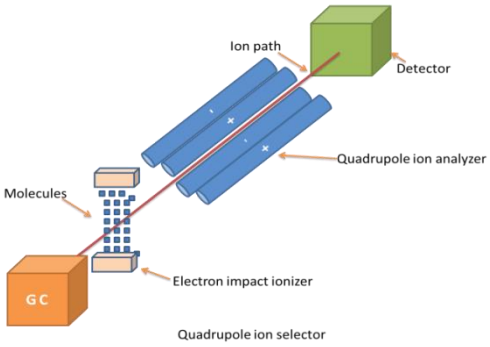

Figure 2.1: Quadrupole ion selector

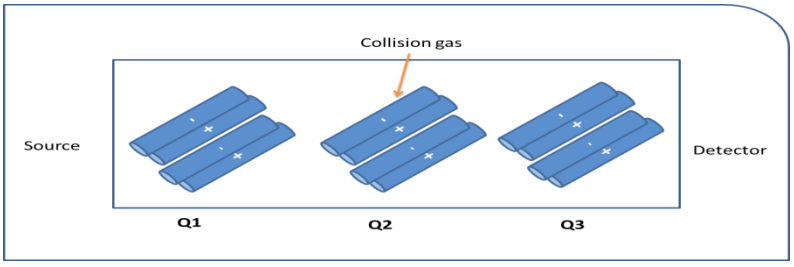

Figure 2.2: Triple quadrupole system. The first (Q1) and third (Q3) are mass spectrometers and the centre (Q2) is a collision cell.

2.3. NMR spectroscopy

Application of NMR spectroscopy for the structural elucidation, stereochemistry determination and even conformational analysis of molecules has been successfully utilized in phytochemical studies of plant secondary metabolites and drug discovery. Currently, 1D (^{1}H, ^{13}C, ^{15}N), 2D (COSY, TOCSY, NOESY, HSQC, HMBC) experiments are basically used in routine analysis of natural products. Certain nuclei such as ^{1}H, ^{13}C, ^{15}N, ^{17}O, ^{19}F, etc.. possess intrinsic spin properties and can act like a magnet. NMR is functioned by exposing these nuclei to magnetic field followed by measuring amount of energy required to put various nuclei in resonance. When a magnetic field is applied, these nuclei tend to spin in the direction of the magnetic field. If a sample is placed in a magnetic field and is subjected to radio-frequency radiation (energy) at the appropriate frequency, nuclei in the sample can absorb the energy. The frequency of the radiation necessary for absorption of energy depends on characteristic of (type) of nucleus (e.g., ^{1}H or ^{13}C) and its chemical environment. When a radiofrequency pulse that corresponds to the frequency of nuclear precession is applied, the nucleus can align itself either with the external field (+) or against it (−). Excited nuclei may lose their energy by processes known as relaxation. Two relaxation mechanisms are (1) spin lattice relaxation (the return of nuclei to their original alignment with the applied magnetic field) (2) spin–spin relaxation (the loss of the coherent spinning of the nuclei). The times of these relaxation processes are known as T_1 and T_2, respectively. NMR is an element-specific technique since each nucleus has its characteristic resonance frequency. Those nuclei that have no spin and do not exhibit magnetic resonant effects cannot be studied through NMR, for example the naturally abundant ^{12}C, ^{16}O, and ^{32}S have zero spin (Pradhan *et al*., 2017; Sim &Fane, 2017).

The nuclei that contain odd atomic or mass number or both are very useful for NMR, such as protons (^{1}H), isotope ^{13}C of carbon, fluorine (^{19}F), the isotopes ^{14}N and ^{15}N of the nitrogen. The first two nuclei are by far the most used in natural product chemistry, both in 1D and 2D experiments as detailed below.

^{1}H NMR and ^{13}C NMR are utilized to determine the type and number of hydrogen (H) and carbon (C) atoms in the molecule. The ^{1}H spectrum can be obtained very fast with a

low amount of sample concentration; however, in ^{13}C NMR, the minimum scan time is longer with the concentrated sample needed to acquire a nice informative spectrum due to only 1.1% natural abundance of ^{13}C isotope and its unfavourable gyromagnetic ratio. Based on the surrounding chemical environment, different resonance signals are obtained for protons. Characteristic splitting patterns of the signal are also observed depending upon the magnetic interaction between different nuclei which is also known as spin-spin coupling. Additionally, the total number of protons responsible for a particular signal can be measured by integrating the area under the signal. The chemical shift range of absorption for ^{1}H spectrum goes from 1 to 15 ppm and ^{13}C ranges around 10–200 ppm.

The COSY (COrrelation SpectroscopY) One of the simplest and most powerful methods for the correlation of nearby resonances via the three-bond *J* coupling between protons attached to neighboring carbon atoms. This experiment is based on measurements of direct bondings (scalar couplings, spin-spin coupled) within a molecular structure

The HSQC (Heteronuclear Single Quantum Coherence) experiment is used to determine proton-carbon single bond correlations, where the protons lie along the observed F2 (X) axis and the carbons are along the F1 (Y) axis.

The HMBC (Heteronuclear Multiple Bond Correlation) experiment shows correlations between carbons and protons that are separated by two, three, and, sometimes in conjugated systems, four bonds. Direct one-bond correlations are suppressed. This gives connectivity information much like a proton-proton COSY. The intensity of cross peaks depends on the coupling constant, which for three-bond couplings follows the Karplus relationship. For dihedral angles near 90 degrees, the coupling is near zero. Thus, the absence of a cross peak doesn`t confirm that carbon-proton pairs are many bonds apart.

2.4. Relative configuration analysis

One important step in structural elucidation of natural molecule is recognizing its stereochemical details, that can affect its molecular mode of actions. Nowadays, this step is viewed as the most challenging field in bioorganic chemistry, but several NMR-based approaches have been developed for this purpose. J_{HH} values can be measured in conventional ^{1}H spectra and yield information about dihedral angles between atoms

which help to choose the rotamer that represent the molecule of interest. In addition to proton–proton coupling constants ($^{3}J_{HH}$) and proton–carbon coupling constants ($^{2,3}J_{CH}$), NOE and ROE effects, especially in their 2D versions, NOESY and ROESY, are the most frequently used experiments. Combining Nuclear Overhauser Effects (NOEs) experiments with molecular mechanics calculations have been applied for flexible molecules, particularly for macrocyclic compounds (e.g macrolides) (Matsumori *et al*., 1999). NOEs give data about the 3D relationships between atoms in the space. When two protons are close to each other in space, their magnetic dipoles will interact (or so-called dipole-dipole interaction). This interaction is different from *J*-coupling effect, which is not through space, but rather induced by polarization of bonding electrons in the compound.

For configuration assignments, using $^{3}J_{H,H}$ alone is often insufficient to differentiate between all possible rotamers. Use of long-range proton–carbon coupling constants ($^{2,3}J_{C,H}$) can provide additional specifications making the *J*-based configuration analysis applicable to broader range of molecules. The utility of $J_{C,H}$ couplings in conformational studies has been recognized long time ago (Hansen, 1981) although their application has often been limited to NMR specialists due to the difficulties in their measurement. Determination of $^{2,3}J_{C,H}$ values is not an easy task, mainly because signals from the active $^{1}H–^{13}C$ isotopomers to be detected are obscured by the large $^{1}H–^{12}C$ signals in the conventional ^{1}H spectrum (Parella & Espinosa, 2013). This task becomes more complicated for acyclic molecules which can show several asymmetric centers and this difficulty may explain why great number of acyclic moieties in important natural products had remained stereochemically unassigned for long time ; e.g., aflastatin, (Sakuda *et al*., 1996), prymnesins, (Igarashi *et al*.,1996) and zooxanthellatoxins (Nakamura *et al*., 1995). Due to the number of chiral centers in these compounds, they were very difficult to crystallize and difficult to synthesize their acyclic fragments.

However, recent advancements in 2D NMR techniques made the determination of $^{2,3}J_{C,H}$ possible. Several practical methods have been proposed for the measurement of $^{2,3}J_{C,H}$. including hetero half-filtered TOCSY (HETLOC), modified versions of HSQC-TOCSY, HSQMBC and phase sensitive HMBC (PS-HMBC) (Márquez *et al*., 2001).

HETLOC gives a ^{1}H-^{1}H 2D spectrum, where $^{2,3}J_{C,H}$ is represented by the dislocation, along *F2*, of a doublet cross-peaks split by $^{1}J_{C,H}$ (Matsumori *et al.* 1999). HETLOC has two main advantages, one of which is that it works even for a sample at millimolar concentration and accurate $^{2,3}J_{C,H}$ values can be determined regardless of the size of the *J* coupling. The other advantage of this method is that signs of *J* values can be obtained (Matsumori *et al*. 1999). Nevertheless, HETLOC has some limitations including that it is exclusive for molecules in which all carbons (including those existing between a carbon of interest and its long-range coupling proton) are protonated i.e it cannot measure the coupling constants between protons and quaternary carbons due to dependence of HETLOC upon the TOCSY spin. Additionally, sensitivity of the method is affected by the magnitude of each $^{3}J_{H,H}$ through which TOCSY transfers magnetization. To overcome these restrictions, PS-HMBC can be employed, which is designed to reproduce a ^{1}H signal shape by setting a refocus time before acquisition and by the application of ^{13}C-decoupling during acquisition. By this way, the relative cross-peak intensities arising from the same proton will depend on the magnitude of $^{2,3}J_{C,H}$ (Matsumori *et al*. 1999). $^{2,3}J_{C,H}$ values can fall in the same range of J_{HH} values (typically between 0 and 15 Hz).

Technically, as seen in many natural products, NOEs are optimal for cyclic compounds, but they are usually not useful to assign the conformation of highly flexible carbon chains due to the presence of several conformers. *J*-based method works better for acyclic systems, but it is often inapplicable for cyclic molecules this is due to common deviations from the staggered rotamers in cyclic systems (Matsumori *et al*., 1999). Therefore, to determine complicated organic compounds stereochemistry, the complementary use of both the *J*-based method and NOE analysis is advisable.

The *J*-based configuration assignment method was successfully applied to several natural compounds including maitotoxin (Sasaki *et al*., 1996), which is the largest secondary metabolite known to date, dysiherbaine (Sakai *et al*., 1997), amphidinol (Satake *et al*., 1991) etc.. This method has been subjected to some modifications during the course of its application following the needs of the different compounds (Bifulco *et al*., 2007).

To assign the relative stereochemistry (threo and erythro) of a1,2-dimethine system using *J*-based method, we must distinguish between six possible staggered rotamers in the threo and erythro diastereomers (Table 2.1). Only the four rotamers, A-1, A-2, B-1, and B-2,

with small $^{3}J_{H,H}$ can be identified using the *J*-based analysis solely. While, two rotamers A-3 and B-3 with large $^{3}J_{H,H}$ (an H/H-anti orientation) cannot be distinguished by $^{3}J_{H,H}$, $^{2,3}J_{C,H}$ alone. In this case, the NOE (or ROE) experiments can be utilized. When there is weak or no NOE between H-1 and H-4 then the two carbons will be anti to each other (B-3 rotamer), whereas A-3 rotamer, will show NOE between H-1 and H-4.

This interpretation is applied with small and large $^{3}J_{H,H}$ which indicates the presence of a single and dominant (>85% populated) rotamer. In case of medium-valued $^{3}J_{H,H}$, two major rotamers (one with H/H-anti and the other with H/H gauche) orientations should be considered to coexist with conformational interconversion much faster than the NMR time scale. *J*-based method cannot be applied when three staggered conformers have comparable populations, in this case, $^{3}J_{H,H}$ and $^{2,3}J_{C,H}$ will show intermediate values. In our work we adopted HETLOC as a method for measuring $^{2,3}J_{C,H}$ values.

Table 2.1: Possible conformers for vicinal methine systems (1,2 methine) using Murata method (*For vicinal deoxygenated system)

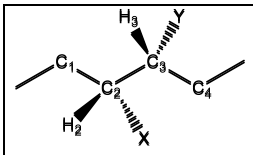 **Measurements of $^{3}J_{H,H}$**	**Method of measurements**	**Possible conformers (using Murata method)**
Small 0-4 Hz (0-Hz)*	**HETLOC/HMBC**	If All $^{2,3}J_{C,H}$ values are typical for gauche or anti select one of these conformers according to $^{2,3}J_{CH}$: 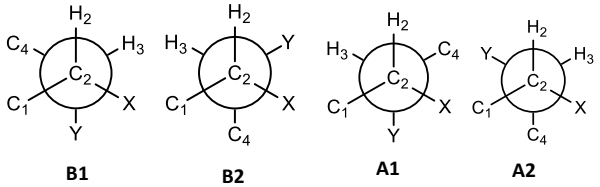 **B1** **B2** **A1** **A2** **Erythro** **Threo**
Medium 4-8 Hz (3-7 Hz)*	**HETLOC/HMBC**	If All $^{2,3}J_{C,H}$ values are typical for gauche or anti Two Alternating rotamers are identified select one of these pairs of conformers according to $^{2,3}J_{CH}$: **Threo** 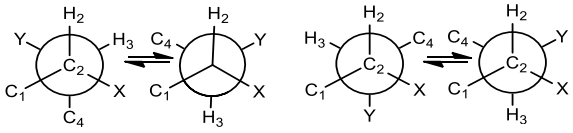 **A2** **A3** **A1** **A3** **Erythro** 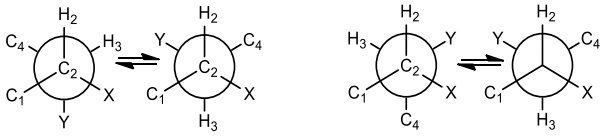 **B2** **B3** **B1** **B3**
Large 8-12 Hz (7-10 Hz)*	**NOE/ROE**	If Long-range NOE is observed between protons on C1 and C4 (C1-C4 gauche rotamer) 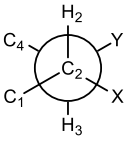 **A3** **Threo** If No Long-range NOE is observed between protons on C1 and C4 (C1-C4 Anti rotamer) 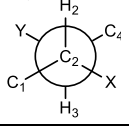 **B3** **Erythro**

Table 2.2: *J*-based configuration of 2,3-disubstituted butane systems

A (Threo)	***J*-value**	**A1**	**A2**	**A3**	**A2↔A3**	**A1↔A3**
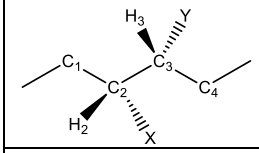	^{3}J (H-2,H-3)	Small	Small	Large	Medium	Medium
	^{3}J (H-2, C4)	Small	Large	Small	Medium	Small
	^{3}J(C1,H-3)	Small	Large	Small	Medium	Small
X= Me, Y= OR	^{3}J (Cx, H-3)	Large	Small	Small	Small	Medium
	^{2}J (C3, H-2)	Small	Large	Large	Large	Medium
X= OR, Y= OR	^{2}J (C2, H-3)	Small	Large	Large	Large	Medium
	^{2}J (C3,H-2)	Small	Large	Large	Large	Medium
B (Erythro)		**B1**	**B2**	**B3**	**B2↔B3**	**B1↔B3**
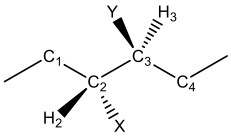	^{3}J (H-2,H-3)	Small	Small	Large	Medium	Medium
	^{3}J (H-2, C4)	Large	Small	Small	Small	Medium
	^{3}J (C1,H-3)	Small	Large	Small	Medium	Small
X= Me, Y= OR	^{3}J (Cx, H-3)	Large	Small	Small	Small	Medium
	^{2}J (C3, H-2)	Large	Small	Large	Medium	Large
X= OR, Y= OR	^{2}J (C2, H-3)	Small	Large	Large	Large	Medium
	^{2}J (C3,H-2)	Large	Small	Large	Medium	Large

2.5. General Experimental Section for this PhD thesis:

2.5.1. Part conducted at University of Naples Federico II

Optical rotations ($CHCl_3$) were measured at 589 nm on a P2000 Jasco (Dunmow, UK) polarimeter. NMR spectra were recorded on a Bruker Avance Neo 700 MHz (700 and 175 MHz for ^{1}H and ^{13}C NMR, respectively). Chemical shifts are referenced to the residual solvent signal (CD_3OD-d_4: δ_H 3.31, δ_C 49.0; DMSO-d_6: δ_H 2.50, δ_C 39.5). Homonuclear ^{1}H connectivities were determined by COSY experiments; one-bond heteronuclear $^{1}H–^{13}C$ connectivities by the HSQC experiment; and two- and three-bond $^{1}H–^{13}C$ connectivities by gradient-HMBC

experiments optimized for a $^{2,3}J$ value of 8 Hz. Through-space ^{1}H connectivities were obtained using a ROESY experiment with a mixing time of 200 ms. The HETLOC was acquired on a 700 MHz NMR with the dipsi2etgpjcsix1 pulse program. Default acquisition parameters were used except for the following modifications: td (f2) = 4096; td (f1) = 256; ns = 64; cnst2 = 140.0; cnst16 = 1.0; gpz1 = 13.0%; gpz2 = 19.0%; gpz3 = 30.0%. The HETLOC spectrum was zero-filled to 8192 and 2048 in the F2 and F1 dimensions, respectively. Column chromatography was performed on Sephadex LH-20 column (Pharmacia, Uppsala, Sweden). RP-HPLC-UV−vis separations were performed on an Agilent instrument, using a 1260 Quat Pump VL system, equipped with a 1260 VWD VL UV−vis detector, Supelco Ascentis C18, 5 μ 10 mm × 250 mm columns, and a Rheodyne injector. HPLC-RI separations were performed on a Knauer (Berlin, Germany) 1800 apparatus equipped with a refractive index detector and LUNA (normal phase, SI60, or reverse-phase RP18, 250 mm × 4 mm) (Phenomenex) columns. Thin-layer chromatography (TLC) was performed on plates coated with silica gel 60 F254 Merck, 0.25 mm. TLC were analyzed using n-BuOH/CH_3COOH/H_2O (60:15:25, v/v) as eluent and ceric sulfate in H_2SO_4 a spray reagent.

PBS (A0965-9010), $CaCl_2$ (A3779-1000), TritonX-100(A1388-0500) were all from Applichem (Germany). Insulin (I6634), (2-(*N*-(7-nitrobenz-2-oxa-1,3-diazol-4-yl)amino)-2-deoxyglucose)(2-NBDG), 2-deoxyglucose(2-DG), (4′, 6-diamidino-2-phenylindole) (DAPI) and Bovine Serum Albumine (BSA) were from Sigma Aldrich (Germany). Formaldehyde (7040) was from JTBaker (The Netherlands).

2.5.2. Part conducted at King Saud University

Optical rotations were measured in analytical grade methanol using a JASCO P-2000 polarimeter (JASCO, 2967-5, Tokyo, Japan). The 1D and 2D NMR data were acquired using a Bruker AVANCE spectrometer (Bruker, Billerica, MA, USA) (500 MHz for ^{1}H and 125 MHz for ^{13}C). Chemical shifts (δ) in ppm, relative to tetramethylsilane, were calculated basing on the residual solvent signal, and *J* scalar coupling constants are reported in Hz (Hertz). The ESI-MS analyses were measured on an Triple Quadrupole 6410 QQQ LC/MS mass spectrometer (Agilent, Santa

Clara, CA, USA) with ESI ion source (gas temperature was 350 °C, nebulizer pressure was 60 psi, and gas flow rate was 12 L/min), operating in the negative and positive scan modes of ionization through direct infusion method using $CH_3OH\backslash H_2O$ (4:6 v/v) at a flow rate of 0.5 mL/min. Column chromatography procedures were performed using silica gel 70–230 mesh, RP-18, Sephadex LH-20 (each from; E. Merck, Darmstadt, Germany). TLC analysis was performed using precoated silica gel 60 F_{254} and RP-18 (Merck, Darmstadt, Germany) plates, and spots were visualized via exposure under UV light (254/365 nm) and by spraying with different spray reagent. Analytical grade solvents and reagents were purchased from Sigma-Aldrich (St. Louis, MO, USA). Deuterated methanol (CD_3OD-d_4) and dimethylsulfoxide (DMSO-d_6) were obtained from Cambridge Isotope Laboratories (Tewksbury, MA, USA).

References:

Bifulco, G.; Dambruoso, P.; Gomez-Paloma, L.; Riccio, R. **(2007)**. Determination of relative configuration in organic compounds by NMR spectroscopy and computational methods. *Chem. Rev.*, 107, 3744-3779.

Hansen, P.E. **(1981)**. Carbon–hydrogen spin–spin coupling constants, *Progress in Nuclear Magnetic Resonance Spectroscopy*, 14, 175–295.

Ho, C. S., Lam, C. W., Chan, M. H., Cheung, R. C., Law, L. K., Lit, L. C., Ng, K. F., Suen, M. W., & Tai, H. L. **(2003)**. Electrospray ionisation mass spectrometry: principles and clinical applications. *The Clinical biochemist*. Reviews, 24(1), 3–12.

Hofstadter, S. A.; Smith, R. D. **(1996)**. Electrospray Ionization Mass Spectrometry. *J. Chem. Ed.* , 73, A82.

Igarashi, T., Satake, M., Yasumoto, T. J. **(1996).** Prymnesin-2: A Potent Ichthyotoxic and Hemolytic Glycoside Isolated from the Red Tide Alga Prymnesium parvum .*Am. Chem. Soc.*, 118, 479-480.

Márquez, B.L., Gerwick, W.H., Williamson, R.T. **(2001)**. Survey of NMR experiments for the determination of nJ(C,H) heteronuclear coupling constants in small molecules. *Magnetic Resonance in Chemistry*, 39, 499–530.

Matsumori,N., Kaneno, D., Murata, M., Nakamura, H., Tachibana, K. **(1999)**. Stereochemical determination of acyclic structures based on carbon–proton spin-coupling constants. A method of configuration analysis for natural products. *J. Org. Chem*., 64,866–876.

Murata, M., Matsuoka, S., Matsumori, N., Kaneno, D., Paul, G.K., Tachibana, K. **(1999)** Structure elucidation of marine natural products. *J. Am. Chem. Soc.*, 121,870–87.

Nakamura, H.; Asari, T.; Murai, A.; Kan, Y.; Kondo, T.; Yoshida, K.; Ohizumi, Y. J. **(1995).** Zooxanthellatoxin-A, a Potent Vasoconstrictive 62-Membered Lactone from a Symbiotic Dinoflagellate . *Am. Chem. Soc*., 117, 550-551.

Parella, T., Espinosa, J.F. **(2013).** Long-range proton–carbon coupling constants: NMR methods and applications. *Progress in Nuclear Magnetic Resonance Spectroscopy*, 73 17–55.

Pradhan, S., Rajamani, S., Agrawal, G., Dash, M., Samal, S.K. **(2017)**. 7 - NMR, FT-IR and raman characterization of biomaterials, Editor(s): Maria Cristina Tanzi, Silvia Farè, Characterization of Polymeric Biomaterials, Woodhead Publishing, Pages 147-173

Sakai, R., Kamiya, H., Murata, M., Shimamoto, K. J. **(1997)**. Dysiherbaine: A New Neurotoxic Amino Acid from the Micronesian Marine Sponge Dysidea herbacea. *Am. Chem. Soc.* 119, 4112-4116.

Sakuda, S.; Ono, M.; Furihata, K.; Nakayama, J.; Suzuki, A.; Isogai. **(1996)**. Aflastatin A, a Novel Inhibitor of Aflatoxin Production of Aspergillus parasiticus, from Streptomyces A. *J. Am. Chem. Soc.*, 118, 7855-7856.

Sasaki, M.; Matsumori, N.; Maruyama, T.; Nonomura, T.; Murata, M.; Tachibana, K.; Yasumoto, T. Angew. **(1996)**. The Complete Structure of Maitotoxin, Part I: Configuration of the C1-C14 Side Chain Chem., *Int. Ed. Engl.* , 35, 1672-1675.

Sasidharan, S., Chen, Y., Saravanan, D., Sundram, K. M., & Yoga Latha, L. **(2011)**. Extraction, isolation and characterization of bioactive compounds from plants ` extracts. *African journal of traditional, complementary, and alternative medicines*. 8(1), 1–10.

Satake, M., Murata, M., Yasumoto, T., Fujita, T., Naoki, H. J. **(1991)**. Amphidinol, a polyhydroxy-polyene antifungal agent with an unprecedented structure, from a marine dinoflagellate, Amphidinium klebsii. *Am. Chem. Soc.*, 113, 9859-9861.

Sim, L.N., Fane, A.G. **(2017)**. Advanced Monitoring of Membrane Fouling and Control Strategies,Editor(s): Enrico Drioli, Lidietta Giorno, Enrica Fontananova, Comprehensive Membrane Science and Engineering (Second Edition), Elsevier,Pages 72-103.

CHAPTER 3

PHYTOCHEMICAL AND BIOLOGICAL STUDY OF *CISSUS ROTUNDIFOLIA* GROWING IN SAUDI ARABIA

3.1. Genus *Cissus*

The genus *Cissus* belongs to the Vitaceae family, which includes the common fruit grapes (*Vitis vinifera*). One of the main secondary metabolites in grapes, resveratrol, one of the better known nutraceutical, has well-established medicinal properties including anti-diabetic (Szkudelski and Szkudelska, 2011), antineurodegenerative (Sun *et al.*, 2010), anti-cancer (Athar *et al.*, 2009), protection from cardiovascular disease (Bertelli and Das, 2009), increase of longevity, to name a few. Additionally, Vitaceae family includes about 350 species, some of which are used in traditional medicine to treat different diseases.

Cissus species were reported to possess anti-diabetic, antimicrobial, antiosteoporotic, hypoglycemic, antioxidant, antitumor, analgesic, anti-inflammatory, gastroprotective, hepatoprotective, immunomodulatory and anti-allergic activities (Al-Mamary, 2002; Alzoreky and Nakahara, 2003; Al-Fatimi *et al.*, 2007). In Australia, Bush Medicine Practitioners use *C. hypoglauca* to treat sore throat. In China and the Far East, *C. assamica*, is used as anti-snake venom, while in South East Asia, including the Indian subcontinent and Sri Lanka, *C. quadrangularis* is used for fracture healing and as an anti-obesity agent (Fernandes & Banu, 2012).

Plants of the genus *Cissus* were reported to contain sterols, triterpenoids, phenolics, flavonoids, stilbene derivatives, coumarin glycosides and iridoids (Beltrame *et al.*, 2002; Singh *et al.*, 2007). For example, compounds isolated from *C. pteroclada* include *β*-sitosterol, bergenin, 11-*O*-galloylbergenin, 11-*O*-(4-hydroxy benzoyl) bergenin, gallic acid and daucosterol (Chi *et al.*, 2011). The leaves of *C. ibuensis* were reported to contain quercetin 3-*O*- rutinoside and flavanoids (Ahmadu *et al.*, 2010). Moreover, phytochemical analysis of *C. assamica* disclosed the presence of lupeol, *n*-hexacosinc acid, isolariciesinol-9-*O*-*β*-*D*-glucopyranoside, daucostenin, 3,3'-dimethyl ellagic acid, *β*-sitosterol and bergenin (Xie *et al.*, 2009). Stilbene *C*-glucosides were reported in *C.*

repens (Wang *et al.,* 2007). Apart from flavanoids, sterols, triterpenoids, iridoids and 3,3,4,4' tetra-hydroxybiphenyl were also isolated from *C. quadrangularis* (Deokule and Waghmare, 2004; Mehta *et al.,* 2001; Nagani *et al.,* 2011; Singh *et al.,* 2007). The chemical constituents of *C. sycoides* include flavonoids, stilbenes, steroids, coumarin, tritepenes, tannins and saponins (Beltrame *et al.,* 2002; Otshudi *et al.,* 2000; Xu *et al.,* 2009). *C. rheifolia* leaves have quinolizidine alkaloids, flavanoids, terpenoids (Saifah *et al.,* 1983) and the stem wood of *C. pallida* has stilbenes, triterpenoids and steroids (Khan *et al.,* 1986). Many of the compounds isolated from the plants belonging to the genus *Cissus* have therapeutic effects.

3.2. Cissus rotundifolia

Cissus rotundifolia (Forssk.) *Vahl* is an edible wild, evergreen perennial tendril climber shrub of family Vitaceae that grows extensively in Yemen and Southern region of Saudi Arabia and Egypt. It is known as a common Arabian wax *Cissus,* and locally (in south Saudi Arabia) as Algalaf. *C. rotundifolia* is consumed by local people as leafy vegetable. By cooking the leaves, various dishes can be prepared according to traditional dietary culture. In Yemen, the boiled leaves of *C. rotundifolia* are eaten with meals as an appetizer and are also used as an antipyretic in the treatment of malaria and dengue fever. In folk medicine, *C. rotundifolia* is used as antidiabetic, antimalarial, in the treatment of gastrointestinal diseases, liver disease, otitis, loss of appetite, burns and skin diseases (Alshawsh *et al.,* 2009 & Al-Fatimi *et al.,* 2007).

Figure 3.1: *Cissus rotundifolia* plant growing in Saudi Arabia

C. rotundifolia growing in Yemen was evaluated for its chemical and nutritional content (Al-Bukhaiti *et al.,* 2019). *C. rotundifolia* plant was found to be a rich source of many essential nutrients, such as carbohydrates (72.54%), protein (12.16%), and dietary fiber (14.10%). Furthermore, *C. rotundifolia* contained important vitamins, including thiamin (5.37 mg/ 100 g DW), riboflavin (1.19 mg/100 g DW), pyridoxine (0.46 mg/100 g DW) and folic acid (0.20 mg/100 g DW). In addition, it contains sufficient amounts of essential amino acids and mineral elements, which could meet the daily requirements of humans.

The phytoconstituents of the plant extract were mainly of phenolics, steroidal saponins, coumarins, stilbenoids and triterpene types (Said *et al.,* 2018). *C. rotundifolia* growing in Egypt showed the presence of triterpenes, carbohydrates, glycosides, tannins, flavonoids, coumarins and saponins (Said *et al.,* 2015). The same research group has suggested a fingerprint profile for the aerial parts of *C. rotundifolia* using HPLC/MS analysis which led to identification of twenty-seven compounds. The identified compounds included four acids (malic acid, aconitic acid, quinic acid and kynurenic acid); two steroidal saponins (1*β*-hydroxy-kryptogenin-1- *O*-α-L-rhamnopyranosyl- (1→2)-*α*-L-arabinopyranoside and Alliospiroside A (25(*S*)-ruscogenin-1-*O*-α-L-rhamnopyranosyl-(1→2)-arabinopyranoside); two coumarins (bergenin and 5,6,7,8- tetrahydroxycoumarin-5*β*-xylopyranoside); two stilbenoids (resveratrol and pallidol); one triterpene (*β*-amyrin) and sixteen phenolic compounds. The phenolic compounds included two phenolic acids, namely gallic acid and vanillic acid, phenolic acid glucoside (vanillic acid hexoside), a xanthoid (mangiferin), in addition to: Isovitexin (apigenin-6-*C*-glucoside), Isoorientin (luteolin-6-*C*-glucoside), cyclolariciresinol hexoside, vanillic acid-hexoside, astragalin (kaempferol-3-*O*-glucoside), isoquercitrin (quercitin-3-*O*-glucoside, quercetin-3-*O*-rhamnoside), kaempferol 3-*O*-α-L-rhamnoside, 3',5-dihydroxy-4',6,7- trimethoxyflavone, Orientin (luteolin 8-*C*-glucoside), pinobanksin, acteoside, formononetin (Said *et al*., 2018). In same study, the plant extract exhibited a significant cytotoxicity against MCF-7, authors have concluded that *C. rotundifolia* can be a potential source of selective cytotoxic agents and further investigations should be undertaken.

C. rotundifolia has been reported to exhibit hypoglycemic (Onyechi *et al.* 1998, Shalabi *et al.*, 2018), hypolipidemic (Bell *et al.*1993, Shalabi *et al.*, 2018), antibacterial (Alzoreky and Nakahara, 2003) and antimalarial activities (Alshawsh *et al.*, 2009).

Ethanolic extract of *C. rotundifolia*, growing in Yemen and its fractions (methylene chloride and *n*-butanol) have shown significant antihyperglycemic, antihyperlipidemic and antioxidant activities (Shalabi *et al.*, 2018). In a similar study, water extract of *C. rotundifolia* has exhibited hypoglycemic effect resembling those of glibenclamide and metformin (Al-Mehdar & Albattah, 2016). The possible mechanism of antidiabetic activity is the stimulation of the activity of the remnant pancreatic cells due to its high content of phenolic compounds (Shalabi *et al.*, 2018). Additionally, ethanolic extract and *n*-butanol fraction of *C. rotundifolia* resulted in a significant elevation of serum calcium and phosphorus levels *in vivo* study and showed protective effect against glucocorticoid-induced secondary osteoporosis (Shalabi *et al.*, 2018). To the best of our knowledge, *C. rotundifolia* growing in Saudi Arabia has never been subjected to phytochemical study, nor the constituents responsible for bioactivities have been disclosed.

3.3. Diabetes mellitus

Blood glucose concentration is strictly controlled by several chemicals and hormones in the body, among which insulin, the hormone produced by the β cell of pancreas. Diabetes mellitus (DM) is a chronic non-infectious disease characterized by the inability of the pancreas to effectively produce sufficient insulin or by the lack of the body ability to properly utilize the produced insulin which results in sustained high blood sugar (hyperglycemia) (Al Dawish *et al*., 2016). Without sufficient insulin activity/level, the uptake of glucose from the blood into the body cells is impaired leading to accumulation of glucose in the blood to abnormal levels. Over prolonged times, uncontrolled hyperglycemia can severely damage several body systems, including the nerves and blood vessels (Martin *et al*., 2014). In 21st century, DM has been considered as one of the main health challenges for mankind with progressively increasing number of patients and has been recognized as a global silent killer both in the developed and developing countries. In 2019, 463 million people worldwide are suffering from diabetes according to the International Diabetes Federation (IDF), this number is expected to rise by 2045 to

700 million. In the Middle East and North Africa (MENA) regions there are 55 million diabetic patients; this number is expected to rise to 108 million by 2045 (IDF, 2019).

Both genetic and environmental factors play crucial roles in the etiology and development of this chronic disorder (Martin *et al*., 2014). Although DM is incurable, it is a preventable and manageable disease (Nathan *et al*., 2005). Diabetes is an expensive disease due to its prolonged nature, severity of the complications and required management drugs and tests. This imposes a substantial load on both the sufferer as well as the health systems (Hu *et al*., 2015). It is noteworthy that a vast percentage of the reported cases of diabetes are in the age group of 40-59, among whom 80% live in countries with low and middle-income economies (Katulanda *et al*., 2014).

There are two types of DM: i. Type 1diabetes (insulin dependent diabetes mellitus) which is caused by deficiency of insulin secretion by beta cells of the pancreas. ii. Type 2 diabetes (non-insulin dependent diabetes mellitus), which is caused by insulin resistance (reduced sensitivity of target tissues to insulin). In both types of DM, metabolic processes of the digested food are altered with lack of efficient uptake and utilization of glucose by most of body cells, except those of the brain (Guyton and Hall, 2006).

Type 1diabetes is caused by an autoimmune reaction that targets proteins of the islets cells of the pancreas leading eventually to selective distruction of pancreatic β-cells that produce insulin. Around 10% of all diabetes cases are of type 1, with the majority of individuals being diagnosed during their childhood and early adulthood (Holt, 2004).

Type 2 diabetes is a typical multifactorial disease that is controlled by multiple genetic factors combined with environmental factors (including obesity, lack of exercise, stress and aging) (Holt, 2004; Kaku, 2010). Type 2 DM accounts for at least 90% of total DM cases with most cases being diagnosed after the age of 40 years (Gonzalez *et al*., 2009). The increase in the prevalence of Type 2 DM is expected to be much higher in developing (69%) than in developed countries (20%) (Shaw *et al*., 2010).

3.3.1 Insulin-stimulated glucose uptake

The chief stimulator for cellular glucose uptake is insulin. This uptake process is initiated by the insulin binding insulin receptor (IR) on cellular surface (Deshmukh, 2015). Insulin receptors are transmembrane proteins (comprising 2 α and 2 β subunits) that possess intrinsic tyrosine kinase activity. Once insulin binds to IR, conformational changes of the receptor are induced, resulting in auto-phosphorylation and activation of tyrosine kinases, which leads to stimulation of insulin receptor substrates (IRS) including IRS1 (Taniguchi *et al*., 2006). Binding of IRS1 to the regulatory subunit of phosphoinositide 3-kinase (PI3-K) will activate PI3-K, which in turn phosphorylates membrane phospholipids and phosphatidylinositol-4,5-bisphosphate (PIP2). The resulted complex works by activating the 3-phosphoinositide-dependent protein kinases-1 (PDK-1) which results in activation of Akt/ protein kinase B (PKB) and atypical protein kinase C λ and ζ (aPKC λ/ζ), which are serine/threonine kinases (Taniguchi *et al*., 2006). This signaling cascade enables translocation of glucose transporters (GLUT) from cytosol to the plasma membrane, which finally opens the gate for cellular glucose uptake (Bandyopadhyay *et al*.,1997; Bandyopadhyay *et al*.,2000; Wang *et al*.,1999). Once the glucose gets inside the cell, it is converted to glucose-6-phosphate in a reaction activated by hexokinase enzyme. The glucose-6-phosphate is either metabolized for energy through the glycolytic pathways or stored as glycogen by glycogen synthase (Deshmukh, 2015).

3.3.2. Management of diabetes mellitus

DM is untreatable disease, however medical approaches helped to reduce diabetes-related mortality and morbidity and to improve quality of life by controlling hyperglycemia. Diabetes management with minimum side effects is the primary goal of these medical approaches. Since the 90's, insulin, sulfonylureas and metformin have been considered as the cornerstones in management of DM. The interest in developing new anti-diabetic agents has continued to trend worldwide with better figured-out pathophysiology of DM resulting in introduction of several new classes with different mode of actions (e.g thiazolidinediones (TZDs), alpha glucosidase inhibitors, meglitinides, amylin agonists, GLP-1 receptor agonists (GLP-1 RA), DPP4 inhibitors (DPP4-i), colesevelam, bromocriptine, and most recently, SGLT2 inhibitors (White, 2014). Despite fascinating

advance in DM management drugs discovery, nearly half of the diabetic population are reported to be not meeting glycemic goals (Blonde *et al*., 2017) which has its negative impact on the prognosis of the diabetes-related complications (damage of the kidney, liver, eyes, nerves, heart and blood vessels). This necessitates the continual of searching for more effective and safer anti-diabetic agents.

Several anti-diabetic drugs were derived from natural sources. For instance, the natural products inspiring the synthesis of metformin (the first line in the treatment of type 2 DM) was isolated from plant *Galega officinalis*, which was used in folk medicine for several centuries. Another anti-diabetic drug, exenatide (GLP-1 receptor agonist), is a synthetic version of exendin-4, a peptide originally isolated from the salivary secretions of the Gila monster animal (Parkes *et al*., 2012). Additionally, acarbose is a natural anti-diabetic pseudotetrasaccharide, derived from microbial cultures of *Actinoplanes* strain SE 50 (Osadebe *et al*., 2014). With no doubts these drug discoveries from nature are inspiring and encouraging to exert more efforts to uncover novel anti-diabetic agents from natural sources including plant, which was the aim of our current work.

3.4. Results and Discussion

Defatted *C. rotundifolia* aerial parts were extracted with 80% ethanol and the total extract was dissolved in H_2O and partitioned against EtOAc and then *n*-BuOH. This latter phase, selected on the basis of bioactivity (see below) was subjected to bioassay-guided fractionation on Sephadex LH-20 and RP-HPLC to afford the new cissuxinoside (**1**) and cissoic acid (**2**), large amounts of the *C*-glycosides **3-5**, *Z*-4-coumaric acid *β-D*-glucopyranoside (**6**) and 1-*O*-*p*-coumaroyl-*β-D*-glucopyranose (**7**).

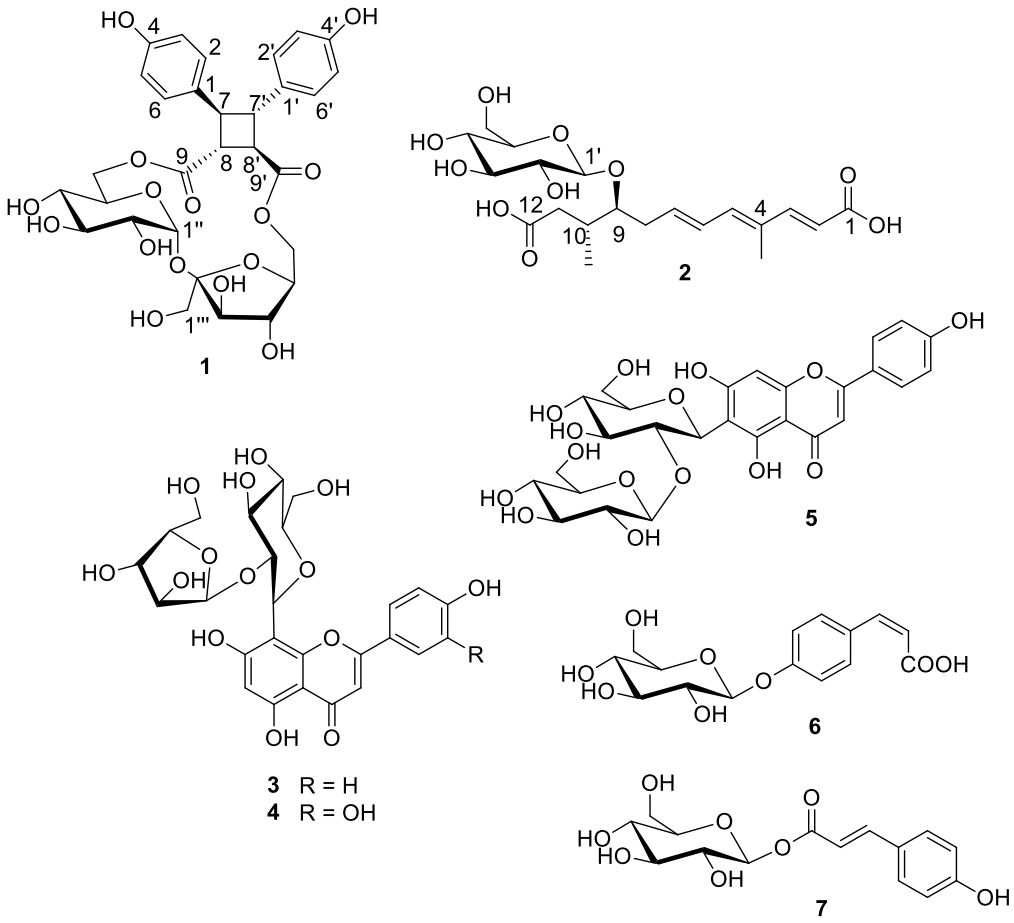

Figure 3.2: Compounds isolated from *C. rotundifolia*

Cissuxinoside (**1**) was obtained as a yellow amorphous solid with molecular formula $C_{30}H_{34}O_{15}$ determined by High Resolution- Electrospray Mass Spectrometry (HR-ESIMS). ^{1}H NMR spectrum of **1** (Table 3.1) showed four 2H-integrating doublets between δ_H 6.50 and 6.85, a pattern suggestive of two 1,4-disubstituted phenyl moieties, and a series of signals located between δ_H 3.00 and 5.35, including one anomeric oxymethine at δ_H 5.34. All the proton signals were associated to the directly linked carbon atoms through the 2D NMR Heteronuclear Single Quantum Coherence spectroscopy (HSQC), while analysis of the Correlation SpectroscopY (COSY) spectrum arranged the proton multiplets in five distinct spin systems, as shown in Figure 3.3. In addition to the two anticipated disubstituted phenyl rings, an AA'BB' system of methine proton signals resonating around δ_H 3.80-4.25 was disclosed (corresponding carbon atoms resonated in the range δ_C 44-46), typical values of a tetrasubstituted cyclobutane

ring. Moreover, an α-glucopyranose system could be deduced from the small value of H-1"/H-2" coupling constant and the large values of H-2"/H-3", H-3"/H-4" and H-4"/H-5". The presence of a ketose sugar unit was inferred from the 2D NMR Heteronuclear Multiple Bond Correlation (HMBC) spectrum, that showed correlations of both H_2-1'" and H-3'" with an anomeric carbon at δ_C 105.0 that, in turn, also showed $^3J_{CH}$ HMBC correlation with H-1", thus clearly pointing to the presence of a sucrose unit. The relatively downfield shifted sugar methylenes H_2-6" and H_2-6'" showed HMBC correlations with the ester carbonyls resonating at δ_C 174.0 and 174.3, respectively. These latter carbonyl signals should be directly attached to the cyclobutane ring, as indicated by their HMBC correlations with the cyclobutane protons, as shown in Figure 3.3 (H-7/C-9 and H-7'/C-9'). The structural arrangement of cissuxinoside (**1**) was defined by the linkage of two 4-hydroxyphenyl moieties to the cyclobutane ring, as implied by the HMBC correlations H-7/C-1, H-7/C-6(C-2), H-7'/C-1', and H-7'/C-6'(C-2'). Thus, cissuxinoside was identified as a 6",6'" diester of sucrose with a truxinic acid unit.

Rotating frame Overhause Effect SpectroscopY (ROESY) spectrum evidenced key correlations H-8/H-6(2), H-8'/H-6' (2') and H-7'/H-8 (Figure 3.3) that, taken together, indicated an *all-trans* relative configuration around the cyclobutane ring, in agreement with a structure of the δ-truxinic type. A further support to this assignment came from a literature search, which revealed that a 7/7' *cis*, 8/8' *cis*, 7/8 *trans*, 7'/8' *trans*- (β-truxinic) stereoisomer of **1** has been reported from *Bidens parviflora* (Wang *et al*., 2003). Accordingly, both ^{1}H NMR values and proton-proton coupling constants of cyclobutane ring protons were significantly different for the two isomers. Truxinic acids likely originate by a head-to-head photochemical cycloaddition of cinnamic or coumaric acid derivatives, while the isomeric truxillic acids, showing phenyl rings attached to alternate cyclobutane methines, should derive form a head-to-tail cycloaddition. Sucrose esters of truxinic or truxillic acids are very unusual in plants and cissuxinoside (**1**) is only the third member of this small family.

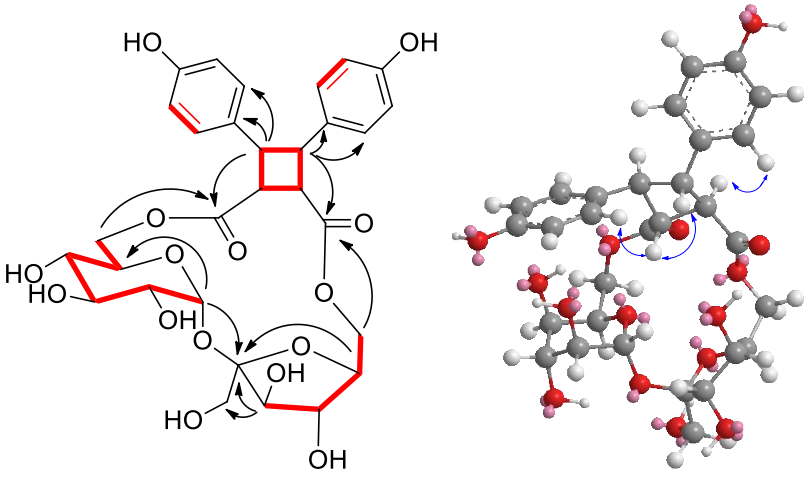

Figure 3.3: *left:* COSY (red) and HMBC (black arrows) detected for cissuxinoside (**1**); *right*: 3D model with key ROESY correlations (blue arrows)

The molecular formula of cissoic acid (**2**) was established as $C_{20}H_{30}O_{10}$ basing on HR-ESIMS data. ^{1}H NMR spectrum of **2** (Table 3.2) showed a series of multiplets in the low-field region (between δ_H 7.40 and 5.80), several signals in the midfield region, some overlapped multiplets around δ_H 2.50 and two 3H-integrating signals. The 2D NMR HSQC spectrum of **2** allowed a detailed interpretation of 1D NMR data associating protons to directly linked carbon atoms (Table 3.2). Thus, the presence of three C-C double bonds (two disubstituted and one trisubstitued), a series of oxymethines and one oxymethylene could be deduced. The low field resonances of the sp^2 methines suggested the existence of a conjugated system, while one of the oxymethines could be identified as anomeric center (δ_C 103.5). In addition, two methyl groups were easily identified in the ^{1}H NMR spectrum at δ_H 0.96 (d) and 1.96 (s), the latter likely occupying an allylic position. The presence of an hexopyranose sugar was confirmed by correlations in the COSY spectrum, that also allowed to arrange the remaining proton multiplets into two spin systems, an isolated double bond and an extended spin system spanning from H-5 to H_2-11 and including a methyl branching at C-10 (Figure 3.4).

Table 3.1. ^{1}H and ^{13}C NMR data of cissuxinoside (**1**) in CD_3OD

Position	δ_H, mult (*J* in Hz)	δ_C, type
1		131.1, C
2 = 6	6.72, *d* (8.5)	129.5, CH
3 = 5	6.52, *d* (8.5)	115.3, CH
4		155.3, C
7	4.23[a]	44.5, CH
8	3.95, *dd* (10.3, 7.8)	44.4, CH
9		174.0, C
1'		131.1, C
2' = 6'	6.84, *d* (8.5)	129.9, CH
3' = 5'	6.57, *d* (8.5)	115.5, CH
4'		155.3, C
7'	4.18, *dd* (10.3, 4.7)	45.5, CH
8'	3.81[a]	44.6, CH
9'		174.3, C
1''	5.34, *d* (3.5)	94.3, CH
2''	3.40, *dd* (9.3, 3.5)	73.0, CH
3''	3.74, *t* (9.3)	73.7, CH
4''	3.09, *t* (9.3)	72.7, CH
5''	4.02[a]	72.6, CH
6''a, 6''b	4.82[a], 3.80[a]	67.2, CH_2
1'''	3.85, *s*	61.5, CH_2
2'''		105.0 C
3'''	4.22[a]	78.9, CH
4'''	4.00[a]	77.2, CH
5'''	4.04[a]	80.3, CH
6'''a, 6'''b	4.31, *dd* (10.8, 8.5), 4.22[a]	68.0, CH_2

a Overlapped with other signals

The 2D NMR HMBC cross-peaks of H-9 with C-1' and of H_3-13 with C-3, C-4 and C-5 provided evidence to join the above subunits. The planar structure of cissoic acid was completed, in agreement with its molecular formula, by interpretation of the HMBC cross-peaks exhibited by both H-2 and H_2-11 with carboxylic acid signals (C-1 and C-12,

respectively), the first resonating at relatively high-fields (δ_C 171.1) due to the double bond conjugation.

The *β*-glucopyranose nature of the sugar unit was deduced by the HMBC correlation H-1'/C-5', by the relatively large proton-proton vicinal coupling constants measurable for the non-overlapped protons H-1', H-2', and H-5' and supported by 2D NMR ROESY contacts H-1'/H-3', H-1'/H-5', H-2'/H-4'. Similarly, the *trans* configuration at Δ^2 and Δ^6 could be deduced by the corresponding proton-proton coupling constants (15.4 and 15.0 Hz, respectively), while *E* configuration was assigned at $\Delta^{4(5)}$ basing on the ROESY cross-peak H_3-13/H-6.

The relative configuration of the C-9/C-10 segment was determined by applying the *J*-based configuration analysis (Matsumori *et al*., 1999; Bifulco *et al*., 2007), based on the measurement of homonuclear and heteronuclear coupling constants (the 2D NMR HETLOC experiment was used to measure exact $^2J_{C,H}$ and $^3J_{C,H}$ values) and ROESY correlations.. Within cissoic acid, two asymmetric centers can be detected, namely C-9 and C-10. Using ROESY experiment, erythro relative configuration of cissoic acid was confirmed by the strong ROESY correlations between H_3-14 and H_2-8, between H-9 and H-10 and between H_2-8 and H_2-11. According to Murata method cissoic acid can be treated as 1,2 asymmetric molecule (i.e the stereogenic carbons are adjacent to each other) and the possible conformers by applying this method are displayed in Table 2.1. Selection of the exact conformer can be achieved by comparing our measured $^3J_{H,H}$ and $^{2,3}J_{C,H}$ to those in Table 2.1. Cissoic acid showed small $^3J_{HH}$ indicating H/H gauche position while the large $^2J_{C\text{-}9/H\text{-}10}$ (-6.0 Hz) indicates that the H-10 and the *O*-Glu group at C-9 must be gauche to each other and as a result also, methyl group at C-10 will be in gauche position with *O*-Glu group. The large $^3J_{C\text{-}8/H\text{-}10}$ (7.9 Hz) will put C-8 and H-10 in anti- orientation while the small $^3J_{C\text{-}11/H\text{-}9}$ (1.8 Hz) means that two nuclei C-11and H-9 are gauche to each other. The configuration in Figure 3.4 exactly fits with these measurements.

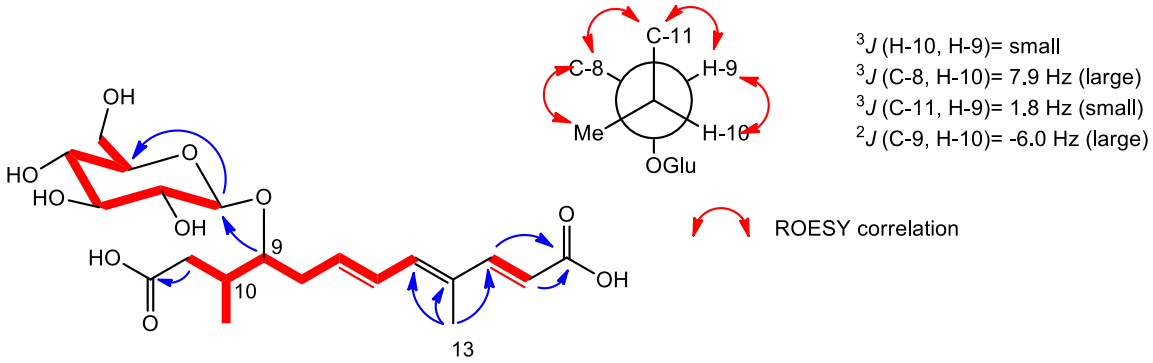

Figure 3.4. *left:* COSY (red) and HMBC (blue arrows) detected for cissoic acid (**2**); *right:* dominant rotamer around C-9/C-10 single bond

Having assumed the D configuration of the sugar unit, determination of the absolute configuration at C-9 and C-10 would completely define the stereostructure of cissoic acid (**2**). The lack of functional groups that could be easily derivatized with chiral auxiliaries suggested us to proceed with a comparison of the experimental and simulated ECD spectra, generated by Time-Dependent Density Functional Theory (TDDFT).

Since the dominant rotamer around the C-9/C-10 axis of **2** had been previously identified, the conformers of **2** resulting from free rotation about C-10/C-11 and C-8/C-9 bonds were selectively investigated using the Gaussian 09 software. This systematic search afforded 80 conformers, which were geometrically optimized at the DFT level using a mpw1pw91 functional and 6-31G(d) basis set. The relative energies of the different conformers were calculated and the equilibrium room temperature Boltzmann-based populations were thus obtained. As shown in Table 3.3, conformers 1 and 2 account for about 90% of the populated ones and the remaining seven conformers are those possessing energies within 3 kcal/mol of the lowest energy conformation and therefore are significantly populated.

Table 3.2. ^{1}H and ^{13}C NMR data of cissoic acid (**2**) in CD_3OD

Position	δ_H, mult (*J* in Hz)	δ_C, type
1		171.1, C
2	5.84, *d* (15.4)	117.1, CH
3	7.33, *d* (15.4)	150.6, CH
4		132.3, C
5	6.44, *d* (11.3)	140.1, CH
6	6.52, *dd* (15.0, 11.3)	128.6, CH
7	6.05, *m*	140.9, CH
8a	2.56[a]	36.8, CH_2
8b	2.04[a]	
9	4.15, *ddd* (3.5, 2.5, 1.5)	80.1, CH
10	1.93[a]	38.2, CH
11a	2.59[a]	37.6, CH_2
11b	2.53[a]	
12		176.4, C
13	1.92, s	12.0, CH_3
14	0.96, *d* (6.9)	14.5, CH_3
1'	4.39, *d* (7.7)	103.5, CH
2'	3.18, *t* (7.7)	75.0, CH
3'	3.36[a]	77.7, CH
4'	3.33[a]	71.2, CH
5'	3.28, *ddd* (7.7, 5.4, 2.3)	77.6, CH
6'a	3.87, *dd* (11.8, 2.3)	62.5, CH_2
6'b	3.70, *dd* (11.8, 5.4)	

a Overlapped with other signals

The excitation energies as well as the oscillator and rotatory strengths of the electronic excitation were calculated for the nine conformational families using the TDDFT methodology and weighed according to the Boltzmann population. Thus, the ECD spectra for 9*S*,10*R* and 9*R*,10*S* were obtained, as reported in Fig. 3.5 The extensive overlapping of the first with the experimental ECD spectrum allowed us a confident assignment of the 9*S*,10*R* configuration to the natural compound.

Table 3.3. Energy and relative population of the main conformers of cissoic acid (**2**)

Conformers	Φ C12-C11-C10-C9	Φ C10-C9-C8-C7	Kcal/mol	ΔG KJ/mol	%pop.
1	-60.10	-68.10	0.00	0.00	59.9
2	-150.10	-68.10	0.42	1.77	29.4
3	74.90	-68.10	2.10	8.78	1.7
4	-60.10	66.90	2.30	9.64	1.2
5	-60.10	66.90	2.30	9.64	1.2
6	-105.10	-68.10	2.35	9.82	1.1
7	150.10	66.90	2.57	10.73	0.8
8	-150.10	66.90	2.57	10.73	0.8
9	-150.10	-23.10	2.58	10.79	0.8
10	-60.10	156.90	2.79	11.69	0.5

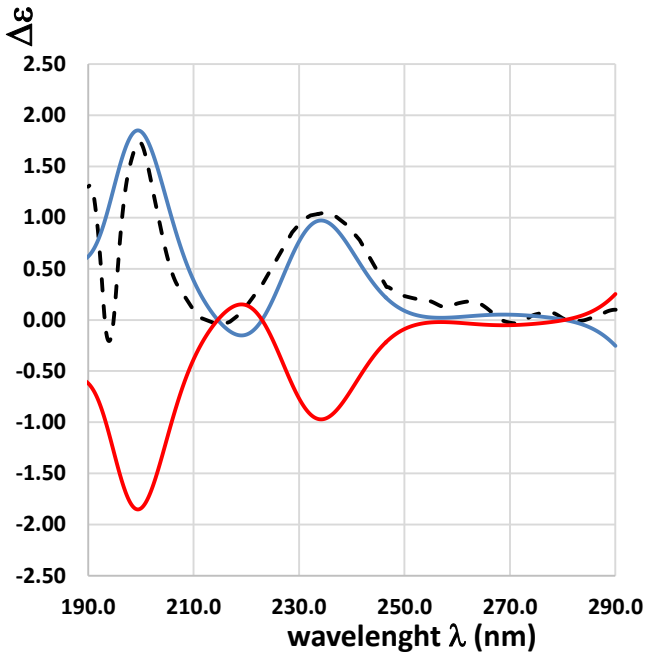

Figure 3.5.: Comparison between experimental (dashed line) and calculated (9*S*,10*R* blue line, 9*R*,10*S* red line) ECD spectra for cissoic acid (**2**).

Cissoic acid (**2**) is an unprecedented glycosylated and extensively conjugated C_{12} dicarboxylic acid bearing two methyl groups at C-4 and C-10. The single related,

although non-glycosylated, diacid analogue of **2** present in the literature has been reported about fifty years ago from the immature seeds of *Phaseolus multiflorus*. (MacMillan & Suter, 1967). Cissoic acid (**2**) could derive from a cytochrome P-450-mediated ω-oxidation of a dimethylated and hydroxylated dodecatrienoic acid. In this sense, it is interesting to notice that a compound very similar to the postulated substrate for this oxidation, 11-hydroxy-4-methyl-2*E*,4*E*,6*E*-dodecatrienoic acid, has been reported from fermentations of a zygomycete of the genus *Mucor sp* (Lorenzen *et al*.,1996).

Compound **3**, $C_{26}H_{28}O_{14}$ by HR-ESIMS, was identified as vitexin-2``-*O*-*β*-D-arabinofuranoside by comparison of its spectral data with those reported for a flavone C-glycoside isolated from *Cotoneaster thymaefolia*. A complete set of 2D NMR spectra was acquired to obtain complete ^{1}H and ^{13}C NMR assignment, reported in the Experimental Section, which was absent in ref. (Palme *et al*., 1994)

Compound **4**, $C_{26}H_{28}O_{15}$ by HR-ESIMS, was assigned as a congener of **3** differing for the presence of a further oxygenated carbon on the aglycone moiety. Accordingly, ^{1}H NMR resonances of the sugar moiety of **4** almost exactly matched those of **3**, while the two compounds differed for the flavone moiety, with **4** showing the typical ^{1}H NMR pattern of luteolin. A detailed investigation of 2D NMR spectra supported the identification of **4** as orientin-2``-*O*-*β*-*D*-arabinofuranoside. The single report of this compound in the literature is a patent reporting on its isolation from *Deschampsia antarctica* and its antineoplastic activity (Gidekel *et al*., 2014). Since no NMR data were available in the patent, a full ^{1}H and ^{13}C NMR assignment of **4** was needed and it is reported in the Experimental Section.

Three further compounds were identified as isovitexin-2'-*O*-*β*-*D*-glucopyranoside (**5**), (Cheng *et al*., 2000) *Z*-4-coumaric acid *β*-*D*-glucopyranoside (**6**), (Wu *et al*., 2003) and 1-*O*-*p*-coumaroyl-*β*-*D*-glucopyranose (**7**) (He & Liu, 2006) by comparison of their spectral data with those reported in the literature.

All the compounds obtained from purification of the bioactive fractions of the BuOH extract were evaluated for their activity in the promotion of glucose uptake in hepatic cell. The fluorescently labeled non-metabolizable glucose analogue 2-(*N*-(7-nitrobenz-2-

oxa-1,3-diazol-4-yl)amino)-2-deoxyglucose (2-NBDG) was used to directly monitor the uptake of the carbohydrate. Similarly to unlabeled glucose, the probe is transported into the cytoplasm by the family of glucose transporters GLUTs. However, due to the replacement of the hydroxyl group in position 2', 2-NBDG cannot isomerize to fructose-6-phosphate and accumulates into the cell without proceeding along the glycolytic pathway. As shown in Figure 3.6, one-hour treatment with **7** (800 mg/L), promoted glucose uptake in HuH7 (2.0 ± 0.2 over vehicle). On the contrary, the other tested compounds **1-6** failed in stimulating glucose uptake. The amount of glucose uptake upon treatment with **7** was comparable to that promoted by 10 nM and 100 nM insulin (1.9 ± 0.1 and 2.2 ± 0.1, respectively) and, in a certain extent; *p*-coumaroyl glycoside **7** might stimulate GLUT transporters using an insulin-like mechanism. Dose response experiments revealed that **7** promotes glucose uptake with an EC_{50} of 7.7 ± 0.1 μM (Figure 3.4).

1-*p*-coumaroyl *β*-D-glucoside had been reported to exert anti-inflammatory activity via Akt phosphorylation, (Vo *et al*., 2014) but to our knowledge it had never been correlated to the antidiabetic activity of plant extracts. Interestingly, compound **7** has been recently detected in the most important Vitaceae plant, grape (*Vitis vinifera*), and in wine (Hixson *et al*., 2016).

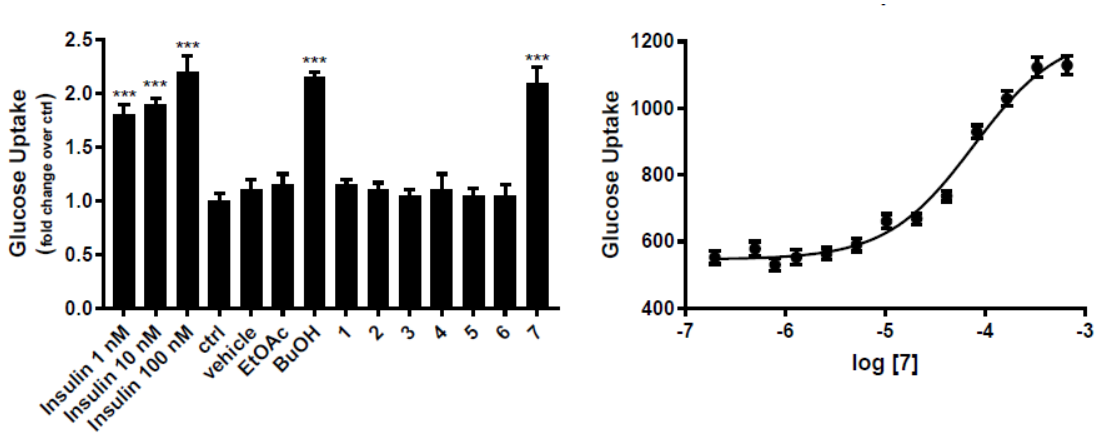

Figure 3.6: *Left.* Glucose uptake of HuH7 cells treated for 1 h with the indicated amount of insulin, compounds **1-7** (800 mg/L), or of vehicle (DMSO) (Data are representative of $n = 3$ measurements, shown is mean ± s.d.; ***$p < 0.001$). *Right* Dose-response curve for **7** promoting glucose uptake in HuH7 cells. The graph is representative of three independent experiments (mean of three replicates ± s.d.)

In summary, a bioassay-guided purification of *C. rotundifolia* extracts revealed the presence of the new cissuxinoside (**1**) and cissoic acid (**2**), belonging to very unusual classes of secondary metabolites. In addition, three rare C-glycosylated flavones (**3**-**5**) were fully characterized, and for two of them (**3**-**4**) NMR data are reported here for the first time. This study identified 1-*O*-(4-coumaroyl)-*β*-D-glucopyranose (**7**) as the main responsible of glucose uptake stimulation effect. However, other concomitant mechanisms likely concur in defining the marked antidiabetic effect of *C. rotundifolia* extract.

3.5. Experimental Section

3.5.1. Plant material

The aerial parts of the *C. rotundifolia* was collected and identified by Dr. Rajakrishnan, Department of Botany and Microbiology, college of science, King Saud University, Riyadh, Saudi Arabia. A voucher specimen of the plant has been deposited in the herbarium of College of science King Saud University, Saudi Arabia. (KSU No: 24329).

Figure 3.7: *C. rotundifolia* collected from Jizan (Southern Saudi Arabia)

3.5.2. Extraction and isolation

C. rotundifolia aerial parts (4.0 Kg) were air-dried at room temperature in the shade and ground using a blender. The obtained powder was defatted in *n*-hexane (2 × 3 L, 8 h each) and then extracted with 80% ethanol (5 × 2 L, 8 h each) at room temperature. The

EtOH extract was filtered and evaporated to obtain a dried material (300 g) that was partitioned between H_2O and EtOAc, and then between H_2O and *n*-BuOH, to afford EtOAc (34.0 g) and n-BuOH (23.0 g) phases. The BuOH phase, selected on the basis of bioactivity, was chromatographed on Sephadex LH-20 column, eluted with MeOH to afford 70 fractions of 20 mL each. Fractions 33, 49-66, 67-68, and 69-70, shown to be the most active in preliminary biological assays (data not shown), were further purified by HPLC on a Supelco Ascentis C18, column. Fraction 33 was separated by semipreparative HPLC (CH_3OH/H_2O, 3:2, flow rate 2.5 mL/min) to afford cissoic acid (**2**, 7.3 mg, Rt 11 min) and two subfractions, whose further purification by analytical RP-HPLC (MeOH/H_2O 3:7, flow rate 0.8 mL/min) yielded *Z*-4-coumaric acid *β-D*-glucopyranoside (**6**, 4.5 mg, Rt 8.8 min) and 1-*O*-*p*-coumaroyl-*β-D*-glucopyranose (**7**, 77.6 mg, Rt 10.6 min). Fraction 49-66 was separated by HPLC (CH_3OH/H_2O, 55:45, flow rate 2.5 mL/min) to afford pure compound **4** (111.4 mg, Rt 8.1 min). Fraction 67-68 was separated by HPLC using CH_3OH/H_2O (50:50, flow rate 2.5 mL/min) to yield compound **3** (93.9 mg, Rt 8.5 min) and isovitexin-2`-O-*β*-D-glucopyranoside (**5**, 39.5 mg, Rt 11.3 min). Fractions 69-70 was separated by HPLC (CH_3OH/H_2O, 50:50, flow rate 2.0 mL/min) to afford pure cissuxinoside (**1**, 5.4 mg, Rt 8.9 min).

*Cissuxinoside (**1**):* yellow amorphous solid, $[\alpha]_D$ -10.8 (c 0.14, CH_3OH); ^1H NMR (CD_3OD, 400 MHz): Table 3.1; ^{13}C NMR (CD_3OD, 125 MHz): Table 3.1; ESIMS *m/z* 633 $[M - H]^-$; HR-ESIMS *m/z* found 633.5873 (calcd for $C_{30}H_{33}O_{15}$ 633.5870).

*Cissoic acid (**2**)*: yellowish amorphous solid, $[\alpha]_D$ -4.6 (c 0.14, CH_3OH); ^1H NMR (CD_3OD, 700 MHz) and ^{13}C NMR (CD_3OD, 175 MHz), see Table 3.2; ESIMS *m/z* 429 [M - H]-; HR-ESIMS *m/z* found 429.4502 ($C_{20}H_{29}O_{10}$ requires 429.4500).

*Vitexin-2"-O-β-D-arabinofuranoside (**3**):* yellow amorphous solid, $[\alpha]_D$ -58.7 (c 0.15, CH_3OH); ^1H NMR (CD_3OD, 500 MHz) δ_H 8.01 (1H, d, *J* = 8.2, H-2', H-6'), 6.94 (1H, d, *J* = 8.2, H-3', H-5'), 6.60 (1H, s, H-3), 6.25 (1H, s, H-6), 5.08 (1H, s, H-1'"), 5.02 (1H, d, *J* = 10.0, H-1"), 4.28 (1H, *dd*, *J* = 9.8, 8.0, H-2"), 3.99 (1H, *dd*, *J* = 12.5, 2.0, H-6"a), 3.88 (1H, overlapped, H-6"b), 3.86 (1H, overlapped, H-2'"), 3.75 (1H, *dd*, *J* = 6.3, 3.8, H-3'"), 3.71 (1H, *t*, *J* = 9.5, H-4"), 3.71 (1H, *t*, *J* = 9.0, H-4"), 3.69 (1H, *t*, *J* = 9.0, H-3"), 3.46

(1H, *m*, H-5"), 3.28 (1H, *dd*, *J* = 12.0, 3.0, H-5'"a), 3.15 (1H, *dd*, *J* = 12.0, 3.0, H-5'"b), 2.70 (1H, *m*, H-4'"); ^{1}H NMR (DMSO-$_{d6}$, 500 MHz) δ_H 8.04 (2H, *d*, *J* = 8.7, H-2', H-6'), 6.88 (2H, *d*, *J* = 8.7, H-3', H-5'), 6.80 (1H, *s*, H-3), 6.24 (1H, *s*, H-6), 4.90 (1H, *bs*, H-1'"), 4.74 (1H, *d*, *J* = 10.0, H-1"), 4.03 (1H, *t*, *J* = 10.0, H-2"), 3.76 (1H, *d*, *J* = 12.0, H-6"a), 3.56 (1H, overlapped, H-2'"), 3.53 (1H, overlapped, H-3'"), 3.51 (1H, *dd*, *J* = 12.0, 6.3, H-6"b), 3.45 (1H, *t*, *J* = 8.9, H-3″), 3.38 (1H, *t*, *J* = 9.4, H-4"), 3.21 (1H, m, H-5"), 2.99 (1H, *dd*, *J* = 12.0, 1.9, H-5'"a), 2.87 (1H, *dd*, *J* = 12.0, 1.9, H-5'"b), 2.36 (1H, *m*, H-4'"); ^{13}C NMR (DMSO-$_{d6}$, 125 MHz), δ_C 182.5 (C-4), 165.1 (C-7), 164.3 (C-2), 161.6 (C-4'), 160.8 (C-5), 156.4 (C-9), 129.4 (C-2', C-6'), 122.1 (C-1'), 116.2 (C-3', C-5'), 108.1 (C-1'"), 104.6 (C-8), 104.0 (C-10), 102.7 (C-3), 98.4 (C-6), 82.9 (C-2'"), 82.7 (C-4'"), 82.5 (C-5"), 79.6 (C-3"), 75.9 (C-3'"), 75.0 (C-2"), 72.3 (C-1"), 71.1 (C-4"), 61.6 (C-6"), 59.2 (C-5'"); ESIMS *m/z* 563 [M - H]$^-$; HR-ESIMS *m/z* found 563.5868 (calcd for $C_{26}H_{27}O_{14}$ 563.5870).

*Orientin-2"-O-β-D-arabinofuranoside (**4**):* yellow amorphous solid, $[\alpha]_D$ -38.9 (c 0.18, CH_3OH); ^{1}H NMR (CD_3OD, 700 MHz) δ_H 7.61 (1H, *d*, *J* = 2.0, H-2'), 7.56 (1H, *dd*, *J* = 8.3, 2.0, H-6'), 6.94 (1H, *d*, *J* = 8.3, H-5′), 6.57 (1H, *s*, H-3), 6.26 (1H, *s*, H-6), 5.08 (1H, *s*, H-1'"), 5.02 (1H, *d*, *J* = 10.0, H-1"), 4.28 (1H, *dd*, *J* = 9.8, 8.0, H-2"), 3.99 (1H, *dd*, *J* = 12.5, 2.0, H-6"a), 3.88 (1H, overlapped, H-6"b), 3.86 (1H, overlapped, H-2'"), 3.75 (1H, *dd*, *J* = 6.3, 3.8, H-3'"), 3.71 (1H, *t*, *J* = 9.5, H-4"), 3.71 (1H, *t*, *J* = 9.0, H-4"), 3.69 (1H, *t*, *J* = 9.0, H-3"), 3.46 (1H, *m*, H-5"), 3.28 (1H, *dd*, *J* = 12.0, 3.0, H-5'"a), 3.15 (1H, *dd*, *J* = 12.0, 3.0, H-5'"b), 2.70 (1H, *m*, H-4'"); ^{13}C NMR (CD_3OD, 175 MHz), δ_C 182.7 (C-4), 165.1 (C-2), 163.1 (C-7), 161.2 (C-5), 157.0 (C-9), 149.3 (C-4'), 145.8 (C-3'), C123.1 (C-1'), 120.7 (C-6'), 116.4 (C-5′), 115.6 (C-3), 114.8 (C-2'), 109.9 (C-1'"), 104.0 (C-8, C-10), 99.2 (C-6), 84.6 (C-4'"), 83.0 (C-2'"), 82.7 (C-5"), 80.6 (C-3"), 77.3 (C-2"), 77.2 (C-3'"), 73.6 (C-1"), 71.8 (C-4"), 62.9 (C-6"), 60.8 (C-5'"); ESIMS *m/z* 579 [M - H]$^-$; HRESIMS *m/z* found 579.5778 (calcd for $C_{26}H_{27}O_{15}$ 579.5770).

3.5.3 ECD calculation

DFT calculations were performed using the Gaussian09 package (Multiprocessor). A systematic conformational search for cissoic acid (**2**) around the C-10/C-11 and C-8/C-9

bonds was carried out at the mpw1pw91 level using the 6-31G(d) basis set. All the conformers obtained were subsequently optimized at the mpw1pw91 level using the 6-31G(d,p) basis set. TDDFT calculations were run using the functional B3LYP and the basis set 6-31G(d,p) including at least 30 excited states in all cases and using IEF-PCM solvation method to mimic MeOH.

3.5.4. 2-NBDG glucose uptake assay

HuH7, human hepatoma cells 7 clone 5 (passage 49), (Ceinge Biotecnologie Avanzate, Naples, Italy) possess stable hepatic phenotype and respond well to insulin stimulation. Cells were cultured in Dulbecco Modified Eagle Medium (DMEM) (41965-039, GIBCO, Thermo Fisher Scientific, Waltham, MA, USA) supplemented with 10% FBS, penicillin and streptomycin in a cell culture incubator at 37°C and with 5% CO2.

HuH7 cells were plated (5 x 10^3/well) in a black, clear bottom, 96-well microtiter plate (Perkin Elmer, U.S.) in a final volume of 100 µL/well of culture medium. Once cells had reached 80-90% of confluence, culture medium was carefully removed and replaced with 100µL of HBSS containing 100 µM 2-DG, 0.4 g/L BSA, and 1.3 mM $CaCl_2$ (in the absence of any growth factors or FBS). Plates were incubated at 37°C for 1 hour. HBSS was then supplemented with insulin (1 nM, 10 nM or 100 nM), used as control, or with the test compounds (800 µg/mL) or fractions (2.0 mg/mL) dissolved in DMSO. Plates were incubated for an additional period of 30 minutes. At the end of this second incubation, cell medium was replaced with HBSS containing 100 µM 2-DG, 0.4 g/L BSA, and 1.3 mM $CaCl_2$ supplemented with 6µM 2-NBDG. Plates were incubated with the fluorescent probe for 45 min to be then washed twice in PBS. Uptake of 2-NDBG was measured in a Perkin Elmer Envision 2105 Multiplate reader (Perkin Elmer, U.S.), using the inbuilt monochromator and the following parameters: λ excitation 471 nm, λ emission 529 nm, monochromator cut off 360 nm. After the measurement of 2-NDBG, cells were fixed in 3.7 % PFA for 30 minutes to be then permeabilized in 0.1 % Triton X-100 in PBS and stained with of the nuclear dye DAPI (30 µM). This second fluorescence measurement correlates with the total number of cells in each well and was used for normalization. DAPI fluorescence was measured using the following parameters: λ

excitation 351nm, λ emission 450 nm. Data analysis for glucose uptake is reported as the ratio between intracellular 2-NDBG fluorescence and DAPI fluorescence ± s.d.

References

Ahmadu, A.A., Onanuga A, Aquino, R. **(2010)**. Flavonoid glycosides from the leaves of Cissus ibuensis hook (vitaceae). *Afr. J. Trad. Complement. Altern. Med.*, 7(3), 225-230.

Al Dawish, M.A., Robert, A.A., Braham, R., Al Hayek, A.A., Al Saeed, A., Ahmed, R.A., AlSabaan, F.S. ***(*2016).*** Diabetes Mellitus in Saudi Arabia: A Review of the Recent Literature. *Current Diabetes Reviews, 12*, 1-10.

AL-Bukhaiti, W.Q., Noman, A., Mahdi, A.A., Abed, S.M., Ali, A.H., Mohamed, J.K., Wang, H. **(2019)** . Proximate composition, nutritional evaluation and functional properties of a promising food: Arabian wax Cissus (*Cissus rotundifolia* Forssk) leaves. *J.Food. Sci. Technol.*, 56(11), 4844–4854.

Al-Fatimi, M., Wurster, M., Schröder, G., Lindequist, U. **(2007)**. Antioxidant, antimicrobial and cytotoxic activities of selected medicinal plants from Yemen. *J. Ethnopharmacol.* 111(3), 657-666.

Al-Mamary, M.A., **(2002).** Antioxidant activity of commonly consumed vegetables in Yemen. *Malays. J. Nutr.* 8(2), 179-189.

Al-Mehdar, Albattah. **(2016)**. Evaluation of Hypoglycemic Activity of Boswellia carterii and *Cissus rotundifolia* in Streptozotocin/Nicotinamide- Induced Diabetic Rats. *Yemeni J.Med. Sci.*,10, 31–39.

Alshawsh, M.A., Mothana, R.A., Al-shamahy, Hassan, A., Alsllami, S.F., Lindequist, U. **(2009)**. Assessment of antimalarial activity against Plasmodium falciparum and phytochemical screening of some Yemeni medicinal plants. *Evidence-based Complementary and Alternative Medicine*. eCAM., 6(4), 453-456. doi:10.1093/ecam/nem148.

Alzoreky, N.S., Nakahara, K. **(2003)**. Antibacterial activity of extracts from some edible plants commonly consumed in Asia. *Int. J. Food Microbiol*., 80, 223- 230.

Athar, M., Back, J.H., Kopelovich, L., Bickers, D.R., Kim, A.L. **(2009)**. Multiple molecular targets of resveratrol: Anti-carcinogenic mechanisms. *Arch. Biochem. Biophys.*, 486(2), 95-102.

Bandyopadhyay, G., Kanoh, Y., Sajan, M.P., Standaert, M.L., Farese, R.V. **(2000).** Effects of adenoviral gene transfer of wild-type, constitutively active, and kinase-defective protein kinase C lambda on insulinstimulated glucose transport in L6 myotubes. *Endocrinology*,141, 4120–4127.

Bandyopadhyay, G., Standaert, M.L., Galloway, L., Moscat, J., Farese, R.V. **(1997).** Evidence for involvement of protein kinase C (PKC)- zeta and noninvolvement of diacylglycerol-sensitive PKCs in insulin-stimulated glucose transport in L6 myotubes. *Endocrinology*.,138, 4721–31.

Bell, S., Onyechi, U.A., Judd, P.A., Ellis, P.R., Ross-Murphy, S.B. **(1993).** An investigation of the effects of two indigenous African foods, *Detarium microcarpum* and *Cissus rotundifolia*, on rat plasma cholesterol levels. *Proceedings of the Nutrition Society*.:52, 372A.

Beltrame, F.L., Ferrei.ra, A.G., Cortez, D.A. **(2002)**. Coumarin glycoside from *Cissus sicyoides*. *Nat. Prod. Lett.*, 16(4), 213-216.

Bertelli, A.A., Das, D.K. **(2009)**. Grapes, wines, resveratrol, and heart health. *J. Cardiovasc. Pharmacol.*, 54(6), 468-476.

Bifulco, G.; Dambruoso, P.; Gomez-Paloma, L.; Riccio, R. **(2007)**. Determination of relative configuration in organic compounds by NMR spectroscopy and computational methods. *Chem. Rev*., 107, 3744-3779.

Blonde, L., Aschner, P., Bailey, C., Ji, L., Leiter, L. A., Matthaei, S., & Global Partnership for Effective Diabetes Management **(2017)**. Gaps and barriers in the control of blood glucose in people with type 2 diabetes. *Diabetes & vascular disease research*, 14(3), 172–183. https://doi.org/10.1177/1479164116679775

Cheng, G.; Bai, Y.; Zhao, Y.; Tao, J.; Liu, Y.; Tu, G.; Ma, L.; Liao, N.; Xu, X. (**2000).** Flavonoids from *Ziziphus jujuba Mill* var. Spinosa. *Tetrahedron*, *56*, 8915-920.

Chi, C.Y., Wang, F., Lei, T., Xu, S.Y., Hong, A.H., Cen, Y.Z. **(2011)**. Studies on the chemical constituents from Cissus pteroclada. *Zhong. Yao. Cai.*, 33(10), 1566-1568.

Das, D.K., Mukherjee, S., Ray, D. **(2010)**. Resveratrol and red wine, healthy heart and longevity. *Heart Fail. Rev.*, 15(5), 467-477.

Deokule, S.S., Waghmare, R.K. **(2004)**. Pharmacognostic study of *Cissus quadrangularis* L. - A bone setting drug. *J. Econ. Taxon. Bot.*, 28(4), 823-829.

Deshmukh, A.S. **(2015)**. Insulin-stimulated glucose uptake in healthy and insulin-resistant skeletal muscle. *Horm. Mol. Biol. Clin. Invest*. 1-12.

Fernandes, G., Banu, J. **(2012)**. Medicinal properties of plants from the genus Cissus: A review. *Journal of medicinal plant research*, 6(16), 3080-3086.

Gidekel, M., Weber R. H., Cafferata, E. G., Gutierrez, A., Sunkel, C., Osorio Navarro. **(2014).** Extracts of deschampsia antartica with antineoplastic activity. *J. U.S. Pat. Appl. Publ.*, US 20140287074 A1 20140925.

González, E.L., Johansson, S., Wallander, M.A., Rodríguez, L.A. **(2009)**. Trends in the prevalence and incidence of diabetes in the UK: 1996 – 2005. J. *Epidemiol. Community Health*. 63, 332-336.

Guyton, A.C., Hall, J.E. **(2006)**. Textbook of Medical physiology. 11th Edition. Elsevier Inc, New Delhi.

He, X.; Liu, R. H. *(***2006).** Cranberry phytochemicals: Isolation, structure elucidation, and their antiproliferative and antioxidant activities. *J. Agric. Food Chem., 54*, 7069-7074.

Hixson,J. L.; Hayasaka, Y.; Curtin, C. D.; Sefton, M. A.; Taylor, D. K. *J.* (**2016).** Hydroxycinnamoyl glucose and tartrate esters and their role in the formation of ethylphenols in wine. *Agric. Food Chem., 64*, 9401-9411.

Holt, G. I. **(2004)**. Diagnosis, epidemiology and pathogenesis of diabetes mellitus an update for Psychiatrists. *Br. J. Psychiatry*. 184, s55- s63.

Hu H, Sawhney M, Shi L, et al. **(2015)**. A Systematic Review of the Direct Economic Burden of Type 2 Diabetes in China. *Diabetes. Ther*., 6, 7-16.

International Diabetes Federation, Diabetes Atlas, Ninth edition (**2019)**.

Kaku, K. **(2010)**. Pathophysiology of type 2 diabetes and its treatment policy. *JMAJ*, 53(1), 41-46.

Katulanda, P., Ranasinghe, P., Jayawardena, R. **(2014).** Prevalence of retinopathy among adults with self-reported diabetes mellitus: the Sri Lanka diabetes and Cardiovascular Study. *BMC Ophthalmol.*, 14, 100.

Khan, M.A., Nabi, S.G., Prakash, S., Zaman, A. **(1986)**. Pallidol, a Resveratrol Dimer from *Cissus-Pallida*. *Phytochemistry*, 25(8),1945-1948.

Lorenzen, K.; Anke, T.; Sterner, O. **(1996)**. 11-Hydroxy-4-methyl-2,4,6-dodecatrienoic acid from fermentations of a Mucor species. *Phytochemistry*, 43, 791-792.

MacMillan, J.; Suter, P. J. **(1967)**. The structure of a C12-acid from the seed of Phaseolus multiflorus. Tetrahedron, 23, 2417-2419.

Martin-Timon I., Sevillano-Collantes, C., Segura-Galindo, A., Del Canizo-Gomez, F.J. **(2014)**. Type 2 diabetes and cardiovascular disease: Have all risk factors the same strength?. *World J. Diabetes*. 5, 444-470.

Matsumori,N., Kaneno, D., Murata, M., Nakamura, H., Tachibana, K. **(1999)**. Stereochemical determination of acyclic structures based on carbon–proton spin-coupling constants. A method of configuration analysis for natural products. *J. Org. Chem*., 64,866–876.

Mehta, M., Kaur, N., Bhutani, K.K. **(2001)**. Determination of marker constituents from *Cissus quadrangularis* Linn. and their quantitation by HPTLC and HPLC. *Phytochem. Anal*., 12(2), 91-95.

Nagani, K.V., Kevalia, J., Chanda, S.V. **(2011)**. Pharmacognostical and phytochemical evaluation of stem of *Cissus quadrangularis* L. *Int. J. Pharm. Sci. Res.*, 2, 2856-2862.

Nathan, D.M., Cleary, P.A., Backlund, J.Y., et al. **(2005)**. Intensive diabetes treatment and cardiovascular disease in patients with type 1 diabetes. *N. Engl. J. Med.*, 353, 2643-53.

Onyechi, U.A., Judd, P.A., Ellis, P.R. **(1998)**. African plant foods rich in nonstarch polysaccharides reduce postprandial blood glucose and insulin concentrations in healthy human subjects. *Br. J. Nutr.*, 80(5), 419- 428.

Osadebe, P., Odoh, U., Uzor, P. **(2014).** Natural Products as Potential Sources of Antidiabetic Drugs. *British Journal of Pharmaceutical Research*, 4. 2075-2095. 10.9734/BJPR/2014/8382.

Otshudi, A.L., Foriers, A., Vercruysse, A., Van Zeebroeck, A., Lauwers, S. **(2000)**. In vitro antimicrobial activity of six medicinal plants traditionally used for the treatment of dysentery and diarrhoea in Democratic Republic of Congo (DRC). *Phytomedicine*, 7(2), 167-172.

Palme E., Bilia A.R., de Feo V., Morelli I. **(1994)**. Flavonoid glycosides from Cotoneaster thymaefolia. *Phytochemistry*.;35:1381–1382. doi: 10.1016/S0031-9422(06)80133-0

Parkes, D., Mace, K.,Trautmann, M. **(2012)**. Discovery and development of exenatide: The first antidiabetic agent to leverage the multiple benefits of the incretin hormone, GLP-1. Expert opinion on drug discovery. 8. 10.1517/17460441.2013.741580.

Said, A. , Aboutabl, E.A. , Melek, F.R. , Abdel Raheem, G., Jaleel, A., Raslan, M. **(2018).** Phytoconstituents profiling of *Cissus rotundifolia* (Forssk.) Vahl. by HPLC-MS/MS, and evaluation of its free radical scavenging activity (DPPH) and cytotoxicity. *Trends. Phytochem. Res.* 2(2), 65-74.

Said, A., Aboutabl, E.A., El Awdan, S., Raslan, M. **(2015a)**. Proximate analysis, phytochemical screening and bioactivities evaluation of *Cissus rotundifolia* (Forssk.) Vahl. (Fam. Vitaceae) and Sansevieria cylindrica Bojer ex Hook. (Fam. Dracaenaceae) growing in Egypt. *Egypt. Pharm. J.* 14(3), 180-186.

Saifah, E., Kelley, C.J., Leary, J.D. **(1983)**. Constituents of the Leaves of *Cissus-Rheifolia*. *J. Nat. Prod.*, 46(3), 353-358.

Shalabi, A., El-Sakhawy, F., Choucry, M., EL Awdan, S., Abdel-Sattar, E. **(2018)**. Assessment of Biological Activities of *Cissus Rotundifolia* (Forssk.) Vahl. Growing In Yemen. *Research Journal of Pharmaceutical, Biological and Chemical Sciences*, 9 (4), 430-440.

Shaw, J.E., Sicree, R.A., Zimmet, P.Z. **(2010)**. Global estimates of the prevalence of diabetes for 2010 and 2030. *Diabetes Res. Clin. Pract*. 87, 4-14.

Singh, G., Rawat, P., Maurya, R. **(2007)**. Constituents of *Cissus quadrangularis*. *Nat. Prod. Res.*, 21(6), 522-528.

Sun, A.Y., Wang, Q., Simonyi, A., Sun, G.Y. **(2010)**. Resveratrol as a therapeutic agent for neurodegenerative diseases. *Mol. Neurobiol.*, 41(2-3), 375-383.

Szkudelski, T., Szkudelska, K. **(2011)**. Anti-diabetic effects of resveratrol. *Ann. N. Y. Acad. Sci.*, 1215: 34-39.

Taniguchi, C.M., Emanuelli, B., Kahn, C.R. **(2006)**. Critical nodes in signalling pathways: insights into insulin action. *Nat. Rev. Mol. Cell. Biol*.,7, 85–96.

Vo, V. A.; Lee, J.W.; Kim, J. Y.; Park, J. H.; Lee H. J.; Kim, S. S.; Kwon, Y. S.; Chun, W. **(2014).** Phosphorylation of Akt Mediates Anti-Inflammatory Activity of 1-p-Coumaroyl *β*-D-Glucoside Against Lipopolysaccharide-Induced Inflammation in RAW264.7 Cells. *Korean J. Physiol Pharmacol*, *18*, 79-86.

Wang, N.; Yao, X.; Ishii, R.; Kitanaka, S. **(2003)**. Bioactive sucrose esters from *Bidens parviflora*. *Phytochemistry*, 62, 741-746.

Wang, Q., Somwar, R., Bilan, P.J., Liu, Z., Jin, J., Woodgett, J.R., Klip, A. **(1999)**. Protein kinase B/Akt participates in GLUT4 translocation by insulin in L6 myoblasts. *Mol. Cell.Biol*.,19:4008–4018.

Wang, Y.H., Zhang, Z.K., He, H.P., Wang, J.S., Zhou, H., Ding, M., Hao, X.J. **(2007)**. Stilbene C-glucosides from *Cissus repens*. *J. Asian Nat. Prod. Res.*, 9(6-8), 631-636.

White, J.R., **(2014)**. A Brief History of the Development of Diabetes Medications. *Diabetes Spectr*, 27(2), 82-6.

Wu, J.; Zhang, S.; Huang, J.; Xiao, Q.; Li, Q.; Long, L.; Huang, L. *(***2003).** New aliphatic alcohol and (Z)-4-coumaric acid glycosides from *Acanthus ilicifolius*. *Chem. Pharm. Bull.*, *51*, 1201-1203.

Xie, Y.H., Deng, P., Zhang, Y.Q., Yu, W.S. **(2009)**. Studies on the chemical constituents from *Cissus assamica*. *Zhong Yao Cai*, 32(2), 210-213.

Xu, F., Matsuda, H., Hata, H., Sugawara, K., Nakamura, S., Yoshikawa, M. **(2009)**. Structures of new flavonoids and benzofuran-type stilbene and degranulation inhibitors of rat basophilic leukemia cells from the Brazilian herbal medicine *Cissus sicyoides*. *Chem. Pharm. Bull.*, 57(10), 1089-1095.

CHAPTER 4

ISOLATION OF SECONDARY METABOLITES FROM *ANVILLEA GARCINII* AND THEIR ANTIMICROBIAL ACTIVITIES

4.1. *Anvillea garcinii*

The genus *Anvillea* is probably the smallest genus of plants that belongs to the family Asteraceae, since it is composed only by two species (*A. garcinii* and *A. platycarpa*) distributed in the region from North Africa to Iran, including several Middle Eastern countries, such as Egypt, Palestine and Saudi Arabia (Chaudhary, 2000)

Anvillea garcinii subsp. *radiata* (Coss & Durieu) Anderb, commonly known as Arabian oxeye, is a shrub with florescent yellow flowers. Flowering time is usually in spring, but it can flower throughout the year. *A. garcinii* is a medicinal plant traditionally used for the treatment of dysentery, gastrointestinal troubles, hepatitis, lung disease, colds, digestive problems, pulmonary infections and in liver diseases (Ghrabi, 2005).

Figure 4.1: *Anvillea garcinii* plant growing in Saudi Arabia

4.2. Phytochemistry & pharmacology of *A. garcinii*

Review of phytochemical analysis of *A. garcinii* (AG) discloses that the secondary metabolites of AG are dominated by two classes: sesquiterpene lactones and flavanoids along with their glycoside derivatives (Abdel-Sattar *et al.,* 1996; Rustaiyan *et al.,*1986; Ulubelen *et al.,*1980; Perveen *et al.,*2018a; Perveen *et al.,*2018b; Tyson *et al.,*1979; Tyson *et al.,*1981).

When illustrating the biologically promising constituents of AG based on the reported data, sesquiterpene lactones will be clearly the main compounds of interest. Previous investigation of the aerial parts of the plant revealed that sesquiterpene lactones of *Anvillea* are chiefly represented by parthenolide-type germacranolide including: parthenolid-9-one (Abdel-Sattar *et al*., 1996), *cis*-parthenolid-9-one (Essam &Andrew, 2000), 8*α*, 9*α*-epoxyparthenolide (Hassany *et al*., 2004), 9*α*-hydroxyparthenolide (Tyson *et al*., 1981), 9*β*-hydroxyparthenolide, 9*β*-hydroxy-1*β*,10*α*-epoxyparthenolide (Rustaiyan *et al*.,1986), and 9*α*-hydroxy-1*β*,10*α*-epoxyparthenolide. Furthermore, recent work on Saudi AG, revealed presence of more compounds belonging to the same class including: garcinamines A–D, 9*α*-hydroxy-1*β*,10*α*-epoxyparthenolide, 9*α*-hydroxyparthenolide, 9*β*-hydroxyparthenolide (Perveen *et al.,* 2018a), 9*α*-hydroxyparthenolide-9-*O*-*β*-D-glucopyranoside (Perveen *et al.,* 2018b).

Second class of AG secondary metabolites is denoted by the flavonoidal composition which includes: hispidulin, nepetin, jaceosidin, quercetin-3-glucoside, patuletin-3-diglucoside, isorhamnetin-3-diglucoside, quercetin-3-rhamnoglucoside, quercetin-3-diglucoside-7- glucoside (Dendougui *et al*., 2006), isorhamnetin-3-glucoside, isorhamnetin-3-rhamnoglucoside, quercetin-3-rhamnoglucoside 3',4'-dimethyl ether, 6-methoxykaempferol-3-galactoside, 6-methoxykaempferol-3-galactoside 7-methyl ether, 6-methoxykaempferol 3-galactoside-7, 4'-dimetnyl ether, 6-methoxykaempferol-3-rhamnoglucoside, 6-methoxyquercetin-3-rhamnoglucoside-3′-methyl ether, 6-methoxyapigenin and 6-methoxyluteolin (Ulubelen *et al*., 1979), spinacetin- 7-glucoside, patuletin-7-glucoside, rutin (Perveen *et al.,* 2018a), spinacetin-3-*O*-[*α*-L rhamnopyranosyl-(1→6)-*β*-D-glucopyranoside]-7-*O*-[*α*-L-rhamnopyranoside], kaempferol-3-*O*-rutinoside , kaempferol 7-*O*-*β*-D-glucopyranoside and quercetin7-*O*-*β*-D-glucopyranoside (Perveen *et al.,* 2018b), Other compounds such as 3,5-*O*-dicaffeoylquinic acid (Saoud *et al*., 2019) have been also reported.

AG was proven to have significant antidiabetic, antihyperlipidemic, hepatoprotective, anti-ulcer and cytotoxic activities (Kharjul *et al*., 2014, Perveen *et al*., 2018a, Perveen *et al.,* 2018b). The isolated sesquiterpenes from aerial parts of AG were shown to possess strong anti-tumor activities in both in vitro and vivo assays (Essam & Andrew, 2000; Tyson *et al*., 1981; Abdel-Sattar *et al.,* 1996; Perveen *et al*., 2018a), in addition to the

speculated role of sesquiterpenes in the reported hepatoprotective activities of *Anvillea* (Perveen *et al*., 2018a). On the other hand, flavonoidal content of AG was believed to be responsible for the anti-ulcer and antioxidant effects of the plant.

These findings encouraged us to further investigate leaves of AG to enrich the sesquiterpenes lactone and flavonoids library of this species and to conduct further biological studies on the isolated compounds, particularly the antimicrobial activities to rationalize the traditional use of the plant in the treatment of infections (e.g pulmonary infections).

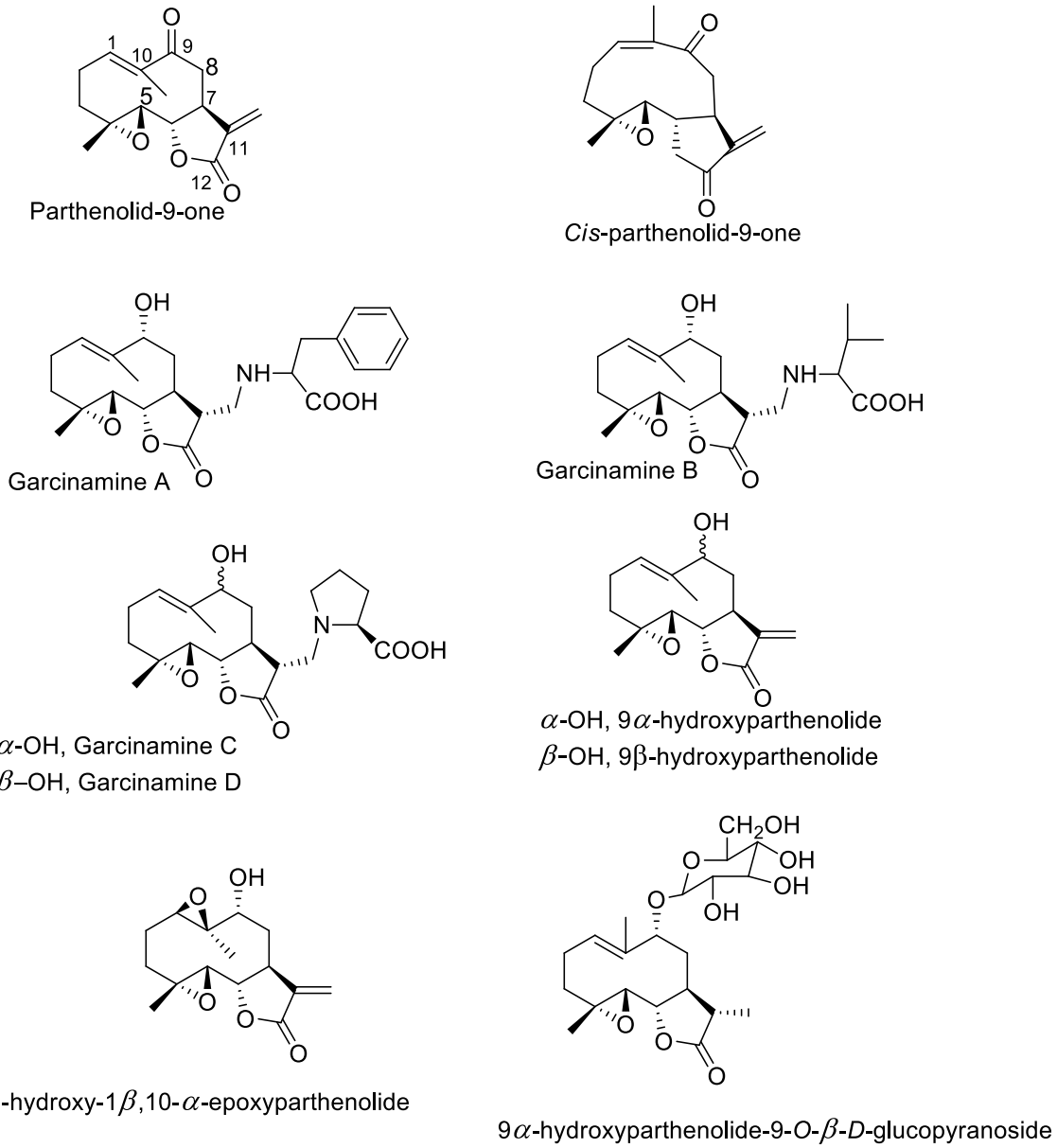

Figure 4.2: Parthenolide-type sesquiterpene lactones isolated from Saudi *A. garcinii*

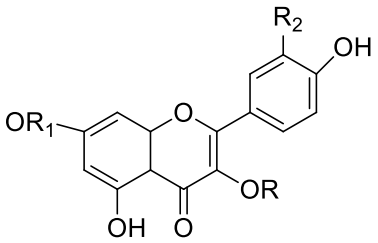

R = 3-*O*-rutinoside, R_1 = H, R_2 = H, Kaempferol 3-*O*-rutinoside
R = H, R_1 = β-*D*-glucoside, R_2 = H, Kaempferol 7-*O*-β-*D*-glucopyranoside
R = H, R_1 = β-*D*-glucoside, R_2 = OH, Quercetin7-*O*-β-*D*-glucopyranoside

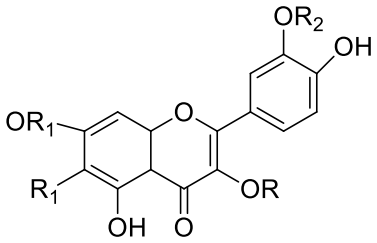

R = H, R_1 = OCH_3, R_2 = β-*D*-glucoside, R_3 = CH_3, Spinacetin-7-glucoside
R = H, R_1 = OCH_3, R_2 = β-*D*-glucoside, R_3 = H, Patuletin-7-glucoside
R = β-*D*-glucose-6-*O*-α -L- rhamnoside, R_1 = H, R_2 = H, R_3 = H, Rutin

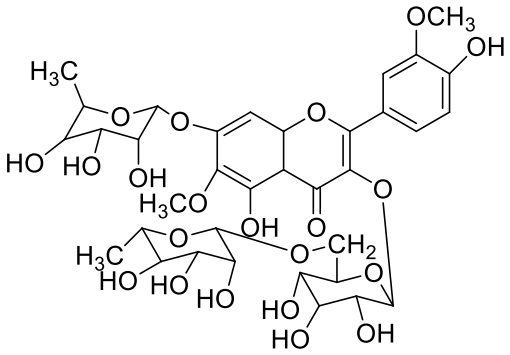

Spinacetin-3-*O*-[α–L- rhamnopyranosyl-(1-6)-β-*D*-glucopyranoside]-7-*O*-[α-L-rhamnopyranoside]

Figure 4.3: Some flavonoids isolated from Saudi *A. garcinii*

4.3. Sesquiterpenes

The interest in the isolation and structure elucidation of sesquiterpene lactones as a group of natural products was increased dramatically during the last decade. This can be attributed to two reasons; first, successful utilization of sesquiterpene lactones as markers in chemotaxonomy (i.e. biochemical systematic) studies, mainly in the Asteraceae.

Second reason is the diverse biological activities range of compounds that belong to this class of natural products, as testified by the considerable attention received by several sesquiterpenes, which resulted in an additional increase in biological activity related publications (Fischer *et al*., 1979).

4.3.1. Sesquiterpenoid biosynthesis

In general, the earlier biosynthetic stages of terpenoid involve reductive processes while the subsequent biomodifications mainly represent oxidative reactions. Hydroperoxides were suggested to be intermediates in the biosynthesis of the various skeletal types of hydroxylated terpenoids which generally involve allylic oxidations as proven by the isolation of sesquiterpene lactone hydroperoxides. Moreover, involvement of sesquiterpene lactone epoxides in major biosynthetic sequences of natural products, particularly in cyclization reactions, is supported by isolation of epoxidated derivatives from plants. It is now generally established that sesquiterpene lactones are derived from farnesyl- or nerolidyl pyrophosphates based on biogenetic assumptions. Sesquiterpene can be classified based on their carbocyclic skeleton in which the suffix "olide" refers to the lactonic function (Fischer *et al*., 1979). The majority of sesquiterpene lactones can be considered biogenetic derivatives of the precursor and largest class, the germacranolides.

4.3.2. Germacranolides biosynthesis

Cyclization of *trans, trans* -farnesyl pyrophosphate (**1**) results in the *trans, trans*-germacradiene intermediate (**2**), that is followed by enzymatic oxidative modifications to finally provide the simplest member of germacranolides, costunolide (**3**) (Scheme 4.1). From the germacradiene the different other skeletal types of sesquiterpene lactones shown in (Scheme 4.2) can be derived.

Two possible biogenetic routes have been suggested for the formation of the lactone ring of these sesquiterpenoids. Possible steps involved in the biogenesis of costunolide (**3**) and inunolide (**10**) are outlined in Scheme 4.2, in which oxidative modifications at C-12 and C-6 or C-8, respectively, takes place as an overall process.

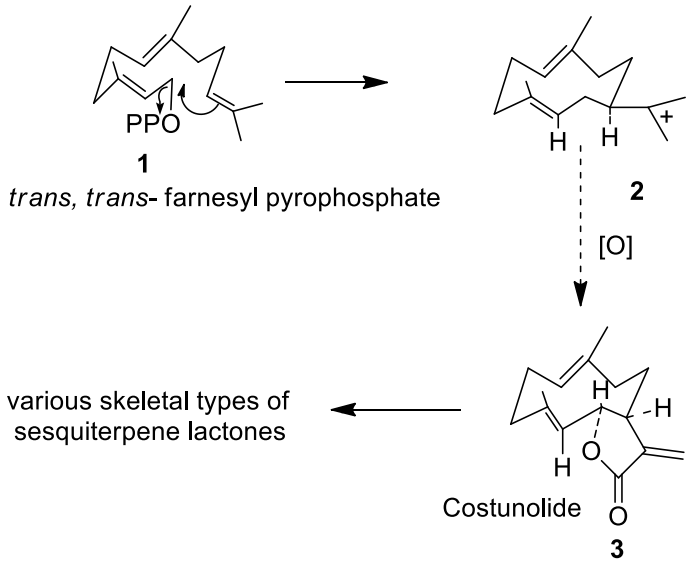

Scheme 4.1: Biogenesis of the germacranolide skeleton

Germacrene A (**4**) is a naturally occurring hydrocarbon in which all non-olefinic carbons are allyllically activated for hydroxylation except C-8. Germacrene A is considered a hypothetical intermediate en route from cation (**2**) to the lactones (**3**) and (**10**). The alcohol derivative (**7**) is formed by introduction of oxygen function at C-12 in germacrene A (**4**) which could proceed either via epoxide intermediate (**5**) or could involve the hydroperoxide (**6**), the latter being formed by an enzymatically-mediated reaction mimicking the reaction of singlet oxygen with olefins. In either case the process involves migration of a double bond from what was originally C-11, C-13 to C-11, C-12. Further oxidative modifications of (**7**) to give aldehyde (**8**), acid (**9**) followed by hydroxylations at C-6 or C-8 would after lactonization give costunolide (**3**) or inunolide (**10**), respectively. The overall steps defined in (Scheme 4.1) appear reasonable, since the oxidation patterns of isopropenyl side chain indicated in (**7**) to (**9**) occasionally accompany the lactonic plant metabolites. Yet, some questions regarding the sequence of oxidations and the detailed mechanism will remain open.

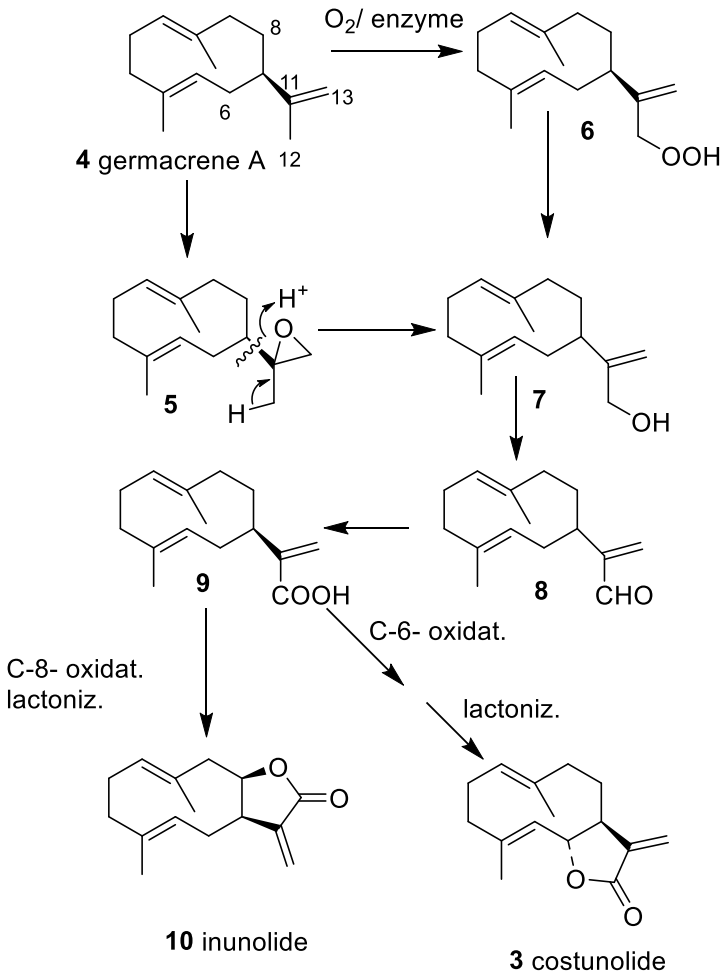

Scheme 4.2: Biogenesis of the lactone ring

One should expect that germacrene B (**11**) is a possible precursor in lactone biosynthesis, since C-8 hydroxylation in a sesquiterpene lactone precursor of type (**11**) would now be favored due to allylic activation of C-8.

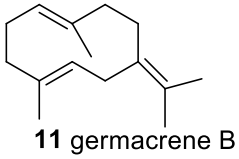

Additionally, in (**11**), among allylic carbons, hydroxylation at C-6 is favored since it represents a doubly allylic carbon center. This can explain predominant formation of C-6-oxygenated sesquiterpenoids. Sesquiterpene lactones of type (**13**) are derived from furanosesquiterpenes (**12**) by autoxidation, and their co-occurrence is common. This

suggests that the lactones are also biogenetically derived from the furan ring as illustrated in (Scheme 4.3):

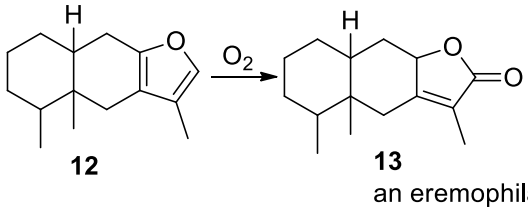

Scheme 4.3: Biogenesis of the lactone ring via furanosesquiterpenes

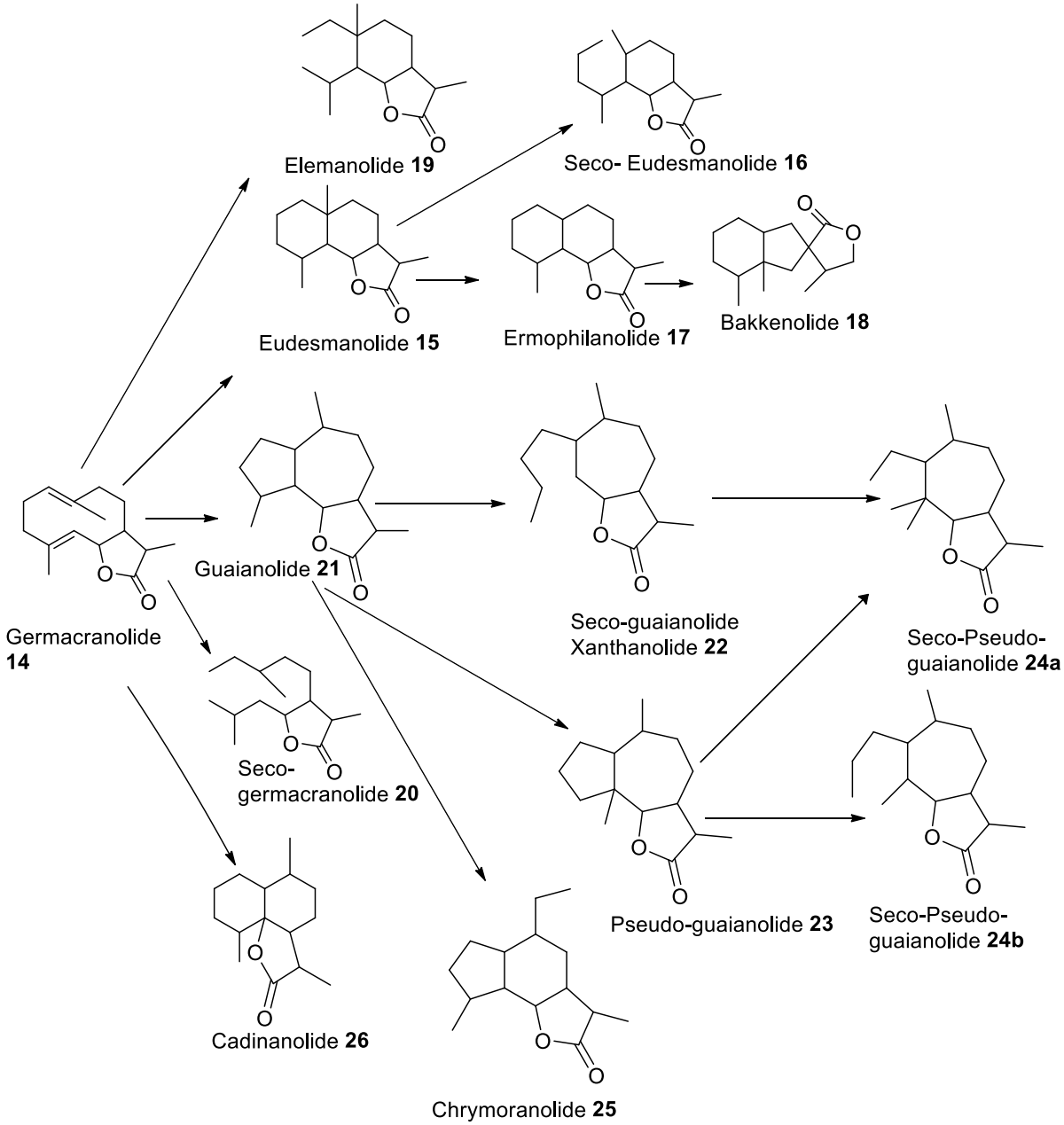

Scheme 4.4: Classes and biogenesis of some known sesquiterpenes

4.3.3. Guaianolide sesquiterpenes

The guaianolide structure consists of a 5,7,5 ring system and the systematic names are seldom used; instead, the compounds are generally mentioned as 6,12-guaianolides (**27**) or 8,12-guaianolides (**28**) (Figure 4.4). If C-7, as displayed, is substituted with hydrogen, then the hydrogen will be *α*-oriented (Figure 4.3). The difference between pseudoguaianolides and guaianolides is in the location of CH_3-15, which in pseudoguaianolides is positioned at C-5 instead of C-4 in guaianolides (Simonsen *et al.*, 2013).

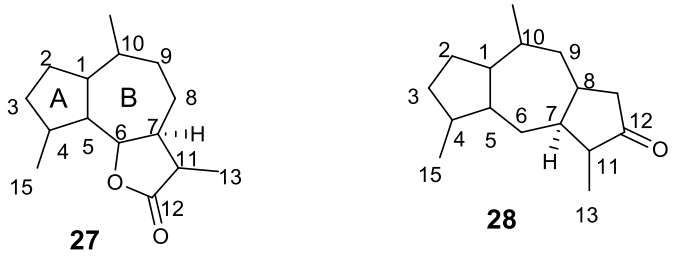

Figure 4.4: The structure of the 6,12-guaianolides **(27)** and 8,12-guaianolides **(28)**

The majority of guaianolides has been isolated from Asteraceae (Composites) followed by Apiaceae (Umbelliferous plants), but in addition, guaianolides have been found in other plants families including: Magnoliaceae, Porellaceae (liverwort), Lamiaceae, and Thymelaeaceae (Simonsen *et al.*, 2013). Furthermore, marine organisms like *Pseudopterogorgia americana* (sea plume) and a Placogorgia species (a gorgonian) have been reported to produce guaianolides.

Several biological activities of guaianolides have been reported, including high antitumor antischistosomal, anthelmintic, antimicrobial and contraceptive properties, etc. (Rodriguez *et al.*, 1976; Drew *et al.*, 2009). This wide spectrum of biological activities attracted an increasing attention toward guaianolides in search for new drug leads, but, due to some toxicity problems, the drug development has been scarce (Yuuya *et al.*,1998; Kupchan *et al.*,1971). However, recent reports for the ability of the thapsigargins (a guaianolide isolated from the genus *Thapsia*, Apiaceae) to inhibit an intracellular calcium pump and subsequently inducing apoptosis has encouraged many researchers to investigate several other guaianolides, with particular regard to *α*-methylene guaianolides and guaianolides containing an *α,β*-unsaturated carbonyl moiety. (Søhoel *et al.*,2006).

4.3.4. Biosynthesis of guaianolides in plants

In all living organisms, farnesyl synthases convert isopentenyl pyrophosphate (IPP) into farnesyl pyrophosphate (FPP) (**1**), the precursor of all sesquiterpene structures. The enzyme generating FPP, FPP synthase, has been extensively studied, and it was shown that the *E,E* conformation of FPP is the predominant product of farnesyl synthases and generally is the substrate for sesquiterpene synthases in eukaryotes (Barton *et al.*,1999). Several possibilities for cyclization reactions of FPP can take place, all of which produce compounds that serve as starting materials for the more than 300 cyclic sesquiterpene skeletons known. These cyclization reactions start with step of isomerization of *trans*-FPP followed by ionization-dependent cyclization and lead to a wide diversity of cyclohexanoid, bicyclohexanoid, cyclodecanoid, or cycloundecanoid ring systems (Scheme 4.5). Internal additions to the remaining double bonds of the initially formed carbocations also occur. Reactions including methyl migrations, Wagner-Meerwein rearrangements, and hydride shifts lead to the generation of the great variety of structures found in nature, among which sesquiterpene lactones, including the guaianolides (Bohlmann *et al.*,1998).

Among the sesquiterpene lactones identified up to now, the one with the better studied biosynthesis is the drug artemisinin (antimalarial drug). A second highly investigated sesquiterpene lactone is the germacranolide costunolide, which exhibits various cytotoxic effects. Both artemisinin and costunolide were isolated from Asteraceae, and although they do not belong to guaianolides, many of the reaction sequences generating these molecules are believed to be similar to those generating guaianolides (Simonsen *et al.*, 2013).

4.3.5. Guaianolide Biosynthesis in Asteraceae

The initial reaction of artemisinin biosynthesis is catalyzed by amorphadiene synthase (ADS) which converts FPP (**1**) to amorpha-4,11-diene (**29**) (Scheme 4.5a). Germacrene A (**12**) was expected as an intermediate, but a single enzyme (ADS) is able to facilitate the complete reaction to **29** (Ro *et al.*, 2006). From **29**, a multifunctional sesquiterpene oxidase, CYP71AV1, catalyzes the production of artemisinic acid (**30**) in yeasts, whereas

the plant pathway goes to artemisinic aldehyde and through dihydroartemisinic acid to artemisin. The last steps in the biosynthesis responsible for converting dihydroartemisinic acid to artemisinin are less clear and are believed to occur spontaneously (Ro *et al.*, 2006; Olofsson *et al.*, 2011). Germacrene A synthases have been isolated from *Artemisia annua* and other asters (Bertea *et al*., 2006).

In a series of studies from 1998 to 2002, Harro Bouwmeester and coworkers isolated several enzymes from chicory that are involved in the biosynthesis of costunolide (**3**). This group also described the formation of **12** from **1** and the subsequent conversion of **12**–**3** in chicory following a similar regime to that of artemisinin. This was further confirmed by Dae-Kyun Ro and coworkers, 2006 with the isolation and characterization of the two enzymes CYP71BL1 and CYP71BL2 that hydroxylate C-8 and C-6, respectively (Scheme 4.5) (de Kraker *et al*., 2002; Ikezawa *et al.*, 2011). In the context of guaianolide biosynthesis, the formation of **3** is remarkable since the lactone ring has been formed before the formation of 5- and 7-membered carbocyclic rings.

From **3**, it is hypothesized that guaianolides are generated via 4,5 epoxidation (Scheme 4.6b) to give parthenolide, which, by an intramolecular attack of the double bond, can undergo opening of the epoxide to afford the three-cyclic skeleton (de Kraker *et al*., 2002; Bouwmeester *et al.,*2002; Dewick, 1995). This reaction mechanism was already proposed in 1995 (Piet *et al.*, 1995). The double bonds are formed due to existence of a hydrogen ion attached to carbon atom neighboring the intermediate C-10 carbocation. This abstraction will ultimately afford different possibilities of $\Delta^{1,10}$, $\Delta^{9,10}$, or $\Delta^{10,14}$ double bonds. Alternatively, the carbocation might be reduced by reaction with a water molecule to give an alcohol at C-10 (Scheme 4.6b).

Biosynthesis of other sesquiterpenes found in Asteraceae and Apiaceae is best hypothesized by considering a 1,10 epoxide as intermediate which undergoes similar intramolecular attack as described above to afford a C-4 carbocation. Double bonds are formed also in a similar manner to afford isomers of $\Delta^{4,5}$, $\Delta^{3,4}$, or $\Delta^{4,15}$ double bonds or the equivalent alcohol at C-4 (Scheme 4.6a). Although enzymes included in the last steps of guaianolide biosynthesis in Asteraceae have not been recognized, studies in *Lactuca floridana* (Asteraceae) support the theory that parthenolide is the intermediate in

guaianolide biosynthesis (Song *et al.*, 1995). This was further supported by the isolation and characterization of the 6-hydroxylase enzyme (CYP71BL2) from *L. floridana*.

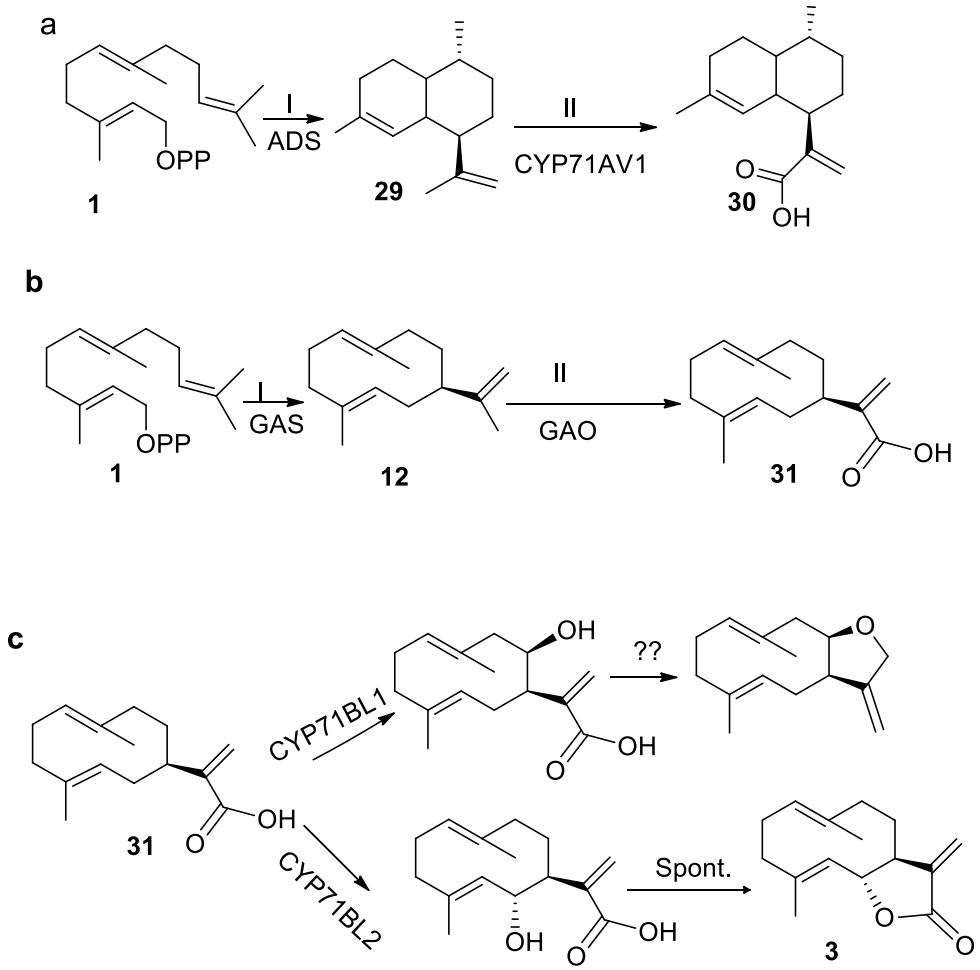

Scheme 4.5: Biosynthesis route to costunolide **3** in Asteraceae compared with artemisinic acid **30** that is spontaneously transformed in artemisinin. (ADS amorphadiene synthase, GAS germacrene A synthase, GAO germacrene A oxidase)

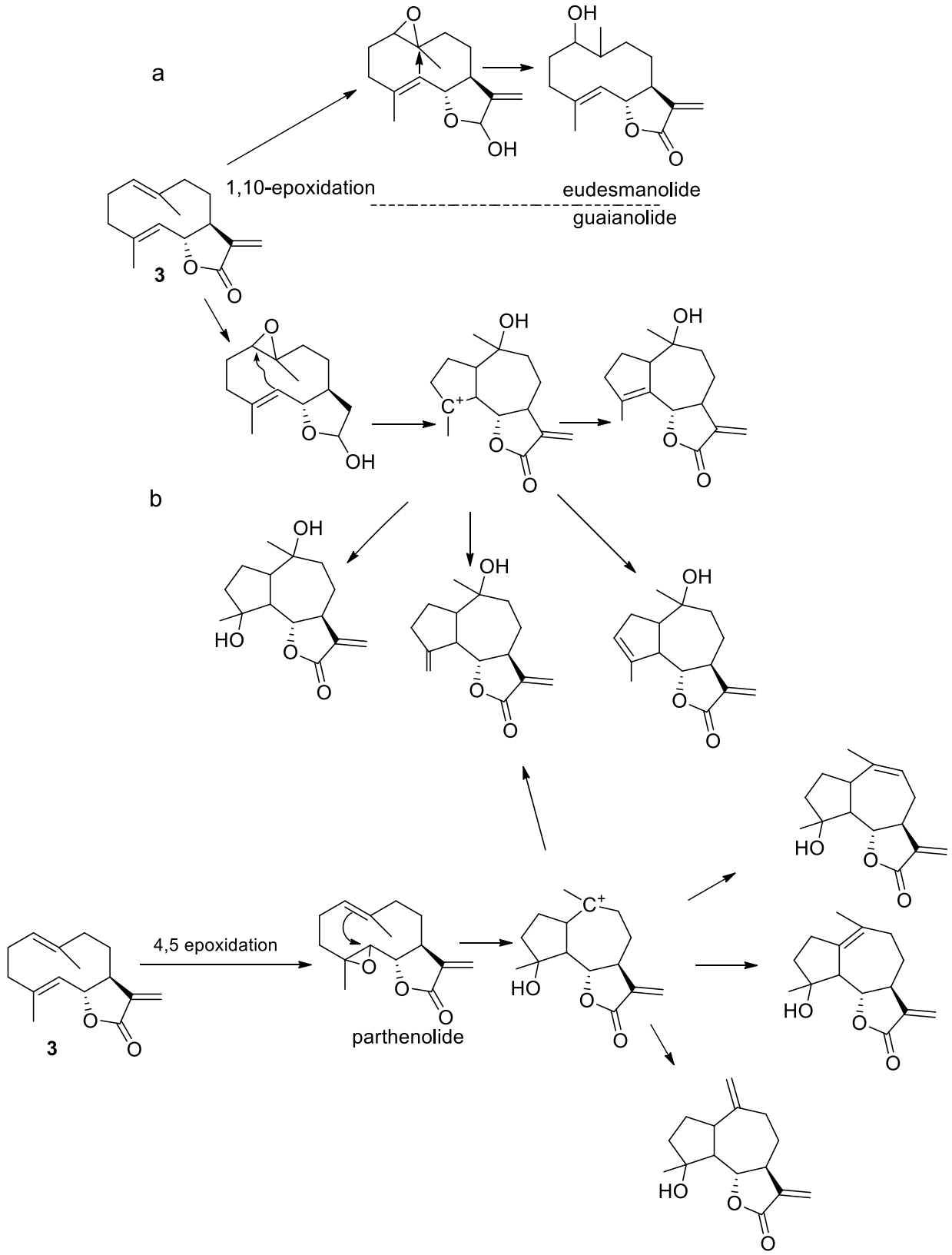

Scheme 4.6: Formation of guaianolides and eudesmanolide in Asteraceae through 1,10 and 4,5 epoxidation of costunolide

4.4. Antimicrobial Resistance

In the late 1940s, antibiotics were firstly introduced to the healthcare for the treatment of bacterial diseases as one of the great inventions of the modern world, which made many to believe that, at last, infectious diseases would disappear once and for ever. Hope was brightly shining that no longer would tuberculosis, dysentery, cholera, pneumonia, enteric diseases can take their heavy toll on humankind and its community systems anymore -- or so it was thought. Indeed, antibiotics deserve much of the credit for saving millions of lives, relieving the suffering of patients and dramatic increase in life expectancy of all ages for more than 60 years (Walsh & Wright, 2005).

Unfortunately, over time, bacteria have developed resistance to antibiotics, creating more difficult-to-treat infectious diseases and ringing the bells for urgent need of developing new antimicrobial agents. Definitely, the use of antibiotics as prophylaxis in human and animal medicine has produced a negative impact on antibiotic therapy overall which eventually led to the increasing number of treatment failures in hospitals and the community providing abundant evidence of this (Hofmann & Meunchen, 2012). In the early days of antibiotic usage, it was difficult to anticipate the extent of the problem regarding antibiotic resistance as it exists today.

Antibiotic resistance was reported to occur when a drug loses its ability to inhibit bacterial growth effectively. Bacteria become ‘resistant’ and continue to multiply in the presence of therapeutic levels of the antibiotics (Zaman *et al*., 2017). Bacterias, when replicates even in the presence of the antibiotics, are called resistant bacterias. Inappropriate use of antibiotic is the main responsible for emerging of resistant strains of microbes.

In 1937, sulfonamides were introduced but shortly after their introduction, sulfonamide resistance was reported, which reveals the same mechanism of resistance that still operates even now, more than 80 years later. Similarly, aminoglycoside-resistant strains of *Staphylococcus aureus* were developed within six years of their production (Gootz, 1990). Methicillin was the first semisynthetic penicillinase-resistant penicillin used in 1961, to target strains of penicillinase-producing *S. aureus*. However, and once again, resistance to methicillin was reported soon after its initiation (Jevons, 1961). In the 1980s, fluoroquinolones were introduced for the treatment of Gram-negative bacterial

infections, yet they were prescribed inappropriately to treat Gram-positive infections which eventually led to the development of fluoroquinolones resistance later (Lowy, 2003). Quinolone resistance emerged as a stepwise attainment of chromosomal mutations, particularly among the methicillin-resistant strains (Zaman *et al.*, 2017). Most recently, vancomycin resistant strains of *S. aureus* (VRSA) were clinically isolated in 2002, after 44 years of vancomycin introduction to the market (Appelbaum, 2006).

Drug-resistant, disease-causing bacteria have multiplied and spread at alarming rates in recent decades as proved by national surveillance data and independent studies. Several reports from the Institute of Medicine (IOM), Centers for Disease Control and Prevention (CDC), National Institutes of Health (NIH) and Food and Drug Administration (FDA) were warning that drug-resistant bacteria are serious public health threat, taking in account that only few novel drugs are produced in a rate that cannot compensate the rapid failure of the antibiotics which can occur in no time. Infections that were once easily curable with antibiotics are becoming difficult, even impossible, to treat, and an increasing number of people are suffering severe illness—or dying—as a result. This would force the healthcare providers to use new, investigational compounds or older, possibly more toxic alternatives, while for some of patients; there simply are no drugs that work.

The recommendations without doubt include researching and developing new antibiotics with novel mechanism of actions to overcome the persistent bacterial resistance. As resistant bacteria proliferate, they will add more financial burdens on our healthcare system with escalating incalculable human cost in terms of pain, grief, and suffering.

4.4.1. Mechanisms of bacterial resistance

Bacterial resistance limited the options of treatment for various infections. However, Gram-negative bacteria that carry carbapenemases, such as New Delhi metallo-beta-lactamase (NDM-1) and extended-spectrum beta-lactamases (ESBL) (Pitout and Laupland, 2008), are particularly worrying since only very few effective antibiotics remain for treating their resulted infections (Walsh, 2011; Poirel, *et al*. 2007).

Some mutant strains of bacteria develop more than one resistance mechanism which in turn increases the threat of the infection. For example, multiple drug resistant (MDR) strains are characterized by enzymes which destroy antibiotics, porin defects, alteration in

cell wall structure, changes in RNA and efflux pumps (Taubes, 2008). Transfer of resistance between bacteria within a species and even between species can occur. MDR genes are encoded by plasmids which are an important part of this process. Beta-lactamases in the periplasmic space of Gram-negative bacteria, destroy beta-lactams including carbapenems. Additionally, efficacy of beta-lactams including meropenem, aminoglycosides, quinolones and tetracyclines can be reduced by overexpression of transmembrane efflux pumps. Furthermore, some bacterial enzymes act by modifying antibiotic which reduces the activity of aminoglycosides and ciprofloxacin. Resistance to quinolones can be induced by mutations of the DNA gyrase and topoisomerase IV genes (Giamarellou, 2009). Other mechanisms of antibiotic resistance activity include (Livermore, 2009):

- Ribosomal mutation or modification which reduces the effect of tetracyclines and aminoglycosides.
- Mutations in lipopolysaccharide structure which affects the efficacy of polymyxin.
- Loss of porins which reduces the efficacy of carbapenems.
- Bypassing of dihydrofolate reductase leads to resistance to trimethoprim.
- Bypassing dihydropteroate synthase results in sulphonamide resistance.

4.4.2. Towards solving the problem

Gram-positives bacteria including methicillin-resistant *Staphylococci* (MRSA) are still vulnerable to a range of old and new antibiotics (Boucher *et al*., 2009). Unfortunately, this does not apply for multi-resistant Gram-negative bacillary bacteria. Nalidixic acid (the forerunner of the plethora of quinolone antibiotics) was the last novel active antibiotic against Gram-negative bacteria. Since that time, large number of analogues in each class of antibiotics have been developed. For some classes, such as cephalosporins and quinolones, market delivery of their analogues has been more feasible than others, for example, the macrolides. However, development of new analogues has not been able to accommodate with the rapid rise in MDR Gram-negative organisms for the current era. Bacteria are now exhibiting multiple-resistant mechanisms against wide range of

established antibiotic classes including beta-lactams and beta-lactam inhibitors, aminoglycosides, quinolones and tetracyclines (Hofmann & Meunchen, 2012).

Economic cost is an important barrier to the development of new novel antibiotics. Unlike any other classes of medicines, unlimited use of antibiotics would lead to development of resistance to those agents and, therefore, increasing clinical failure which will limit the outcome of developing new antibiotic from economical point of view. Antibiotics with sufficient activities against more resistant bacteria will be preserved only for cases in which causative bacteria have been identified, thus limiting its use very significantly as most antibiotics are prescribed empirically. The majority of available antibiotics are now generic due to the lack of novel new agents, resulting in low prices. Economically, spending budgets for launching a new, expensive antibiotic, including one with high activity versus MDR Gram-negative bacteria, would be not recommended (Hofmann & Meunchen, 2012).

Appropriate and prudent use of antibiotics by prescribing doctors is recommended to optimize patient outcomes and minimize the acquisition and spread of antibiotic resistance (Bax *et al*. 1998). However, failure to give them the guidance according to evidence-based data derived from clinical trials makes this recommendation a non reliable practice. Unfortunately, many calls for appropriate use merely mean a nonspecific reduction in use (Bax *et al.,* 1999).

It is possible that no new, novel, broad-spectrum antibiotics active against a broad range of MDR Gram-negative bacteria will be available in the next 10 years. Even after discovery, it takes 8–10 years before an antibiotic becomes generally available for use.

4.4.3. Plant-secondary metabolites as part of the solution

Recent years have witnessed the role of plant-secondary metabolites (PSMs) as the inhibitors of ABC transporter system and hence play a role in reversing antimicrobial resistance. Secondary metabolites, such as terpenoids, function as substrate for ABC transporter systems such as AtrB (in fungi) and NorA efflux pump (in *Staphylococcus aureus*) and thus serve as inhibitors of ABC transporters (Andrade *et al*., 2000; Smith *et al*., 2007). The potential role of PSMs in reversing antimicrobial resistance in some of the medically important microorganisms such as *S. aureus* (including MRSA),

Mycobacterium tuberculosis (including MDR strains) and other medically important microorganisms was studied thoroughly.

For example, compounds like calodenin B, dihydrocalodenin B and other dimeric proanthocyanidins which were isolated from *Ochna macrocalyx* were able to Inhibit MDR *S. aureus* (Tang *et al*., 2003). Similarly flavonoidal compounds including chrysosplenol-D and chrysosplenetin isolated from *Artemisia annua* L. showed synergistic inhibition of MDR *S* . *aureus* (Stermitz *et al*., 2002 ; Wink *et al*., 2012). A glycosidic flavonoid, tiliroside obtained from *Platanus orientalis* and *Herissantia tiubae* Inhibits NorA efflux protein (Falcao-Silva *et al*. ,2009).

For the treatment of MRSA, emodin (a trihydroxyanthraquinone derivative) isolated from *Rheum palmatum* exhibited a synergistic activity with oxacillin (Lee *et al*., 2010). Alkaloids including indole alkaloids canthin-6-one and 8-hydroxycanthin- 6-one from *Allium neapolitanum* were proven to inhibit MRSA growth (O'Donnell and Gibbons 2007) while a benzophenanthridine alkaloids, chelerythrine, from *Zanthoxylum clava-herculis* exhibits antimicrobial effect against MRSA by reversing their drug resistance (Gibbons *et al*., 2003). Furthermore, 5-Methoxyhydnocarpine and pheophorbide A, isolated from *Hydnocarpus kurzii*, Berberis spp., work as Inhibitors of NorA MDR pump (Stermitz *et al*., 2000; 2001; Wink *et al*., 2012). Similarly, N-*trans*-feruloyl 4'-O-methyldopamine from *Mirabilis jalapa* inhibits over expressing NorA pump in *S. aureus* (Michalet *et al*., 2007).

Secondary metabolites that act against *Mycobacterium tuberculosis* include: aegicerin, an antimycobacterial triterpene obtained from *Clavija procera* through reversal of MDR in resistant *M. tuberculosis* (Rojas *et al*., 2006) and piperine from *Piper nigrum* that inhibits over expression of mycobacterial efflux protein (Rv1258c) (Sharma *et al*., 2010). Moreover, two alkaloids (vasicine acetate and 2-acetyl benzylamine) from *Adhatoda vasica* were proven to inhibit MDR starins of *M. tuberculosis* (Ignacimuthu and Shanmugam, 2010). Ellagic acid, tannic acid from several plant species Inhibit the efflux pump in *Acinetobacter baumannii* (Chusri *et al*., 2009).

A macrocyclic bis(bibenzyl) compound, plagiochin, was isolated from *Marchantia polymorpha* with antifungal activity against *Candida albicans* through reversal of the efflux pump (Guo *et al*., 2008). Jatrophane diterpenes from the Iranian spurge *Euphorbia*

squamosa were discovered as a new class of potent inhibitors of multidrug transporters critical for drug resistance in pathogenic yeasts. These compounds (namely deacetylserrulatin B and euphosquamosin C) acted with strong inhibition of the drug-efflux activity of the primary ABC-transporter CaCdr1p, resulting in increased sensitivity to fluconazole in yeast strain overexpressing this transporter (Rawal *et al*., 2014**)**.

4.5. Results and discussion

Nine sesquiterpene lactones were isolated from the *n*-butanol soluble fraction of the ethanol extract of *A. garcinii* leaves and they were identified as four new guaianolides (**32–35**) and five known sesquiterpenes (**36–41**). The structures of the new sesquiterpenes were elucidated by MS and NMR experiments, while those of the known compounds were assigned by comparison with literature data.

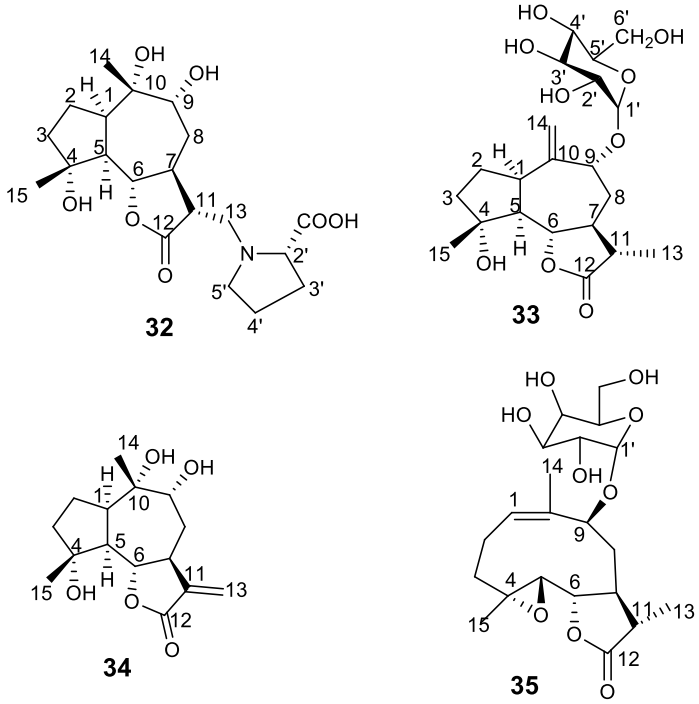

Figure 4.5: Chemical structures of new metabolites isolated from *A. garcinii*

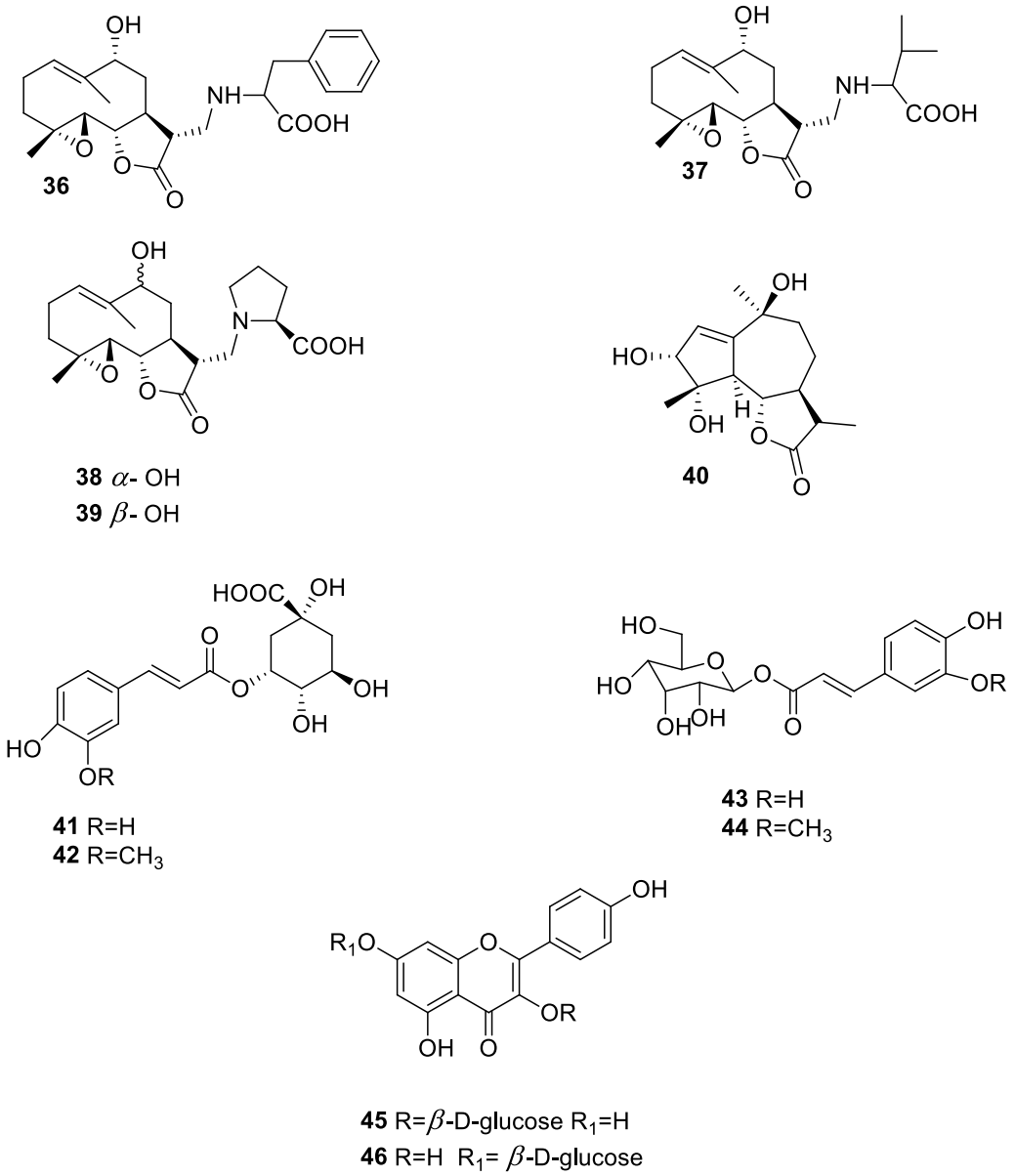

Figure 4.6.: Chemical structures of metabolites isolated from *A. garcinii*

Table 4.1.: ^{1}H (500 MHz) and ^{13}C (125 MHz) NMR data for compounds **32**, **33**, **34** and **35** in CD_3OD

Pos.	Compound **32**		Compound **33**		Compound **34**		Compound **35**	
	δ_H	δ_C	δ_H	δ_C	δ_H	δ_C	δ_H	δ_C
1	3.05 (*m*)	41.0	3.55 (*m*)	35.8	2.80	40.5	5.56 (*dd*, 9.5, 11.5)	129.4
2α	1.88 (*ddd*, *J*= 2.1, 6.3, 12.0 Hz)	24.5	1.66 (*m*)	25.5	1.64 (*dd*, 7.5, 12.5)	24.6	2.61 (*m*)	23.5
2β	1.67 (*ddd*, *J*=5.6, 7.0,12.0 Hz)				1.49 (*dd*, 6.5, 12.5)		2.22 (*m*)	
3a	1.77 (*m*)	40.4	1.77 (*m*)	41.3	1.53 (*m*)	40.4	2.13 (*m*)	35.9
3b							1.22 (*m*)	
4	--	79.6	-	79.7	-	79.6	-	61.8
5	2.26 (*t*, *J*= 12.0 Hz)	54.0	2.12 (*t*, *J*=12.0)	55.2	2.00 (*t*, 11.0)	54.6	2.79 (*d*, 9.0)	65.9
6	4.60 (*dd*, *J*= 9.8, 12.0 Hz)	83.2	3.97(*dd*, *J*=2.0, 12.0)	83.6	4.17 (*dd*, 9.5, 11.0)	82.6	4.04 (*t*, 9.0)	81.4
7	2.49 (*dd*, *J*= 2.1, 12.0 Hz)	40.6	2.20 (*m*)	44.9	2.87 (*br.d*, 9.5)	40.7	2.11 (*br.d*, 9.0)	48.2
8a	2.05 (*dd*, *J*= 2.1, 4.2 Hz)	31.8	2.35 (*m*)	36.8	1.99 (*dd*, 2.5, 6.0)	31.6	2.09 (*dd*, 2.5, 6.0)	35.0
8b	1.83 (*m*)	--	1.37 (*m*)		1.53 (*m*)	-	1.98 (*m*)	-
9	3.77 (*dd*, *J*= 2.1, 4.9 Hz)	76.3	4.43 (*t*, *J*=3.0)	82.1	3.58 (*d*, 2.5)	76.0	4.37 (*t*, 7.5)	83.1
10	--	76.1	-	150.0	-	76.6	-	133.9
11	3.05 (*m*)	41.4	2.20 (*m*)	40.9	-	139.8	2.49	41.7
12		176.8	-	180.0	-	170.8	-	178.7
13a	3.59 (*dd*, *J*= 10.5, 12.6 Hz)	52.8	1.07 (d, *J*= 6.5)	12.0	5.90 (*br.s*)	118.7	1.27 (*d*, 7.0)	12.0
13b	3.45 (*dd*, *J*= 3.5, 12.6 Hz)	--	--		5.36 (*br.s*)	-		
14a	1.20 (*s*)	21.6	5.01(*br.s*)	111.4	0.95 (*s*)	21.8	1.76 (*s*)	10.0
14b	--	--	4.91(*br.s*)					
15	1.34 (*s*)	21.8	1.20 (*s*)	22.7	1.10 (*s*)	22.0	1.36 (s)	16.3
1'		171.8	4.20 (d, *J*= 8.0)	102.1			4.11 (*d*, 7.5)	98.7
2'	4.03 (*dd*, *J*= 4.2, 9.1 Hz)	70.5	3.15 (*m*)	73.7			3.23 (*t*, 7.5)	73.5

3'a	2.44 (*dd, J*= 9.1, 13.3 Hz)	28.6	3.12 (*m*)	76.3			3.17 (*m*)	76.5
3'b	2.26 (*dd, J*= 13.3, 7.7, 4.9 Hz)	--	--	--				
4'a	2.16 (*ddd, J*= 10.5, 7.0, 4.2 Hz)	23.4	3.26 (*m*)	70.0			3.29 (*m*)	70.3
4'b	1.99 (*ddd, J*= 10.5, 6.3, 2.1 Hz)	--	--	--				
5'a	3.84 (*dd, J*= 10.5, 4.9 Hz)	54.1	3.31 (*m*)	76.7			3.31 (*m*)	76.7
5'b	3.25 (*dd, J*= 10.5, 2.8 Hz)		--	--				
6'a	--	--	3.76 (*m*)	61.2			3.67 (*m*)	61.4
6'b	--	--	3.59 (*m*)				3.86 (*m*)	

4.5.1. Structure elucidation of isolated compounds

Compound **32** was obtained as yellow gummy solid. The positive HRESIMS data at *m/z* 398.2233 $[M+H]^+$ suggested the molecular formula $C_{20}H_{32}NO_7$ with six indices of hydrogen deficiency (calcd. for $C_{20}H_{32}NO_7$, 398.2353). The ^{13}C NMR spectrum of **32** showed twenty carbon signals that were attributed to two methyls, seven methylenes (two nitrogen containing methylenes), seven methines (one nitrogen-linked and two oxygenated methines) and four quaternary carbons (two carbonyls and two sp^3 oxygenated carbon) based on the DEPT experiment. Thus, two of the six indices of hydrogen deficiency were accounted for carbonyl carbons, and the remaining four indices were indicative of a four-ring system. Analysis of the 2D HSQC spectrum allowed assignment of two methyl groups attached to carbinol carbons (δ_H 1.20, *s*; δ_C 21.6; δ_H 1.34, *s*; δ_C 21.8), two oxygenated methine groups [δ_H 3.77, *dd*, *J*= 2.1, 4.9 Hz; δ_C 76.3 and δ_H 4.60,*dd*, *J*= 9.8, 12.0 Hz; δ_C 83.2] and one downfield methine [δ_H 2.26 (*t*, *J*=12.0 Hz); δ_C 54.0] (Table 4.1). The ^{13}C NMR spectrum showed characteristic carbon signals for a proline moiety (δ_C 171.8, 70.5, 28.6, 23.4, 54.1), supported by the $^1H-^1H$ COSY spin system from H-2' to H_2–5'. The two COSY spin systems of the sesquiterpenoid core (H-1 to H-3 and H-5 to the H-9, including the H-11/H-13 branching) clearly indicated the nature of 1 as a sesquiterpenoid possessing a proline amino acid substitution (Figure 4.6).

The HMBC spectrum showed $^{3}J_{C\text{-}H}$ correlation of H-9 (δ_H 3.77) with C-14 (δ_C 21.6) and $^{2}J_{C\text{-}H}$ correlation with the oxygenated C-10 (δ_C 76.1), confirmed the presence of the hydroxy group at position 9. In addition, the HMBC spectrum showed ^{3}J correlations from H-6 and H-7 to C-12 and from H_2–13 to C-12 suggesting the presence of a γ-lactone moiety (Figure 4.7). The HMBC ^{3}J correlations from H_3–15 to C-3, C-4 and C-5, and from H_3–14 to C-10, clearly indicated the placement of tertiary alcohol groups at C-4 and C-10, respectively. The coupling of H-11 with a downfield-shifted diastereotopic methylene group at δ_H 3.59 and 3.45, strongly suggested the attachment of the nitrogen atom of L-proline at C-13. The point of attachment of L-proline moiety was further confirmed by the HMBC spectrum, in which H_2–13 showed ^{3}J correlations with C-2′ (δ_C 70.5) and C-5′ (δ_C 54.1). All these observations suggested that compound **32** was a proline containing trioxygenated guaianolide (Zhou *et al.,* 2018; Milutinovic *et al.,* 2018). Clear NOESY correlations were observed between pair H-6/H_3-15, H-6/H_3-14 and H-9/H_3-14, suggesting that 9-OH was in an *α*- configuration (Meng *et al.,* 2001). The network of ROESY correlation of **32** is shown in (Figure 4.7). The structure of **32** was thus determined as 4*α*,9*α*,10*α*-trihydroxy-13*α*-(N-prolyl)-guaia-12,6-*α*-olide and named garcinamine E. In structure **32**, the absolute configuration commonly found for guaianolide and the L configuration of proline have been assumed.

It can be argued that amino acid adducts of sesquiterpenoids are artifact formed during the extraction/purification processes. However, it seems worthy of note mentioning that the postulated sesquiterpene lactone originating **32** (having a $\Delta^{11(13)}$ hexomethylene in place of the proline) is nevertheless new and is an anticipated natural product of this plant.

The molecular formula of compound **33** was established as $C_{21}H_{31}O_9$ for *m/z* 451.2031 $[M+Na]^+$ by positive ESIMS. The proton NMR spectrum of compound **33** showed typical signals for two methyl groups (δ_H 1.07, *d, J*=6.5 Hz; 1.20, *s*) and a pair of sp^2 methylene protons (δ_H 5.01 and 4.91, both *br.s*), two oxymethine protons (δ_H 3.97, *dd, J*= 2.0, 12.0; 4.43, *t, J*= 3.0) and an anomeric proton signal (δ_H 4.20, *d, J*= 8.0) for a glycosyl moiety. Interpretation of ^{13}C and DEPT NMR spectra of 2 indicated the presence of two methyl groups at δ_C 12.0 and 22.7, one sp^2 methylene at δ_C 111.4 and three sp^3 methylenes at δ_C 25.8, 41.3 and 36.8, two hydroxy methine at δ_C 83.6 and 82.1, one carbinol carbon at δ_C

79.7 and two sp^2 unprotonated carbons at δ_C 150.0 and 180.0 (Table 4.1). The ^{13}C NMR spectrum further showed the signal of glucose moiety at δ_C 102.1, 73.7, 76.3, 70.0, 76.7 and 61.2 (Table 4.1). These NMR spectroscopic data suggested that compound 2 was a glycosylated guaianolide sesquiterpene lactone (Wu *et al*., 2018). The ^{1}H and ^{13}C NMR data of **33** were similar to those of **32**, except for the three differences including:

a) appearance of a 3H doublet signal [δ_H 1.07 (*d*, *J*= 6.5); δ_C 12.0] attributable to H_3-13 methyl replacing the *N*-proline amino acid moiety of **32** at C-13

b) the presence of a 10(14) exocyclic methylene group [δ_H 5.01 (*br.s*), 4.91 (*br.s*); δ_C 111.4]

c) and the presence of hexose sugar unit.

Cross-peaks in the HMBC spectrum between H_2-14 and C-1 [δ_C 35.8] and C-9 [δ_C 82.1], confirmed the position of a secondary alcohol group at C-9. The linkage of the sugar unit at this position was further confirmed by the strong HMBC ^3J correlation between H-1′ (δ_H 4.20) and C-9 (δ_H 4.20, δ_C 82.1) (Figure 4.7). The large coupling constant of the anomeric proton (*d*, *J*= 8.0) suggested the *β*-configuration of the hexose sugar in the pyranose form. The remaining proton signals of the sugar portion appeared widely overlapped in the region between δ_H 3.10 and 3.80 ppm, thus preventing an assignment based on the proton-proton coupling constants. However, acid hydrolysis of **33** allowed the isolation of the sugar unit, which was identified as D-glucose through co-TLC and the sign of its optical rotation. The relative configuration of the terpenoid core of **33** was established by analysis of coupling constants and NOESY correlations. The NOESY spectrum of **33** gave the correlations between H-6 and H_3-15 and between H-7 and H_3-13. Assuming the *α*-orientation of H-7 (Milutinovic *et al.*, 2018; Meng *et al*., 2001; Wu *et al*., 2018), H-1 and H-5 must be *α*-configured, while H-6, H-9, and H-11 must have *β*-configurations (Figure 4.7). On the basis of these evidences, the structure of compound **33** was established as 4*α*-(*β*-glucopyranosyl)-oxy-9*α*-hydroxyguaia-10(14)en-12,6*α*-olide.This compound has an evident structural relationship with **32**, differing for dehydration at Δ10(14), glucosylation at *O*-9, and lack of the proline residue.

Compound **34** was isolated as a white powder with molecular formula $C_{15}H_{22}O_5$, determined by HR-ESIMS (*m/z* 281.1400 $[M–H]^–$; calculated for $C_{15}H_{21}O_5$, 281.1394),

indicating five unsaturation degrees. The ^{1}H NMR spectrum of **34** showed the presence of a pair of sp^2 methylene protons at (δ_H 5.90 and 5.36, each *br.s*); two oxygenated methines protons at δ_H 3.58 (1H, *d*, *J* = 2.5 Hz) and 4.17 (1H, *dd*, *J* = 9.5, 11.0 Hz); three relatively deshielded methines at δ_H 2.00 (1H, *br.d*, *J* = 11.0 Hz), 2.87 (overlapped) and 2.84 (overlapped); three methylene protons, and two methyl singlets at δ_H 0.95 and 1.10 (see Table 4.1). The ^{13}C NMR spectral data of **34** were analyzed with the help of the 2D NMR HSQC spectrum and revealed the presence of one ester carbonyl at δ_C 170.8; one sp^2 methylene at δ_C 118.7 and an additional unprotonated sp^2 carbon at δ_C 139.8; two oxymethine carbons at δ_C 82.6 and 76.0 and two unprotonated oxygenated carbons at 79.6 and 76.6. The remaining carbon atoms were assigned as three sp^3 methylenes at δ_C 24.6, 31.6 and 40.3, three sp^3 methines at δ_C 40.5, 40.7 and 54.6, and two methyl carbons at δ_C 21.7 and 22.0.

The guaianolide-type skeleton of compound **34** was assembled basing on the 2D NMR COSY and HMBC spectra. COSY spectrum allowed to disclose the single extended spin system (highlighted in red in Figure 4.8), which was arranged on the bicyclic system on the basis of the HMBC correlations from methyl singlets H_3-14 and H_3-15. HMBC correlations from the methylene H-13 to C-12, C-11 and C-7 and from H-6 to C-12, completed the definition of the planar structure of **34**. NOESY correlations H-6/H_3-15, H-6/H_3-14 and H-9/H_3-14, and the network of ROESY correlation of **34** shown in (Figure 4.8), indicated the relative configuration of compound **34**. Using all above mentioned data, compound **34** was thus elucidated as 4α,9α,10α-trihydroxyguaia-11(13)-en-12,6α-olide.

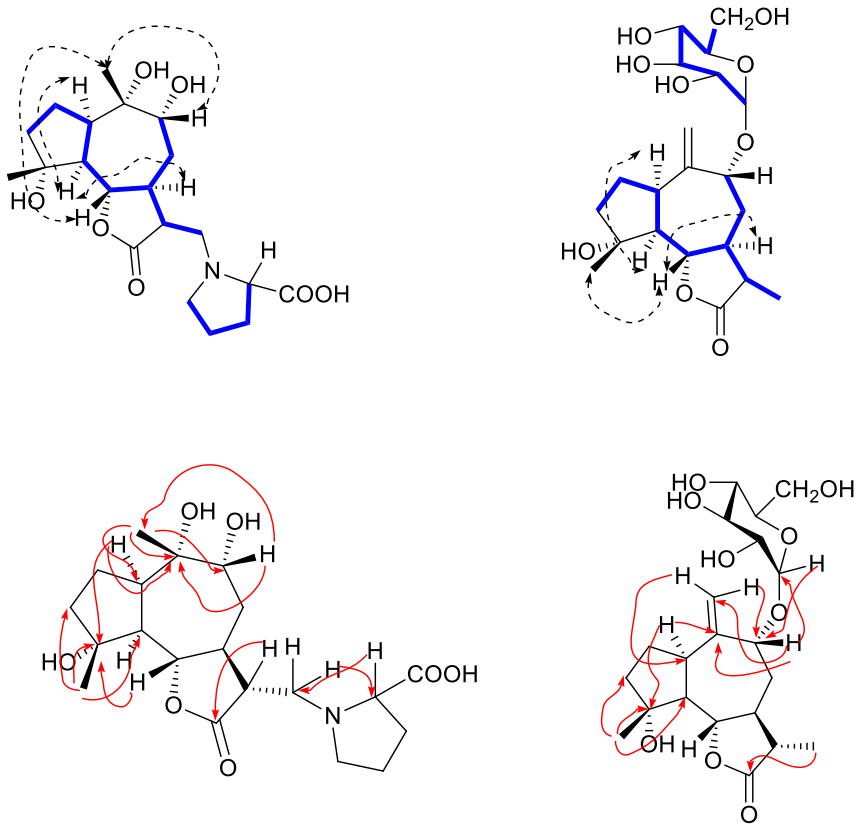

Figure 4.7: Key COSY(▬) , ROESY (⇢), and HMBC (→) correlations of **32** & **33**.

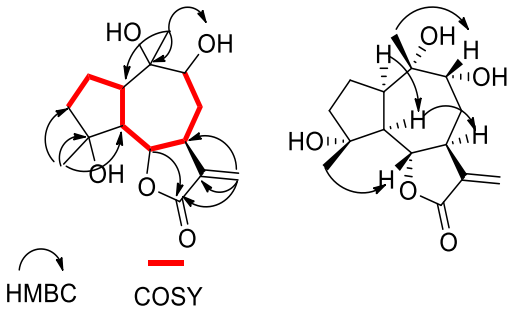

Figure 4.8. Some key 2D NMR correlations of **34** (*left*: COSY and HMBC; *right*: NOESY).

Compound **35** was obtained as an optically active ($[\alpha]^{25}$ D = -55, *c* = 0.10, CH_3OH) yellow gummy solid with molecular formula, $C_{21}H_{32}O_9$, as established by HR-ESIMS. The ^{13}C NMR spectrum, which was interpreted taking into account data from 2D NMR HSQC and HMBC experiments, indicated the presence of one ester carbonyl (δ_C 178.7),

two olefinic carbons (δ_C 129.4 and 133.9); one anomeric carbon (δ_C 98.7), seven additional oxygenated methines (δ_C 83.1, 81.4, 76.7, 76.5, 73.5, 70.3 and 65.9); one oxygenated unprotonated carbon (δ_C 61.8); one oxygenated methylene (δ_C 61.4) and eight additional sp^3 carbons, including two methines, three methylenes and three methyls (Table 4.1). Accordingly, the ^{1}H NMR spectrum of **35** (Table 4.1) showed a sp^2 methine signal at δ_H 5.56, a series of oxymethine/oxymethylene protons between δ_H 4.37 and 3.17, three methyl signals, namely a deshielded singlet at δ_H 1.76, a singlet at δ_H 1.36 and a doublet at δ_H 1.27. These data were indicative of a sesquiterpene lactone glycoside nature for compound **35**, whose structure was assigned on the basis of 2D NMR correlations and comparison with data for 9*α*-hydroxyparthenolide-9-*O*-*β*-D-glucopyranoside, reported earlier from the same plant (Perveen *et al*., 2018b). Also, in the case of **35** the sugar unit was assigned as a *β*-D-glucopyranoside on the basis of the coupling constant H-1′/H-2′ (J = 7.5 Hz) and acid hydrolysis of **35** affording the free sugar unit identified as D-glucose through co-TLC and optical rotation sign. Inspection of COSY and HMBC correlations supported the 9-hydroxyparthenolide aglycone skeleton for **35** and linkage of the D-glucose moiety was further confirmed by HMBC experiment in which H-1′ (δ_H 4.10) showed ^3J correlation with C-9 (δ_C 83.1). Therefore, we supposed that compound **35** should be epimeric to the known 9*α*-hydroxyparthenolide-9-*O*-*β*-D-glucopyranoside. According to the literature, if the 9-hydroxy group has *α*-orientation, then the C-9 carbon shows the signal at δ_C 70-72 ppm, while in the case of the *β*-oriented 9-hydroxy group, the C-9 carbon signal resonated at lower fields in the ^{13}CNMR spectrum. The downfield carbon signal of C-9 (δ_C 83.1) of compound **35** confirmed the *β*-orientation of the hydroxy group (Hassany *et al*, 2004). Further support to this assignment came from: a) the methyl group at C-10 carbon atom was shifted from δ_C 16.4 to δ_C 10.0; b) the NOESY cross-peak of H-7 with H-9 pointed to the *α*-orientation of both protons. Thus, compound **35** was identified as the new 9*β*-hydroxyparthenolide-9-*O*-*β*-D-glucopyranoside.

The known compounds isolated from the chloroform and *n*-butanol fractions were identified by comparison of their spectroscopic data with those reported in the literature. Selected spectra of these compounds are reported as Supplementary Materials. These compounds include: Garcinamine A **36**, Garcinamine B **37**, Garcinamine C **38**,

Garcinamine D **39** (Perveen *et al*.,, 2018a) , 3*α*,4*α*,10*β*-trihydroxy-11*β*-guai-1-en-12,6*α*-olide **40** (Tan *et al*., 1998), chlorogenic acid **41** (Tosovic & Markovic, 2016), 3-*O*-feruloylquinic acid **42** (Erel *et al*, 2011), 1-*O*-caffeoyl-*β*-*D*-glucopyranose **43** (Azam *et al*.,2019), 1-*O*-feruloyl-*β*-*D*-glucopyranose **44** (Delazar *et al*., 2017), kaempferol-3-*O*-glucopyranoside **45** (Aisah *et al*., 2017), and kaempferol-7-*O*-glucopyranoside **46** (Lee *et al*., 2018). Phenolic derivatives [**41-46**] are reported from *A. garcinii* for the first time.

4.5.2. Biological activities

The isolated compounds (**32–46**) were tested for their antimicrobial activity against pathogenic fungi and bacteria (Table 4.2 &Table 4.3). The results showed that the new guaiane sesquiterpenes **32** and **33** displayed low to moderate antifungal effect against *C. albicans* and *C. parapsilosis* and potent antibacterial activities against *S. aureus* and against *E. fergusonii* with minimum inhibitory concentration (MIC) values of 0.32 and 1.4 μgmL−1, and 1.7 and 3.5 μgmL^{-1}, respectively. The other two new guaianolides **34** and **35** also showed strong antifungal activities against tested human pathogenic fungi, with a growth inhibitory activity around 80% at 50 μg mL^{-1} against *C. albicans* and *C. parapsilosis*. In addition, **34** and **35** possess activity against *S. aureus, B. licheniformis*, and against *E. fergusonii* bacteria with MIC ranging from 2.3 to 6.3 μg mL^{-1}. The rest of sesquiterpenes (**36–40**) showed obvious antifungal activities against both *C. albicans* and *C. parapsilosis* as well. These compounds showed marked inhibition of growth of the tested Gram-positive bacterial pathogens, *S. aureus* and *B. licheniformis.* In terms of gram-negative bacterial pathogens, the only active sesquiterpene was compound **40** which showed strong activity with MIC of 3.9 μg mL^{-1}. Among the non-sesquiterpenoids isolated compounds chlorogenic acid **41** showed a significant inhibition against pathogenic fungi (Table 4.2) and strong antibacterial activity against the Gram-negative bacteria *E. xiangfangensis* and *E. fergusonii*. Ester derivatives **43** and **44** showed neither antifungal nor antibacterial activity at 25 μg mL^{-1}.

Table 4.2: *In vitro* antifungal activities of compounds **32–46**.

Compounds	**Growth inhibition (%, mean ± SD)**	
	Candida albicans	*Candida parapsilosis*
32	32.3 ± 2.4	22.3 ± 4.8
33	41.6 ± 4.2	34.9 ± 3.4
34	83.4 ± 3.3	81.3± 2.6
35	79.8 ± 5.3	76.5 ± 4.5
36	67.3 ± 2.1	78.2 ± 1.8
37	56.6 ± 1.2	58.9 ± 3.2
38	63.2 ± 3.1	67.4 ± 4.3
39	65.0 ± 4.9	71.0 ± 2.9
40	85 ± 3.4	80 ± 2.7
41	61.2 ± 3.3	69.5 ± 2.4
42	23.6 ± 5.2	18.9 ± 3.7
43	19.5 ± 2.9	21.7 ± 3.4
44	15.8 ± 3.2	10.9 ± 4.7
45	42.7 ± 4.4	51.8 ± 2.5
46	45.3 ± 3.7	49.9 ± 4.8
Itraconazole	54.7 ± 2.6	51.5 ± 4.1

[a] Results expressed as mean ± standard deviation (SD).

Table 4.3: *In vitro* antimicrobial activities of compounds **32–46**.

Compounds	**MIC (µg mL-1)**				
	Staphilococcus aureus	*Bacillus licheniformis*	*Escherichia xiangfangensis*	*Escherichia fergusonii*	*Pseudomonas aeruginosa*
32	0.32	>25	>25	1.7	>25
33	1.4	>25	>25	3.5	>25
34	2.3	2.3	> 25	5.7	> 25
35	3.4	3.1	> 25	6.3	> 25
36	13.4	10.8	>25	>25	>25
37	4.2	3.5	>25	>25	>25
38	5.1	4.7	>25	>25	>25
39	9.5	12.6	>25	>25	>25
40	5.2	4.4	3.8	> 25	> 25
41	> 25	> 25	5.2	4.6	> 25
42	> 25	> 25	> 25	> 25	> 25
43	> 25	> 25	> 25	> 25	> 25
44	> 25	> 25	> 25	> 25	> 25
45	9.4	> 25	> 25	6.8	> 25
46	> 25	7.5	> 25	8.4	> 25
Amikacin	0.523	0.523	0.523	0.523	0.523

[b] Results expressed as MIC µgmL−1.

4.6. Experimental part

4.6.1. Plant material

The fresh leaves of *A. garcinii* were collected two times: first time in February 2016 and second time in March 2018 from the old industrial area 15 km South West of Al-Kharj city, Saudi Arabia, and identified by Dr. M. Atiqur Rahman, College of Pharmacy, Medicinal, Aromatic and Poisonous Plants Research Center, King Saud University, Saudi

Arabia. A voucher specimen (No. PSAU-CPH-6-2014) has been kept in the herbarium of College of Pharmacy, Prince Sattam Bin Abdulaziz University, Saudi Arabia.

Figure 4.9: *Anvillea garcinii* collected from Al-Kharj

4.6.2. Extraction and isolation

The shade dried powdered leaves of *A. garcinii* (2.0 kg) were extracted with 80% ethanol at room temperature (3×15 L). Total ethanol extract was concentrated under reduced pressure using a rotary evaporator (Büchi Rotavapor RII, Flawil, Switzerland). The crude extract (130 g) was suspended in H_2O (1.0 L) and extracted successively with chloroform and *n*-butanol and then the residual water fraction was lyophilized. The *n*-butanol soluble fraction (35 g) was subjected to Sephadex LH-20 column (75 g) and eluted with a gradient of water: methanol (9.0:1.0→7.0:3.0), to afford seven fractions (fractions 1–7) based on their TLC behaviour.

Fraction 2 (1.5 g) was further subjected to C-18 silica gel column chromatography, eluted under medium-pressure with a gradient of water: methanol (8.5:1.5→6.0:4.0), to obtain two sub-fractions (Fr.2.1) and (Fr.2.2). Fr2.2 (800 mg) was loaded on C-18 silica gel column and eluted with a gradient mixture of water: methanol (8.0:2.0→7.0:3.0), which yielded compound **32** (15 mg). Fraction 3 (1.0 g) was applied to C-18 silica gel column using water: methanol (8.0:2.0→1.0:1.0) to yield compounds **36** (12 mg) and **37** (10 mg).

Fraction 5 (1.2 g) was rechromatographed on Sephadex LH-20 column with water: methanol (50:50–100:0) to afford two sub-fractions (Fraction 5.1 and 5.2). Fraction 5.1 (50 mg) was subjected to C-18 silica gel column using water: methanol (50:50–100:0) to yield compounds **38** (3.0 mg) and **39** (5.0 mg).

Fraction 7 (0.5 g) was separated on Sephadex LH-20 column with a gradient mixture of water: methanol (9.0:1.0→7.0:3.0), finally was divided on silica gel column with $CHCl_3$/MeOH (8.5:1.5) to afford compound **33** (9.0 mg).

A second collection of *A. garcinii* leaves (0.5 kg) was extracted with 100% methanol at room temperature (3 × 2.5 L). Total methanol extract was concentrated under reduced pressure using a rotary evaporator (Büchi Rotavapor RII, Flawil, Switzerland). The crude extract (50 g) was suspended in H_2O (0.5 L) and extracted successively with chloroform and *n*-butanol and then the residual water fraction was lyophilized. The *n*-butanol soluble fraction (30 g) was subjected to normal silica gel open column and eluted with a gradient of CH_2Cl_2:CH_3OH (9.5:0.5→1.0:9.0), to afford nine major fractions 1–9 based on their TLC image. Fraction 3 (0.8 g) was further subjected to RP C-18 column chromatography, eluted under medium-pressure with a gradient of water: methanol (4.0:6.0→9.0:1.0), to obtain two sub-fractions which was further loaded on RP C-18 silica gel column and eluted with a gradient mixture of water: methanol (6.0:4.0→1.0:9.0), and yielded compound **34** (10 mg) and **40** (8 mg). Fraction 5 (0.3 g) was applied to RP C-18 column using water: methanol (8.0:2.0→1.0:1.0) to yield compound **35** (15 mg). Fraction 6 (0.6 g) was rechromatographed on Sephadex LH-20 column with water: methanol (1:1–100:0) to afford two compounds **41** (10 mg) and **42** (12 mg). Fraction 7 (0.5 g) was separated on Sephadex LH-20 column with a gradient mixture of water: methanol (9.0:1.0→7.0:3.0), finally was divided on silica gel column with $CHCl_3$/MeOH (8.5:1.5) to afford compound **43** (6.0 mg) and **44** (11 mg). Subfraction 8 (0.2 g) was further purified by HPLC (flow rate 1 ml/min; wavelength 254 nm; CH_3OH–0.01% HCOOH:H_2O, 4:6) to afford **45** (15 mg, Rt 25.5 min). Sub-fraction 9 (0.1 g) was purified by HPLC (flow rate 1.0 ml/min; wavelength 254 nm; CH_3OH–0.01%HCOOH: H_2O, 1:1) to afford compound **46** (12 mg, Rt 27.5 min).

*Acid hydrolysis of **33** and **35***

Compounds **33** (1.2 mg) and **35** (3 mg) were acid-hydolyzed. Each compound was dissolved in 0.6 mL of a solution of 1N HCl–methanol (1:1). The mixture was refluxed at 65 ^{0}C for 60 min. The reaction mixture was concentrated *in vacuo*, water was added and the whole mixture was extracted with ethyl acetate. The aqueous portion was filtered, the filtrate was evaporated, and D-glucose was identified from the sign of its optical rotation ($[\alpha]^{25}_D$ +52.0^0) and co-TLC (*n*-butanol: water: acetic acid, 8:2:10, *Rf* 0.17) with an authentic sample of D-glucose (Merck).

Garcinamine E **(32)**: [4*α*,9*α*,10*α*-trihydroxy-13*α*-(*N*-prolyl)-guaia-12,6*α*-olide] (1). Yellow gummy solid, $[\alpha]_D^{25}$ +72 (c 0.10, MeOH); ^{1}H NMR (700 MHz, in CD_3OD and DMSO) and ^{13}C NMR (175 MHz, in CD_3OD) see Table 4.1; +ESIMS *m/z* 398.2233 [M+H]+ (calc. 398.2353 for $C_{20}H_{32}NO_7$).

4α-(β-glucopyranosyl)-oxy-9α-hydroxyguaia-10(14) en-12,6α-olide **(33)**. Yellow gummy solid, $[\alpha]_D^{25}$ +55 (c 0.10, MeOH); ^{1}H NMR (500 MHz, in CD_3OD) and ^{13}C NMR (125 MHz, in CD_3OD) see Table 4.1; +ESIMS *m/z* 451.1943 $[M+ Na]^+$ (calc. 451.1944 for $C_{21}H_{32}NaO_9$).

4α,9α,10α-trihydroxyguaia-11(13)en-12,6α-olide (**34**). Yellow gummy solid, $[\alpha]_D^{25}$ +72 (c 0.10, MeOH); ^{1}H NMR (500 MHz, in CD_3OD) and ^{13}C NMR (125 MHz, in CD_3OD): see Table 4.1; Negative ions ESIMS: *m/z* 281.1400 $[M–H]^-$; calculated for $C_{15}H_{21}O_5$, 281.1394.

9β-hydroxyparthenolide-9-O-β-D-glucopyranoside (**35**). Yellow gummy solid, $[\alpha]_D^{25}$ +55 (c 0.10, MeOH); ^{1}H NMR (500 MHz, in CD_3OD) and ^{13}C NMR (125 MHz, in CD_3OD): see Table 4.1; Positive ions ESIMS: *m/z* 451.1948 $[M+ Na]^+$, calculated for $C_{21}H_{32}NaO_9$, 451.1944.

4.6.3. Antibacterial assay

To detect the antibacterial activity of the isolated compounds, the previously reported method (Ebrahim *et al.*, 2016) was used. The pathogenic Gram-negative bacteria, *Pseudomonas aeruginosa* (NR-117678.1), *Escherichia fergusonii* (CU928158.2) and *Enterobacter xiangfangensis* (CP017183.1) and the Gram-positive, *Bacillus licheniformis* (KX785171.1) and *Staphylococcus aureus* (CP011526.1) were suspended for 24 h in a

nutrient broth. After spreading the sample on Muller Hinton agar plate, the wells were filled with 10 µL of the sample using amikacin as positive control. The diameters of the inhibition zone were calculated by measuring the clear area with no microbial growth. The experiment was repeated three times and the mean was calculated. Minimal inhibitory concentration (MIC, µg mL−1) which represented the lowest concentration that inhibits the bacterial growth was detected as well (Berghe & Vlietinck, 1991)

4.5.4. Antifungal assay

Well diffusion and broth microdilution techniques were used in this study in order to test the antifungal effect of isolated compounds according to Gong and Guo protocol (Gong &Guo, 2009). In SDA plate the sample solutions (100 µL), approximately 3×106 colony-forming units (CFU) mL−1 of *Candida albicans* and *Candida parapsilosis* were smeared. 10 µg of the isolated compounds were loaded in wells of the SDA plates and incubated at 37 °C for 1 day. The antifungal itraconazole was used as positive control and the zone of inhibition diameters (in mm) were detected and the rates of growth inhibition were obtained according the following formula taking on consideration±SD as means: %Growth inhibition rate = (dc − ds)/(dc − d0) × 100 Where dc: Diameter of the untreated control fungus, ds: Diameter of the sample-treated fungus and d0: Diameter of the fungus cut.

References

Abdel-Sattar, E., Galal, A. M., Mossa. (**1996)**, Antitumor germacranolides from *Anvillea garcinii. G. S. J. Nat. Prod., 59*, 403-405.

Aisah, L.S., yun, Y.F., Herlina, T., Julaeha, E., Zainuddin, A., Nurfarida, I., Hidayat, A.T., Supratman, U., Shiono, Y. **(2017)** Flavonoid compounds from the leaves of *Kalanchoe prolifera* and their cytotoxic activity against P-388 murine leukemia cells. *Nat. Prod. Sci., 23*, 139–145.

Andrade, A.C., Del Sorbo, G.,Van Nistelrooy, J.G., Waard, M.A. **(2000)**. The ABC transporter AtrB from *Aspergillus nidulans* mediates resistance to all major classes of fungicides and some natural toxic compounds. *Microbiology* 146, 1987–1997.

Appelbaum, P. **(2006)**. The emergence of vancomycin ‐ intermediate and vancomycin ‐ resistant *Staphylococcus aureus*. *Clin Microbiol Infect*., 12, 16–23.

Azam, F., Chaudhry, B.A., Ijaz, H., Qadir, M.I. **(2019).** Caffeoyl-*β-D*-glucopyranoside and 1,3-dihydroxy-2-tetracosanoylamino-4-(E)-nonadecene isolated from *Ranunculus muricatus* exhibit antioxidant activity. *Sci. Rep.*, *9*, 15613.

Barton, S.D., Nakanishi, K., Meth-Cohn, O. **(1999).** Comprehensive natural products chemistry. Elsevier Science, Amsterdam.

Bax, R.P., Anderson, R., Crew, J. *et al* **(1998)**. Antibiotic resistance—What can we do?. *Nat. Med*., 4(5), 545–546.

Bax, R.P., Gabbay, F., Phillips, I. **(1999)**. The Witley Park Study Group. *Clin. Microbiol. Infect.*, 5(12), 774–778.

Berghe, A., Vlietinck. **(1991)**. Screening methods for antibacterial and antiviral agents from higher plants. *Methods Plant Biochem*, 6, 47–68.

Bertea, C.M., Voster, A., Verstappen, F.W.A., Maffei, M., Beekwilder, J., Bouwmeester H.J. **(2006).** Isoprenoid biosynthesis in Artemisia annua: cloning and heterologous expression of a germacrene A synthase from a glandular trichome cDNA library. *Arch. Biochem. Biophys.*, 448 (1–2), 3–12.

Bohlmann, J., Meyer-Gauen, G., Croteau R. **(1998).** Plant terpenoid synthases: molecular biology and phylogenetic analysis. *Proc. Natl. Acad. Sci.*, USA 95(8), 4126–4133.

Boucher, H.W., Talbot, G.H., Bradey, J.S., Edwards, J.E., Gilbert, D., Rise, L.B. et al **(2009)**. Bad bugs, no drugs: no ESKAPE! An update from the Infectious Diseases Society of America. *Clin. Infect. Dis.*, 48, 1–12.

Bouwmeester, H.J., Kodde, J., Verstappen, F.W.A., Altug, I.G., De Kraker, J.W., Wallaart, T.E. **(2002).** Isolation and characterization of two germacrene A synthase cDNA clones from chicory. *Plant Physiol.*, 129(1),134–144.

Chaudhary, SA. **(2000)**. Flora of the Kingdom of Saudi Arabia, Volume II, Ministry of Agri. and Water, Riyadh, Saudi Arabia.

Chusri, S., Villanueva, I., Voravuthikunchai, S. P., Davies, J. **(2009)**. Enhancing antibiotic activity: A strategy to control Acinetobacter infections. *Journal of Antimicrobial Chemotherapy*, 64 (6), 1203–1211.

De Kraker, J.W., Franssen, M.C.R., Joerink, M., de Groot, A., Bouwmeester, H.J. **(2002).** Biosynthesis of costunolide, dihydrocostunolide, and leucodin. Demonstration of cytochrome P450- catalyzed formation of the lactone ring present in sesquiterpene lactones of chicory. *Plant Physiol.*, 129(1), 257–268.

Delazar, A., Nazemiyeh, H., Afshar, F.H., Barghi, N., Esnaashari, S., Asgharian, P. **(2017).** Chemical compositions and biological activities of *Scutellaria pinnatifida* A. Hamilt aerial parts. *Res. Pharm. Sci.*, *12*, 187–195.

Dendougui, H., Jay. M., Benayache, F., Benayache, S. **(2006).** Flavonoids from Anvillea radiata Coss. & Dur. (Asteraceae). *Biochemical Systematics and Ecology*, 34(9), 718-720.

Dewick, P.M. **(1995).** The biosynthesis of C5-C20 terpenoid compounds. *Nat. Prod. Rep.*, 12(5), 507–534.

Drew, D.P., Krichau, N., Reichwald, K., Simonsen, H.T. **(2009)**. Guaianolides in apiaceae: perspectives on pharmacology and biosynthesis. *Phytochem. Rev.*, 8(3), 581–599.

Ebrahim, W., El-Neketi, M., Lewald, L.I., Orfali, R., Lin, W., Rehberg, N., Kalscheuer, R., Daletos, G. & Proksch, P. **(2016).** Metabolites from the fungal Endophyte Aspergillus austroafricanus in axenic culture and in fungal−bacterial mixed cultures. *J. Nat. Prod.*, 79, 914–922.

Erel, S.B., Karaalp, C., Bedir, E., Kaehlig, H., Glasl, S., Khan, S., Krenn, L. **(2011).** Secondary metabolites of *Centaurea calolepis* and evaluation of cnicin for anti-inflammatory, antioxidant, and cytotoxic activities. *Pharm. Biol.*, *49*, 840–849.

Essam, A.S., Andrew, T.M. **(2000)**. *Cis*-Parthenolid-9-one from *Anvillea garcinii*. *J. Nat. Prod. 63*, 1587–1589.

Falcao-Silva, V. S., Silva, D. A., Souza Mde, F., Siqueira-Junior, J. P. **(2009)**. Modulation of drug resistance in *Staphylococcus aureus* by a kaempferol glycoside from *Herissantia tiubae* (Malvaceae). *Phytotherapy Research*, 23 (10), 1367–1370.

Fischer, N.H., Olivier, E.J., Fischer, H.D. **(1979).** The biogenesis and chemistry of sesquiterpene lactones. *Fortschr. Chem. Org. Naturst.*, 38:47–390.

Ghrabi Z. **(2005)**. A guide to medicinal plants in North Africa. Malaga, Spain: IUCN Center for Mediterranean Cooperation, pp. 35.

Giamarellou, H. **(2009)**. Multi-drug resistant Gram-negative infections. *Drugs*, 69(14), 1879–1901.

Gibbons, S., Leimkugel, J., Oluwatuyi, M., Heinrich, M. **(2003)**. Activity of Zanthoxylum clavaherculis extracts against multi-drug resistant methicillin-resistant Staphylococcus aureus (mdr-MRSA). *Phytotherapy Research*, 17 (3), 274–275.

Gong, L., Guo, S. **(2009).** Endophytic fungi from Dracaena cambodiana and Aquilaria sinensis and their antimicrobial activity, *Afr. J. Biotechnol*., 8, 731.

Gootz, T.D. **(1990)**. Discovery and development of new antimicrobial agents. *Clin Microbiol. Rev*., 3, 13–31.

Guo, X. L., Leng, P., Yang, Y., Yu, L. G., Lou, H. X. **(2008)**. Plagiochin E, a botanic-derived phenolic compound, reverses fungal resistance to fluconazole relating to the efflux pump. *Journal of Applied Microbiology*, 104 (3), 831–838.

Hassany, B., Hanbali, F., Akssira, M., Mellouki, F., Haidour, A., Barrero, A.F. **(2004)**. Germacranolides from *Anvillea radiate. Fitoterapia, 75*, 573–576.

Hofmann, F.B., Meunchen. **(2012)**. Handbook of Experimental Pharmacology. Vol. 211. DOI 10.1007/978-3-642-28951-4.

Ignacimuthu, S., & Shanmugam, N. **(2010)**. Antimycobacterial activity of two natural alkaloids, vasicine acetate and 2-acetyl benzylamine, isolated from Indian shrub *Adhatoda vasica* Ness. leaves. *Journal of Biosciences*, 35 (4), 565–570.

Ikezawa, N., G€opfert, J.C., Nguyen, D.T., Kim, S-U., O'Maille, P.E., Spring, O., Ro, D-K. **(2011).** Lettuce Costunolide Synthase (CYP71BL2) and its homolog (CYP71BL1) from sunflower catalyze distinct regio- and stereoselective hydroxylations in sesquiterpene lactone metabolism. *J. Biol. Chem.* 286(24), 21601–21611.

Jevons, M.P. **(1961)** "Celbenin"-resistant staphylococci. *Br. Med. J.*, 1, 124–125.

Kharjul, M., Gali, V., Kharjul, A. **(2014).** Antidiabetic potential of ethanolic extracts of Citrus maxima fruit peel and *Anvillea garcinii*. *Int. J. Pharm. Inno.,* 4, 8–18.

Kupchan, S.M., Eakin, M.A., Thomas, A.M. **(1971)**. Tumor inhibitors. 69. Structure-cytotoxicity relations among the sesquiterpene lactones. *J. Med. Chem.,* 14(12), 1147–1152.

Lee, S.B., Shin, J.S., Han, H.S., Lee, H.H., Park, J.C., Lee, K.T. **(2018).** Kaempferol 7-*O*-*β*-D-glucoside isolated from the leaves of *Cudrania tricuspidata* inhibits LPS-induced expression of pro-inflammatory mediators through inactivation of NF-κB, AP-1, and JAK-STAT in RAW 264.7 macrophages. *Chem. Biol. Interact*., *284,* 101–111.

Lee, Y.S., Kang, O.H., Choi, J.G., Oh, Y.C., Keum, J.H., Kim, S.B., Jeong, G.S., Kim,Y.C., Shin, D.W., Kwon, D.Y**.(2010)**. Synergistic effect of emodinin combination with ampicillin or oxacillin against methicillin-resistant *Staphylococcus aureus*. *Pharm. Biol.* 48, 1285–1290.

Livermore, D.M. **(2009)**. Has the era of unbeatable infections arrived?. *J. Antimicrob. Chemother*., 64. (suppl 1):i29–i36.

Lowy, F.D**. (2003)**. Antimicrobial resistance: the example of *Staphylococcus aureus* . *J. Clin. Invest.*, 111, 1265–1273.

Meng J.C., Huc Y.F., Chen J.H. & Tan R.X. **(2001).** Antifungal highly oxygenated guaianolides and other constituents from Ajania fruticulosa. *Phytochemistry*, 58, 1141–1145.

Michalet, S., Cartier, G., David, B., Mariotte, A. M., Dijoux-franca, M. G., Kaatz, G. W., Stavri, M., & Gibbons, S. **(2007)**. N-caffeoylphenalkylamide derivatives as bacterial efflux pump inhibitors. *Bioorganic & Medicinal Chemistry Letters*, 17 (6), 1755–1758.

Milutinovic, V., Niketic, M., Krunic, A., Nikolic, D., Petkovic, M., Usjak, L., Petrovic S. **(2018).** Sesquiterpene lactones from the methanol extracts of twenty-eight Hieracium species from the Balkan Peninsula and their chemosystematic significance. *Phytochemistry*, 154, 19–30.

O'Donnell, G., Gibbons, S. **(2007)**. Antibacterial activity of two canthin-6-one alkaloids from *Allium neapolitanum*. *Phytotherapy Research*, 21 (7), 653–657.

Olofsson, L., Engstrom, A., Lundgren, A., Brodelius, P. **(2011)**. Relative expression of genes of terpene metabolism in different tissues of Artemisia annua L. *BMC. Plant. Biol.*, 11(1), 45.

Perveen, S., Al-Taweel, A.M., Yusufoglu, H.S., Fawzy, G.A., Foudah, A., Abdel- Kader, M.S. **(2018a).** Hepatoprotective and cytotoxic activities of Anvillea garcinii and isolation of four new secondary metabolites. *J. Nat. Med.*, 72, 106–117.

Perveen, S., Fawzy, G.A., Al-Taweel, A.M., Orfali, R., Yusufoglu, H.S., Abdel- Kader, M.S. **(2018b)**. Antiulcer activity of different extract of *Anvillea garcinii* and isolation of two new secondary metabolites. *Open. Chem*., *16*, 437–445.

Piet, D.P., Schrijvers, R., Franssen, M.C.R., De Groot, A. **(1995)**. Biotransformation of germacrane epoxides by Cichorium intybus. *Tetrahedron*, 51(22), 6303–6314.

Pitout, J.D.D., Laupland, K.B. **(2008)**. Extended B-lactamase producing Enterobacteriaceae: an emerging problem. *Lancet Infect. Dis.* 8, 159–166

Poirel, L., Pitout, J.D., Nordmann, P. **(2007)**. Carbapenemases: molecular diversity and clinical consequences. *Fut. Microbiol*., 2, 501–512.

Rawal, M.K. Shokoohinia, Y., Chianese, G., Zolfaghari, B., Appendino, G., Orazio Taglialatela-Scafati, O., Prasad, R., Di Pietro, A. **(2014)**. Jatrophanes from Euphorbia squamosa as Potent Inhibitors of Candida albicans Multidrug Transporters. *Journal of Natural Products* 77 (12), 2700-2706. DOI: 10.1021/np500756z.

Ro, D.K., Paradise, E.M., Quellet, M., Fisher, K.J., Newman, K.L., Ndungu, J.M., Ho, K.A., Eachus, R.A., Ham, T.S., Kirby, J., Chang, M.C.Y., Withers, S.T., Shiba, Y., Sarpong, R., Keasling, J.D. **(2006).** Production of the antimalarial drug precursor artemisinic acid in engineered yeast. *Nature* 440(7086), 940–943.

Rodriguez, E., Towers, G.H.N., Mitchell, J.C. **(1976)**. Biological activities of sesquiterpene lactones. *Phytochemistry*, 15(11), 1573–1580.

Rojas, R., Caviedes, L., Aponte, J. C., Vaisberg, A. J., Lewis, W. H., Lamas, G., Sarasara, C., Gilman, R. H., Hammond, G. B. **(2006)**. Aegicerin, the first oleanane triterpene with wideranging antimycobacterial activity, isolated from *Clavija procera*. *Journal of Natural Products*, 69 (5), 845–846.

Rustaiyan, A., Dabiri, M., Jakupovic, J. **(1986)**. Germacranolides from *Anvillea garcinii*. *Phytochemistry, 25*, 1229–1230.

Saoud, H., Jelassi A., Hlila M.B, Goudjil M.B., Ladjel S., Jannet H.B **(2019)**. Biological activities of extracts and metabolites isolated from *Anvillea radiata* Coss. & Dur. (Asteraceae), *South African Journal of Botany*, 121, 386-393. ISSN 0254-6299, https://doi.org/10.1016/j.sajb.2018.10.033.

Sharma, S., Kumar, M., Nargotra, A., Koul, S., & Khan, I. A. (2010). Piperine as an inhibitor of Rv1258c, a putative multidrug effl ux pump of *Mycobacterium tuberculosis*. *Journal of Antimicrobial Chemotherapy*, 65 (8), 1694–1701.

Simonsen, H.T., Weitzel, C., Christensen, S.B. **(2013).** Guaianolide Sesquiterpenoids: Pharmacology and Biosynthesis. *Natural Products : Phytochemistry, Botany and Metabolism of Alkaloids, Phenolics and Terpenes* 98, 3069-3098.

Smith, E.C., Kaatz, G.W., Seo, S. M., Wareham, N., Williamson, E. M., Gibbons,S**. (2007)**.The phenolic diterpene totarol inhibits multidrug efflux pump activity in *Staphylococcus aureus*. *Antimicrob. AgentsChemother.* 51, 4480–4483.

Søhoel, H., Jensen, A.M.L., Møller, J.V., Nissen, P., Denmeade, S.R., Isaacs, J.T., Olsen, C.E., Christensen, S.B. **(2006).** Natural products as starting materials for development of second-generation SERCA inhibitors targeted towards prostate cancer cells. *Bioorg. Med. Chem.*, 14(8), 2810–2815.

Song, Q., Gomez-Barrios, M.L., Hopper, E.L., Hjortso, M.A., Fischer, N.H. **(1995).** Biosynthetic studies of lactucin derivatives in hairy root cultures of *Lactuca floridana*. *Phytochemistry*, 40(6), 1659–1665.

Stermitz, F. R., Beeson, T. D., Mueller, P. J., Hsiang, J., Lewis, K. **(2001)**. *Staphylococcus aureus* MDR efflux pump inhibitors from a Berberis and a Mahonia (sensu strictu) species. *Biochemical Systematics and Ecology*, 29 (8), 793–798.

Stermitz, F. R., Lorenz, P., Tawara, J. N., Zenewicz, L. A., Lewis, K. **(2000)**. Synergy in a medicinal plant: Antimicrobial action of berberine potentiated by 5′methoxyhydnocarpin, a multidrug pump inhibitor. *Proceedings of the National Academy of Sciences of the United States of America*, 97 (4), 1433–1437.

Stermitz, F. R., Scriven, L. N., Tegos, G., Lewis, K. **(2002)**. Two fl avonols from *Artemisa annua* which potentiate the activity of berberine and norfl oxacin against a resistant strain of *Staphylococcus aureus*. *Planta Medica*, 68 (12), 1140–1141.

Tan, R.X., Tang, H.Q., Hu, J., Shuai, B. **(1998).** Lignans and sesquiterpene lactones from *Artemisia sieversiana* and *Inula racemosa*. *Phytochemistry, 49*, 157–161.

Tang, S., Bremner, P., Kortenkamp, A., Schlage, C., Gray, A. I., Gibbons, S., Heinrich, M. (2003). Bifl avonoids with cytotoxic and antibacterial activity from Ochna macrocalyx. *Planta Medica*, 69 (3), 247–253.

Taubes, G. (2008). The bacteria fight back. *Science*. 321(5887), 356–61.

Tosovic, J., Markovic, S. **(2016).** Structural and antioxidative features of chlorogenic acid. *Croat. Chem. Acta*, *89*, 535–541.

Tyson, R.L., Chang, C.J, McLaughlin, J.L., Cassady, J.M. **(1979).** A novel sesquiterpene lactone from *Anvillea garcinii* (Burm.). *J. Nat. Prod*., *42*, 680-681.

Tyson, R.L., Chang, C.J., McLaughlin, J.L., Aynehchi, Y., Cassady, J.M. **(1981).** 9-*α*-Hydroxyparthenolide, a novel antitumor sesquiterpene lactone from *Anvillea garcinii* (Burm.) DC. *Experientia*, *37*, 441-442.

Ulubelen, A., Mabry, T., Aynehchi, Y. **(1979)**. Flavonoids of *Anvillea Garcini. J. Nat. Prod*., *42*, 624-626. 10.1021/np50006a007.

Walsh, C.T., Wrigh,t G. (2005) Introduction: antibiotic resistance. *Chem. Rev*.,105:391–394.

Walsh, T.R., Weeks, J., Livermore, D.M., Toleman, M.A. **(2011)**. Dissemination of NDM-1 positive bacteria in the New Delhi environment and its implications for human health: an environmental point prevalence study. The *Lancet Infectious Diseases*, 11(5), 355–362.

Wink, M., Ashour, M. L., El-Readi, M. Z. **(2012)**. Secondary metabolites from plants inhibiting ABC transporters and reversing resistance of cancer cells and microbes to cytotoxic and antimicrobial agents. *Frontiers in Microbiology*, 3 , 130.

Wu, Q.X., He, X.F., Jiang, C.X., Zhang, W., Shi, Z.N., Li, H.F., Zhu, Y. **(2018)**. Two novel bioactive sulfated guaiane sesquiterpenoid salt alkaloids from the aerial parts of Scorzonera divaricate. *Fitoterapia*, 124, 113–119.

Yuuya, S., Hagiwara, H., Suzuki, T, Ando, M., Yamada, A., Suda, K., Kataoka, T., Nagai, K. **(1998)**. Guaianolides as immunomodulators. synthesis and biological activities of dehydrocostus lactone, mokko lactone, eremanthin, and their derivatives. *J. Nat. Prod*, 62(1), 22–30.

Zaman, S.B, Hussain, M.A., Nye, R. , Mehta, V., Mamun, K.T., Hossain, N. **(2017).** A Review on Antibiotic Resistance: Alarm Bells are Ringing. *Cureus*, 9(6), 1403-1412. DOI 10.7759/cureus.1403.

Zhou, Q.M., Chen, M.H., Li, X.H., Peng, C., Lin, D.S., Li, X.N., He, Y., Xiong, L. **(2018)**. Absolute configurations and bioactivities of Guaiane-type Sesquiterpenoids isolated from Pogostemon cablin. *J. Nat. Prod*, 81, 1919–1927.

CHAPTER 5.
CONCLUSIONS

Two Saudi plants, *Cissus rotundifolia* and *Anvillea garcinii* were selected to be phytochemically and biologically studied with aim of rationalizing their folk medicinal use among Saudi population. *C. rotundifolia* growing in Saudi Arabia had not been subjected to phytochemical analysis prior to our project. We have undertaken a bioassay guided investigation of the extracts obtained from leaves of a Saudi sample of *C. rotundifolia* aimed at finding compounds active in the promotion of glucose uptake in hepatic cell. A bioassay-guided purification of *C. rotundifolia* extracts revealed the presence of two new metabolites, cissuxinoside (new sucrose diester of truxinic acid) and cissoic acid (unprecedented glycosylated and extensively conjugated C12 dicarboxylic acid bearing two methyl groups at C-4 and C-10). Both compounds, cissuxinoside and cissoic acid belong to very unusual classes of secondary metabolites. Moreover, three rare C-glycosylated flavones (vitexin-2"-*O*-*β*-*D*-arabinofuranoside, orientin-2"-*O*-*β*-*D*-arabinofuranoside, and isovitexin-2'-*O*-*β*-*D*-glucopyranoside) were fully characterized and for two of them, NMR data are reported here for the first time. Additionally, two coumaric acid derivatives (Z-4-coumaric acid *β*-*D*-glucopyranoside, and 1-*O*-p-coumaroyl-*β*-*D*-glucopyranose). This study identified 1-p-coumaroyl *β*-*D*-glucoside as the main responsible of glucose uptake stimulation effect. However, other concomitant mechanisms likely concur in defining the marked antidiabetic effect of *C. rotundifolia* extract.

Anvillea garcinii, the second plant in our project, is a medicinal plant used in the Arab region for intestinal diseases, lungs and liver diseases, digestive problems, and as an anti-diabetic. It was subjected to repeated chromatographic purifications which led to the isolation of four new sesquiterpene lactones (4*α*,9*α*,10*α*-trihydroxyguaia-11(13)en-12,6*α*-olide;9-*β*-hydroxyparthenolide-9-*O*-*β*-*D*-glucopyranoside; 4*α*,9*α*,10*α* trihydroxy-13*α*-(N-prolyl) -guaia-12,6*α*- olide and 4*α*-(*β*-glucopyranosyl) -oxy-9*α*-hydroxyguaia-10(14)en-12,6*α*-olide) along with five known germacranolides (garcinamine A, garcinamine B, garcinamine C, garcinamine D, 3*α*,4*α*,10*β*-trihydroxy-11*β*-guai-1-en-12,6*α*-olide) .in

addition to the isolated flavonoids and polypenolics (chlorogenic acid, 3-*O*-feruloylquinic acid, 1-*O*-caffeoyl-*β*-*D*-glucopyranose, 1-O-feruloyl-*β*-*D*-glucopyranose, kaempferol-3-*O*-glucopyranoside, and kaempferol-7-*O*-glucopyranoside). The structures of the new compounds were established using spectroscopic (1D, 2D NMR) and spectrometric methods (ESIMS). The isolated compounds were tested for their antimicrobial activity against pathogenic fungi and bacteria. The isolated sesquiterpenoids have shown remarkable activities against some of the tested pathogens including *Candida albicans*, *C. parapsilosis, S. aureus, B. licheniformis,* and against *E. fergusonii*.

Overall, the results presented in this PhD thesis confirm the potential of Saudi flora to provide interesting leads for pharmacological development and encourage further studies in this direction. Compared to other floras, plants of the Saudi region have been much less studied and, therefore, we can anticipate that next years will see a significant increase in communications from this part of the world. The collaboration with foreign research institutions, as happened in the present work, will be instrumental in realizing this objective.

CHAPTER 6

SPECTRAL DATA

6.1. Spectral data for CHAPTER 3

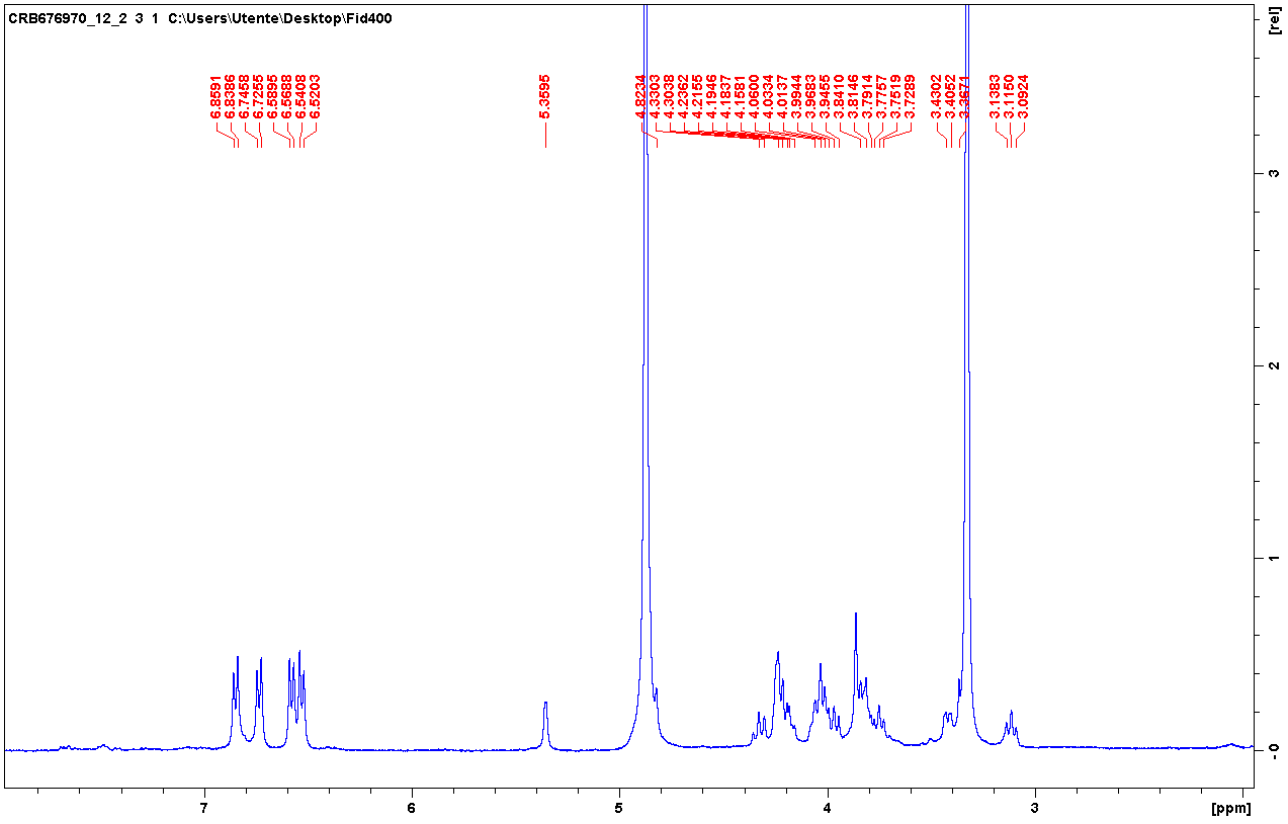

Figure 6.1: ^{1}H NMR in CD_3OD (400 MHz) of cissuxinoside (**1**)

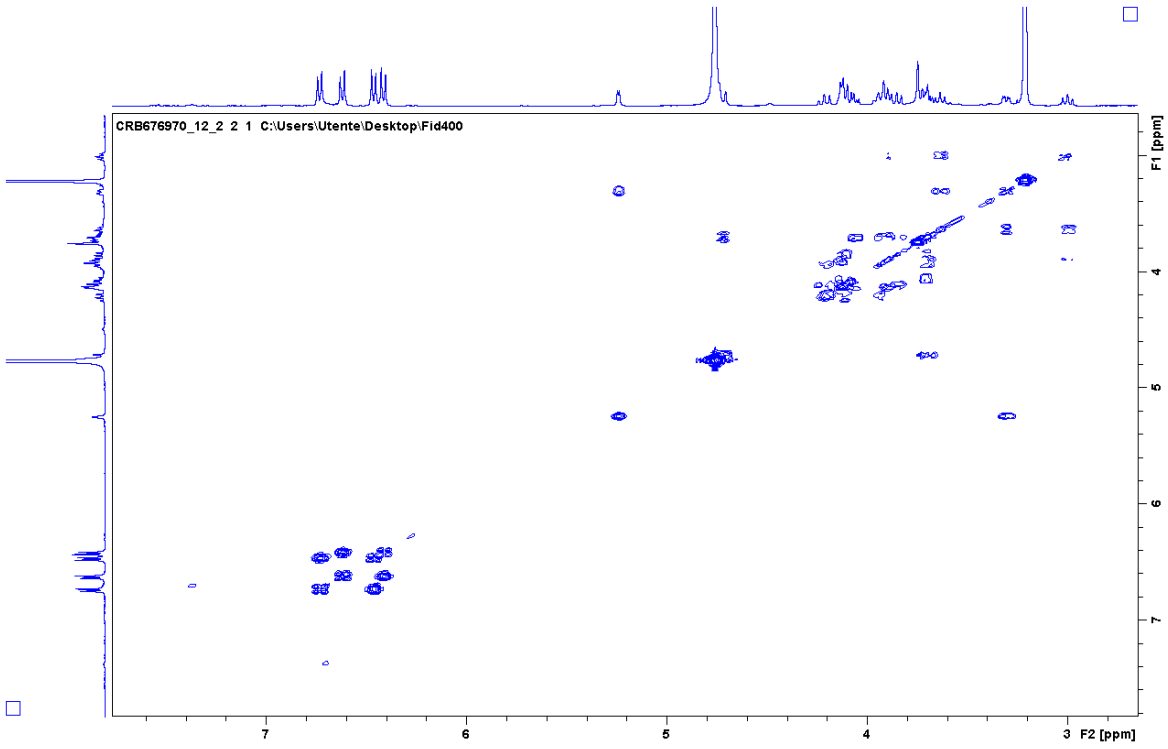

Figure 6.2: 2D NMR COSY in CD_3OD (400 MHz) of cissuxinoside (**1**)

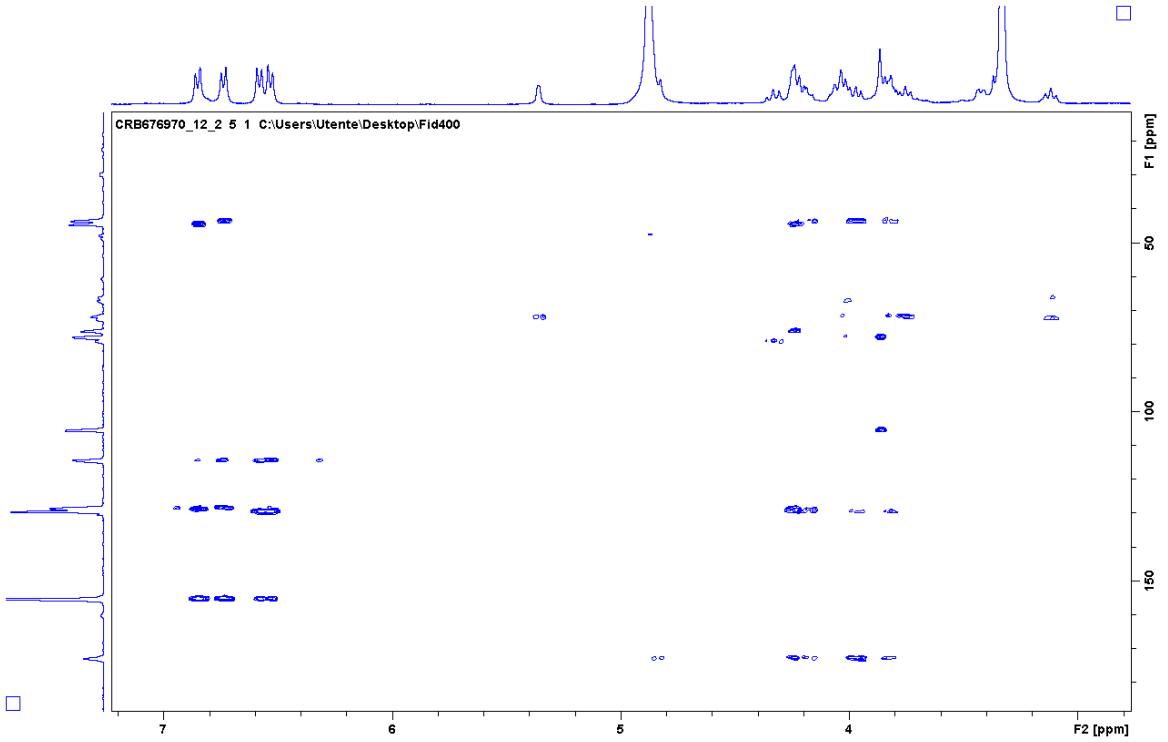

Figure 6.3: 2D NMR HMBC in CD_3OD (400 MHz) of cissuxinoside (**1**)

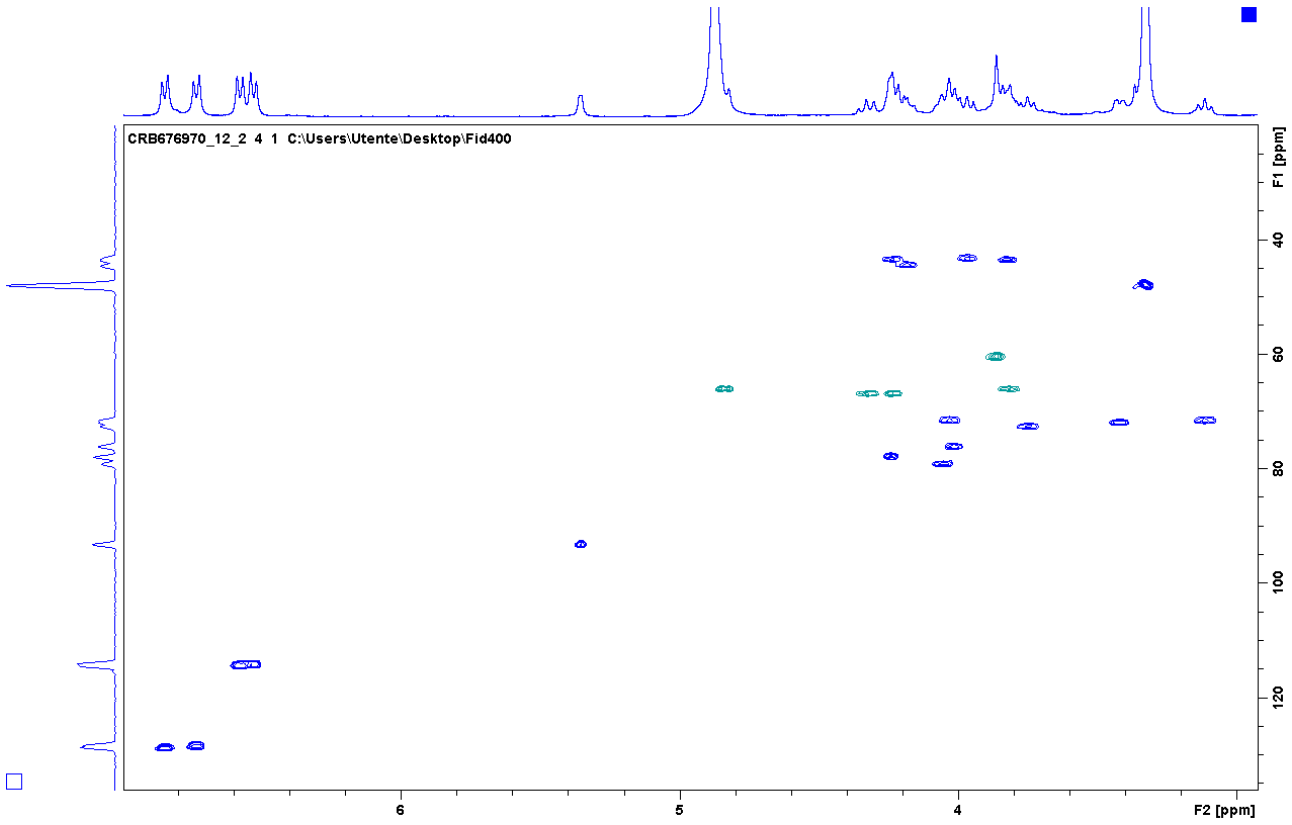

Figure 6.4: 2D NMR HSQC in CD_3OD (400 MHz) of cissuxinoside (**1**)

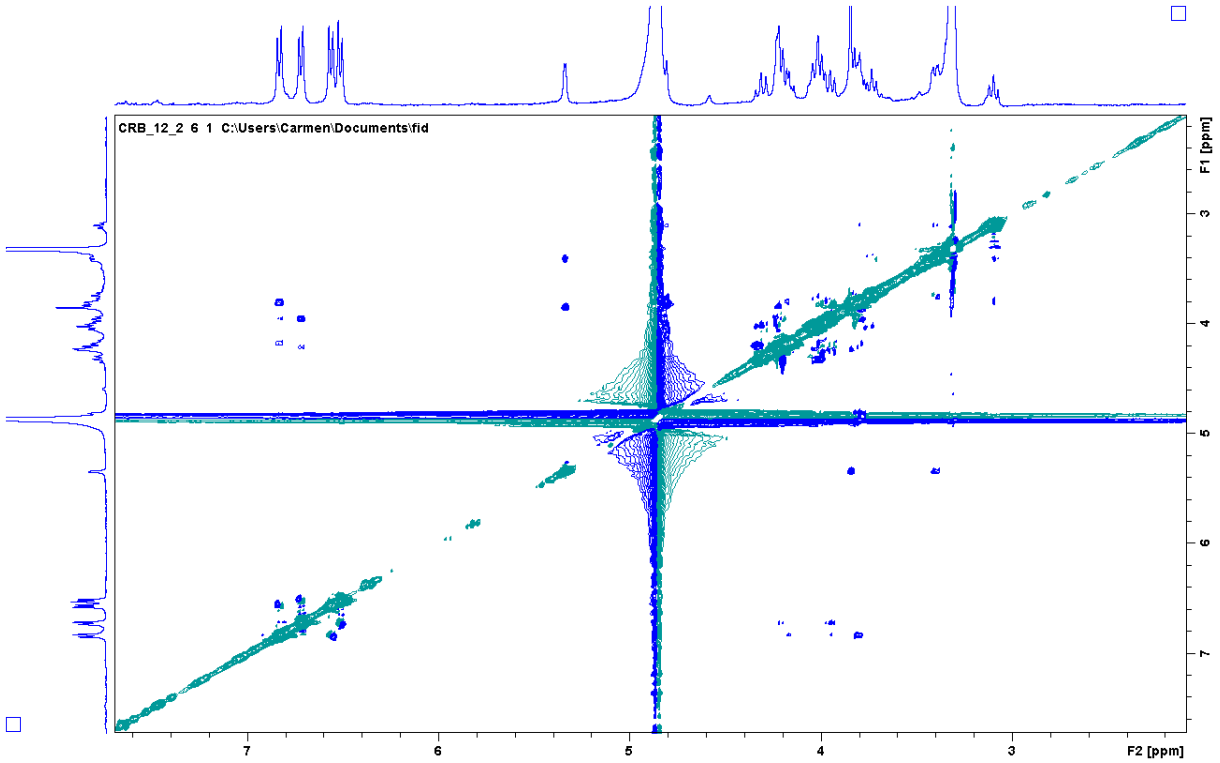

Figure 6.5: 2D NMR ROESY in CD_3OD (400 MHz) of cissuxinoside (**1**)

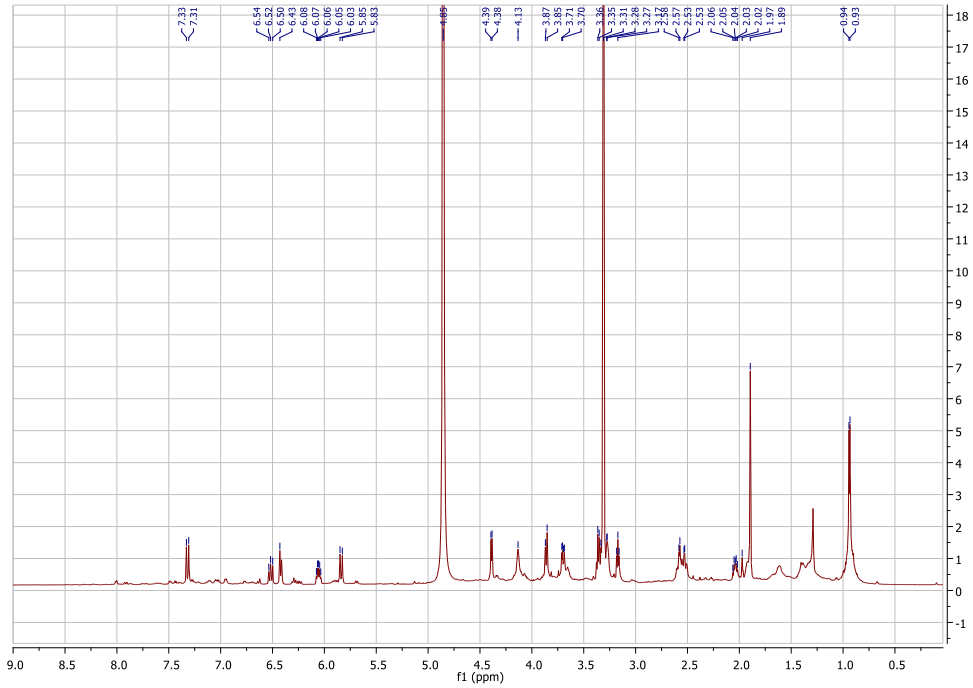

Figure 6.6: ^{1}H NMR spectrum (700 MHz) of cissoic acid (**2**) in CD_3OD

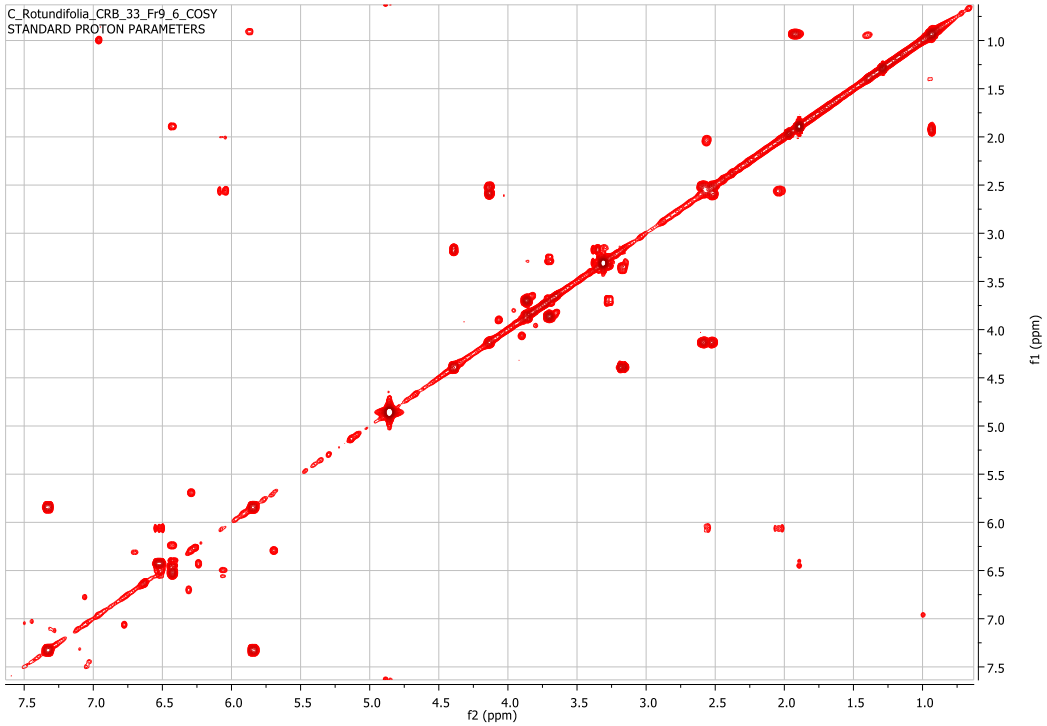

Figure 6.7: 2D NMR COSY in CD_3OD (700 MHz) of cissoic acid (**2**)

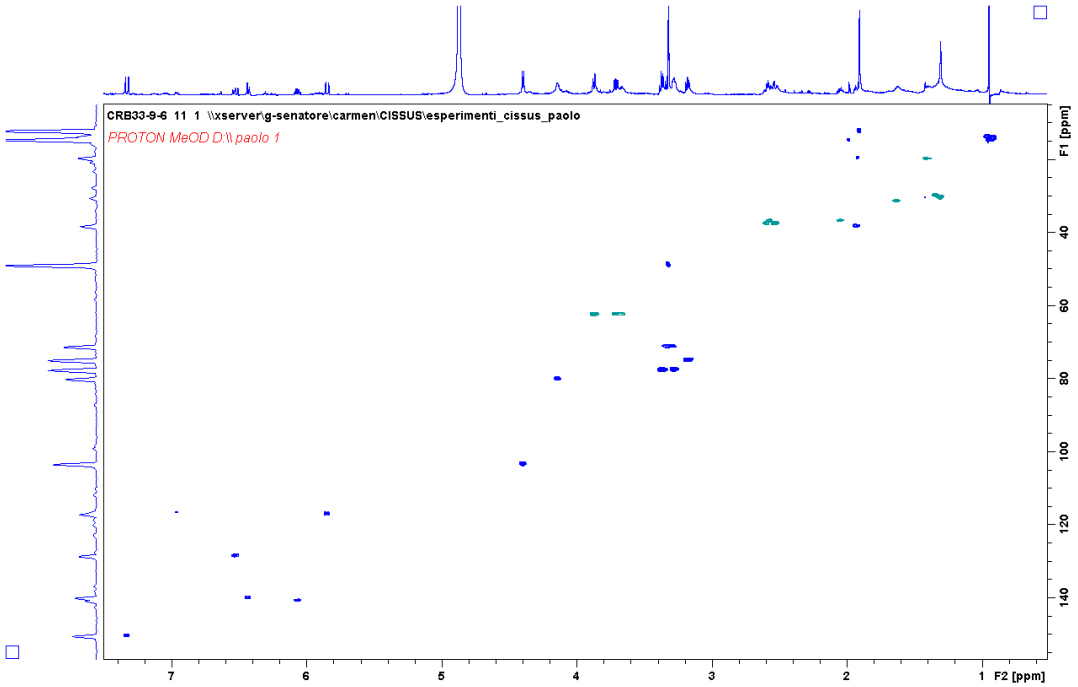

Figure 6.8:2D NMR HSQC in CD_3OD (700 MHz) of cissoic acid (**2**)

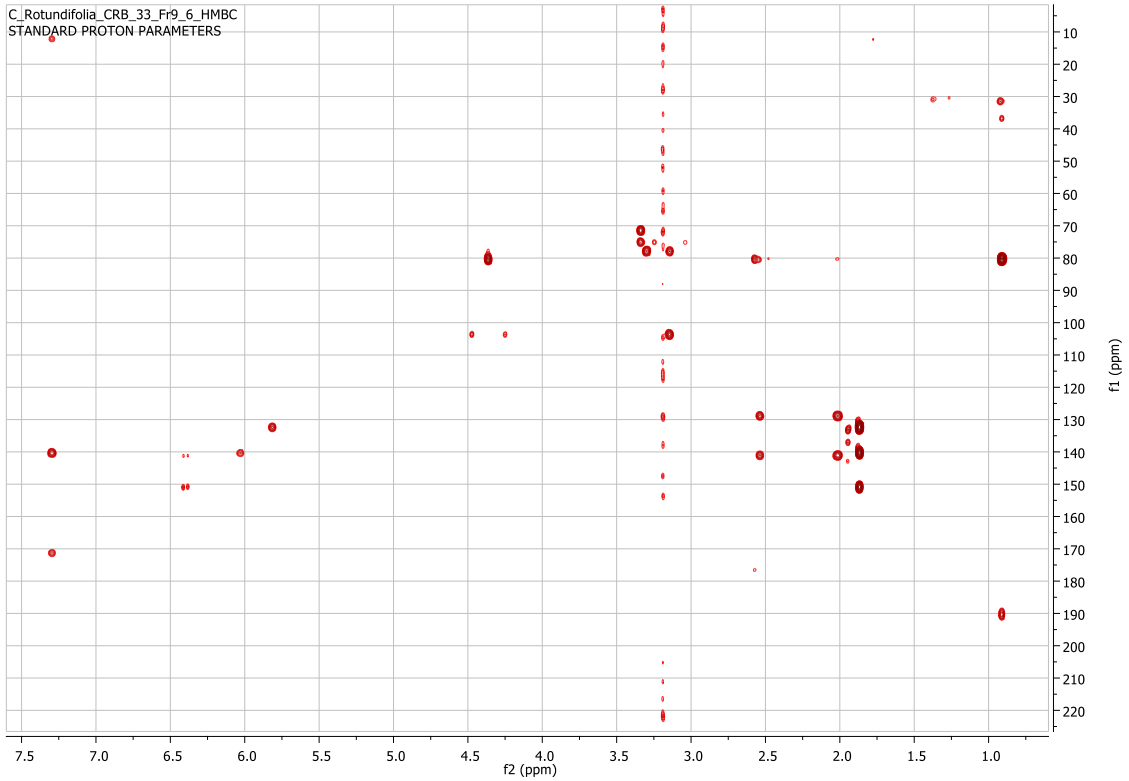

Figure 6.9:2D NMR HMBC in CD_3OD (700 MHz) of cissoic acid (**2**)

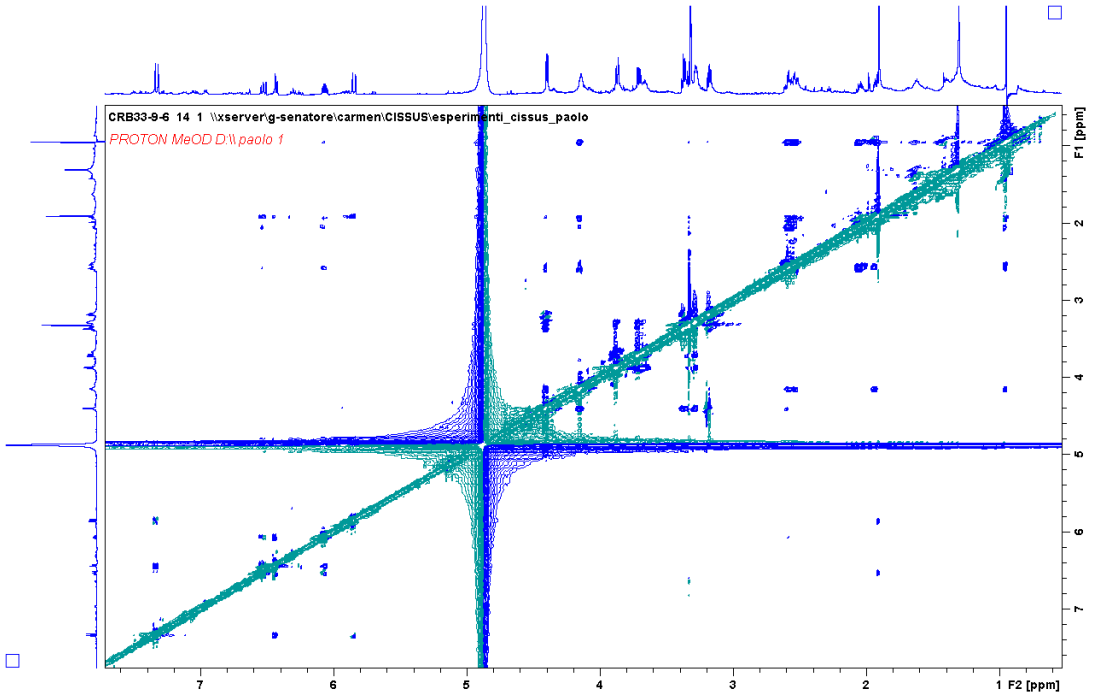

Figure 6.10:2D NMR ROESY in CD_3OD (700 MHz) of cissoic acid (**2**)

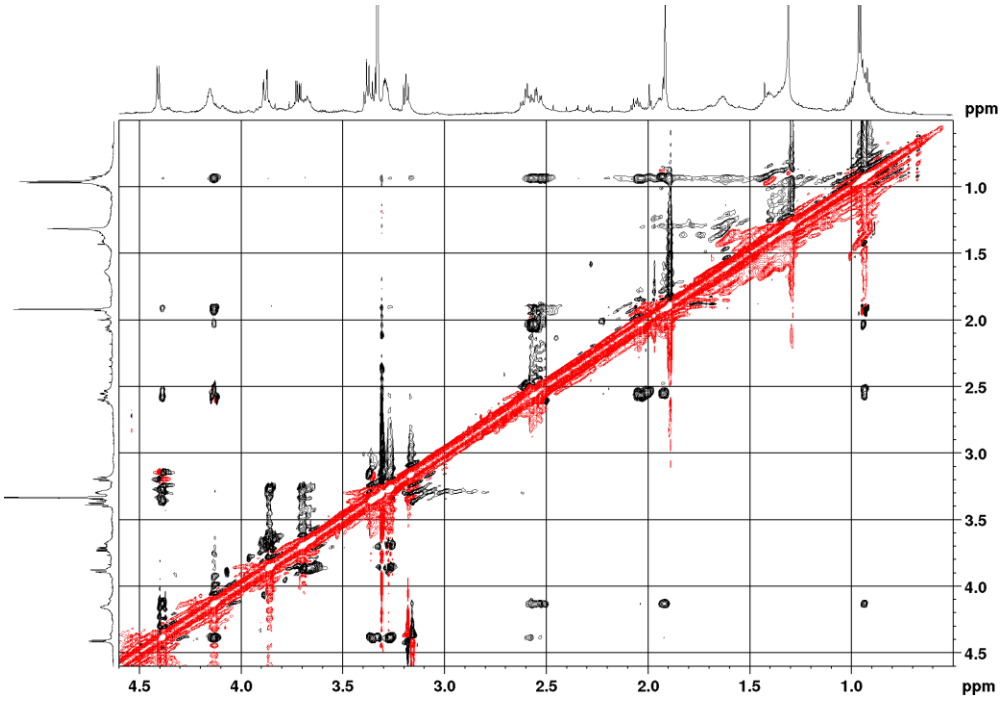

Figure 6.11: Expansion of high-field region of the 2DNMR ROESY of cissoic acid (**2**)

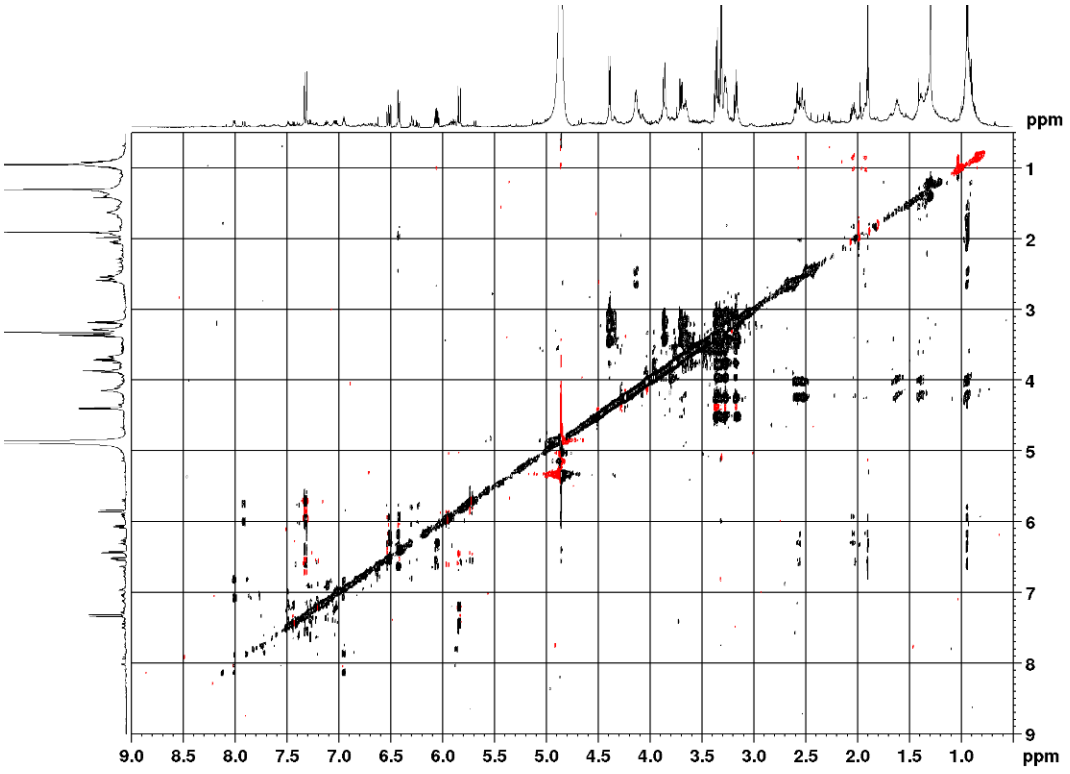

Figure 6.12: 2D NMR HETLOC in CD_3OD (700 MHz) of cissoic acid (**2**)

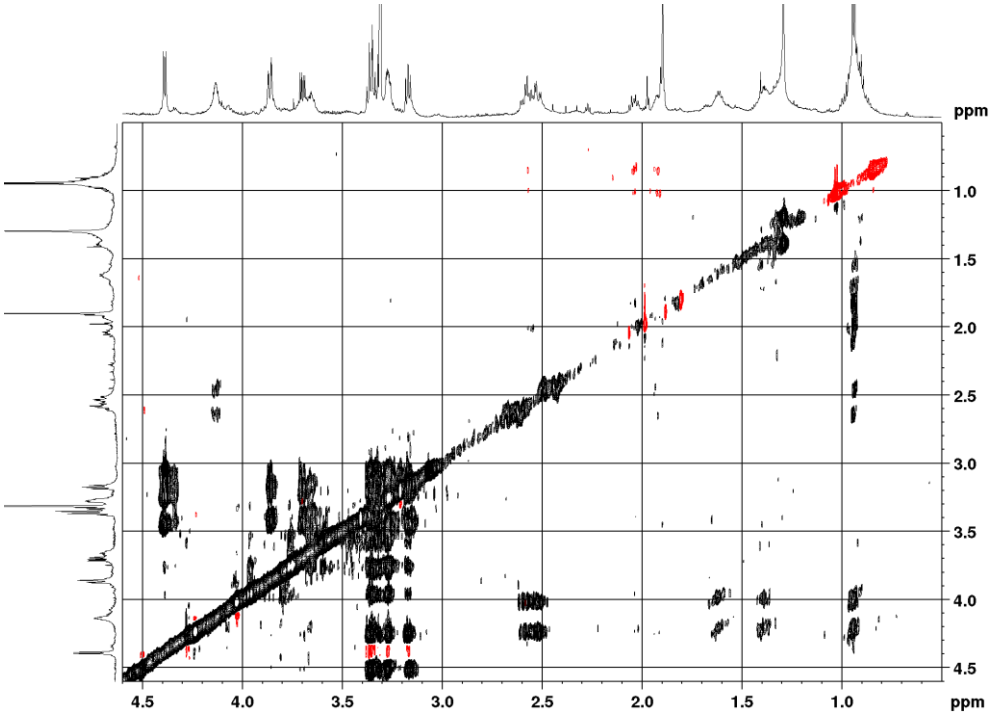

Figure 6.13: Expansion of the high-field region of the 2D NMR HETLOC of cissoic acid (**2**)

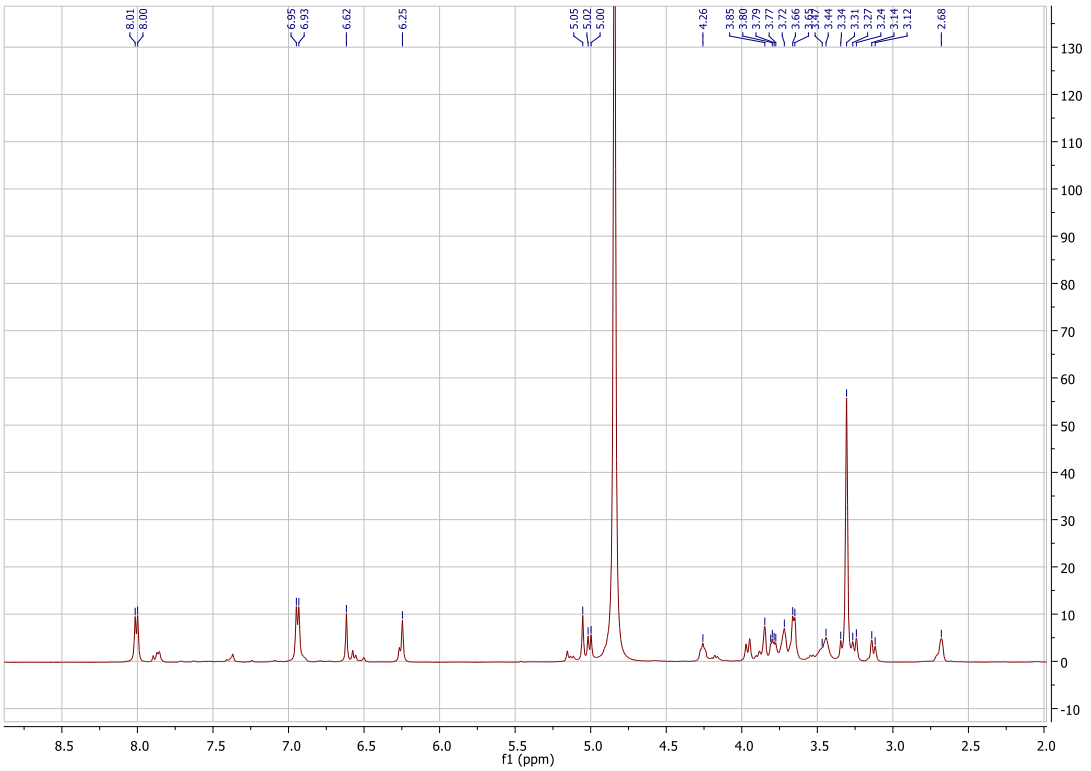

Figure 6.14: ^{1}H NMR in CD_3OD (500 MHz) of compound **3**

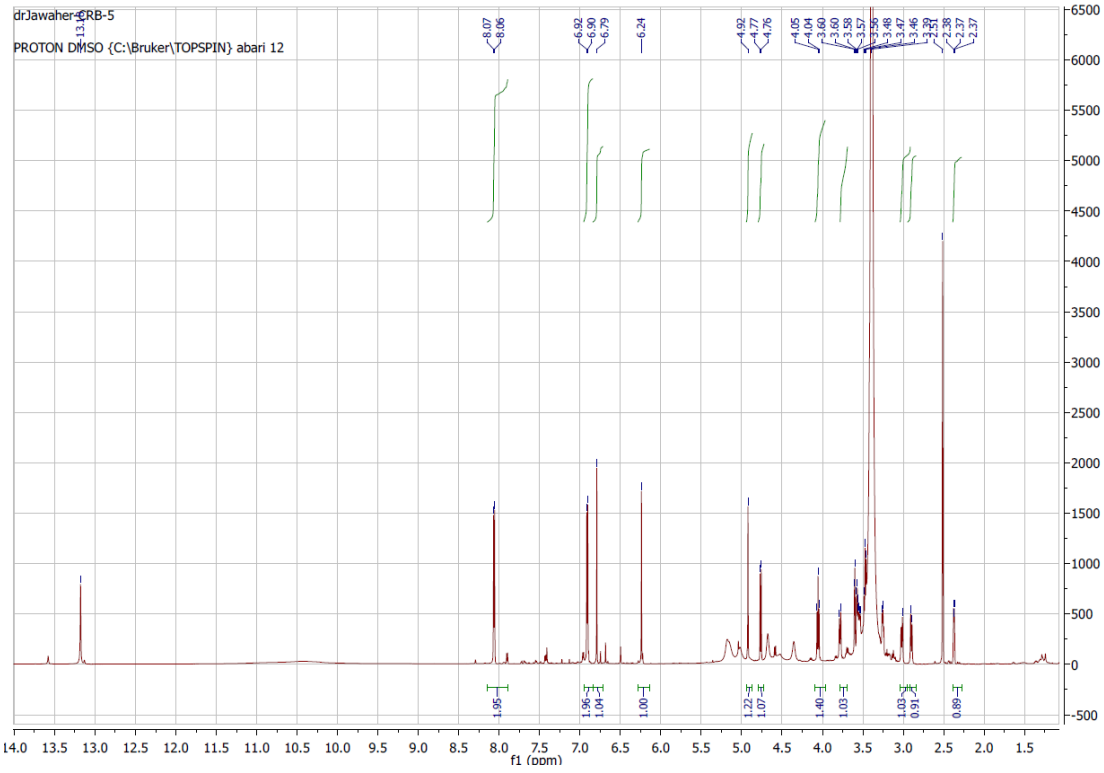

Figure 6.15: ^{1}H NMR in DMSO-d_6 (500 MHz) of compound **3**

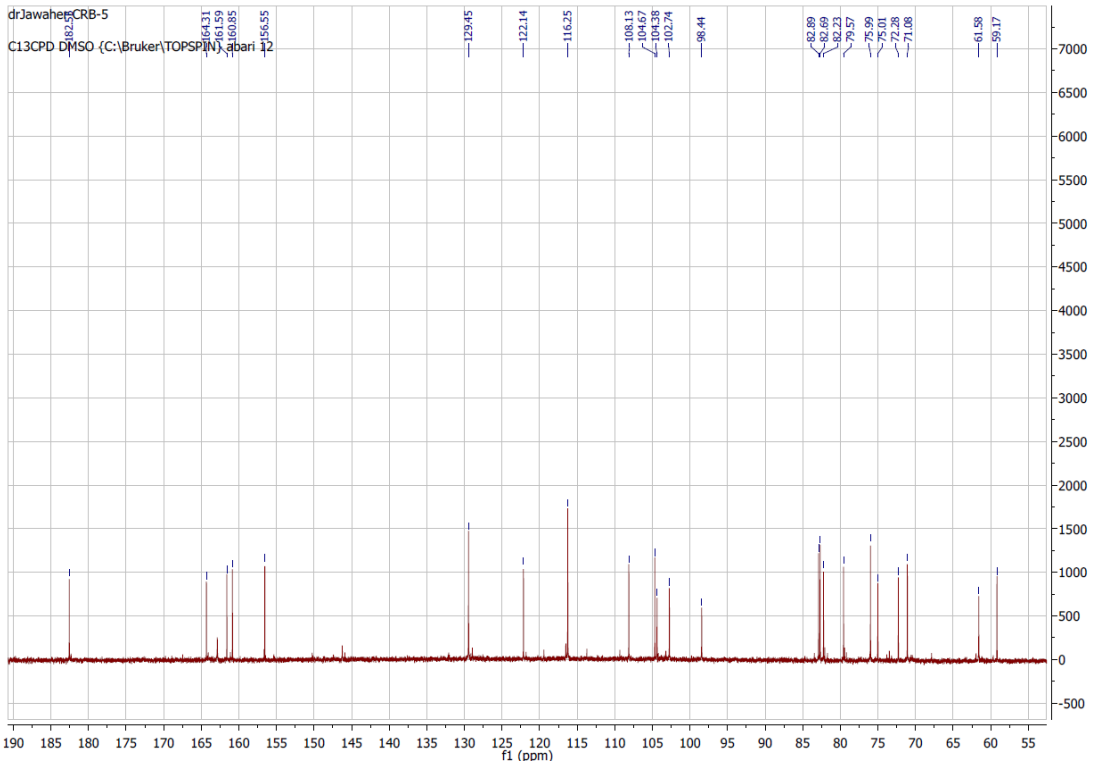

Figure 6.16: ^{13}C NMR in DMSO-d_6 (125 MHz) of compound **3**

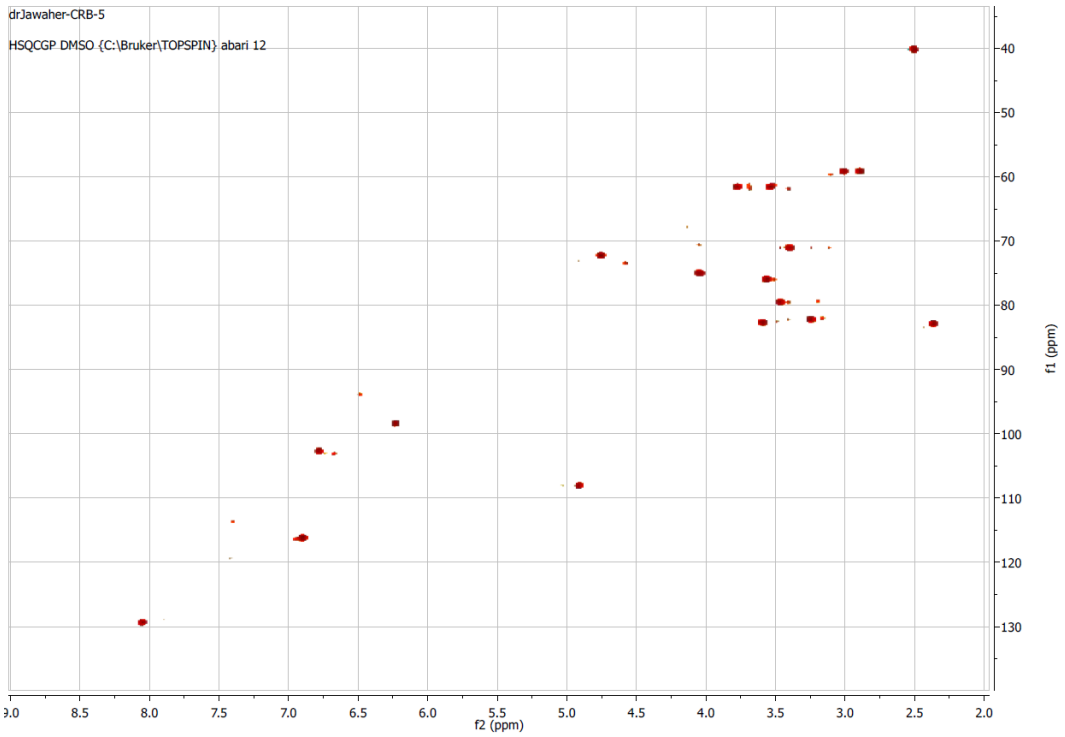

Figure 6.17:2D NMR HSQC in DMSO-d_6 of compound **3**

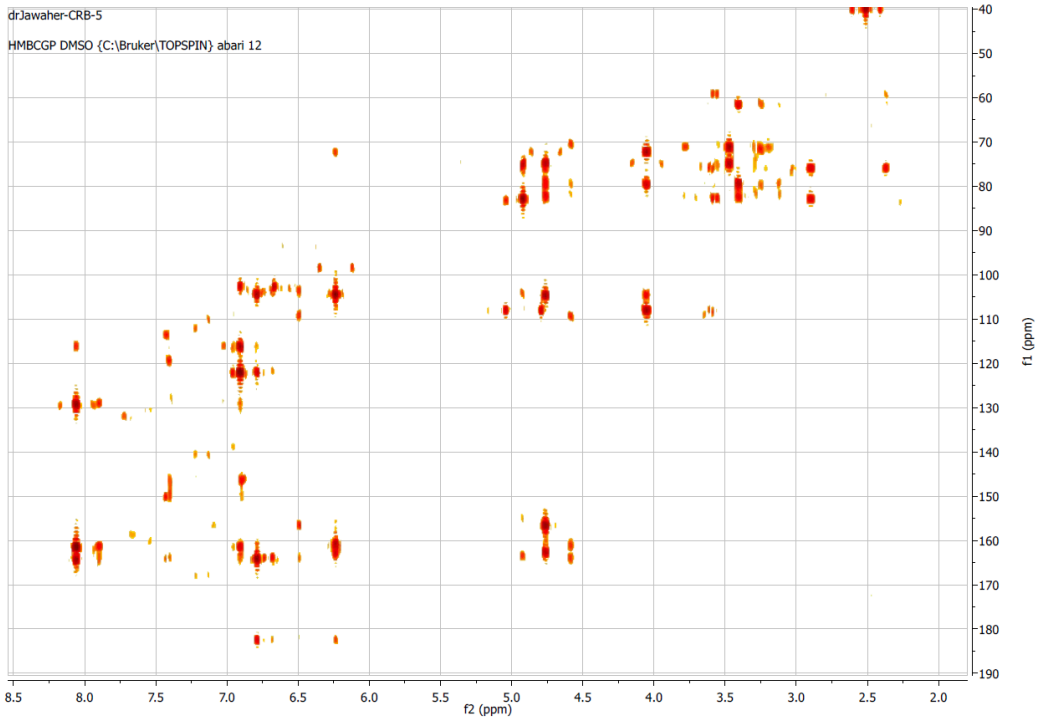

Figure 6.18: 2D NMR HMBC in DMSO-d_6 of compound **3**

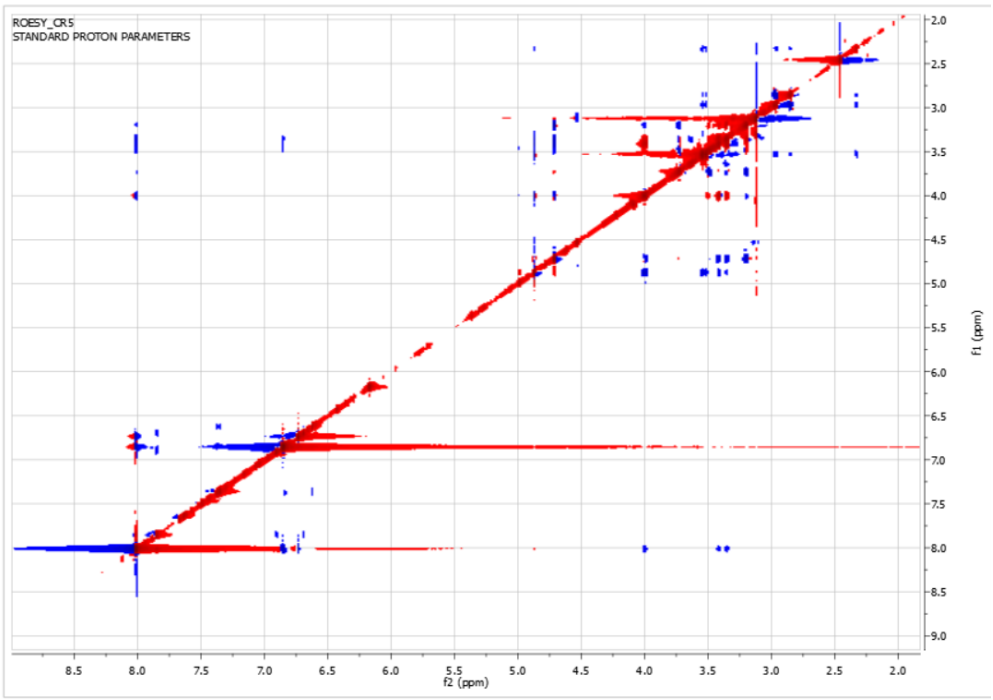

Figure 6.19: 2D NMR ROESY in DMSO-d_6 of compound **3**

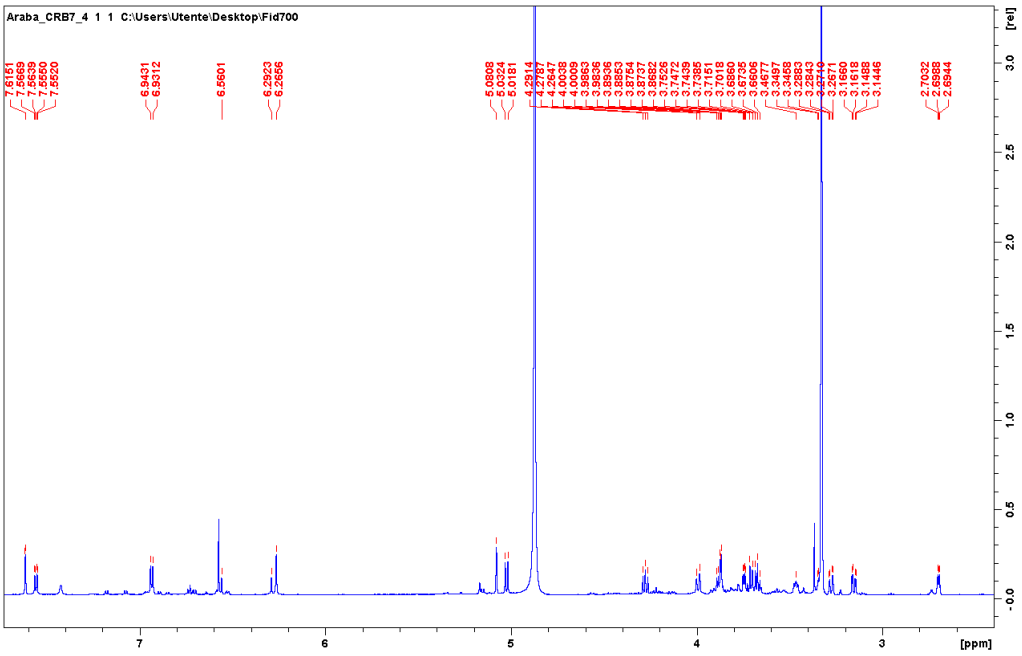

Figure 6.20: ^{1}H NMR in CD_3OD (700 MHz) of compound **4**

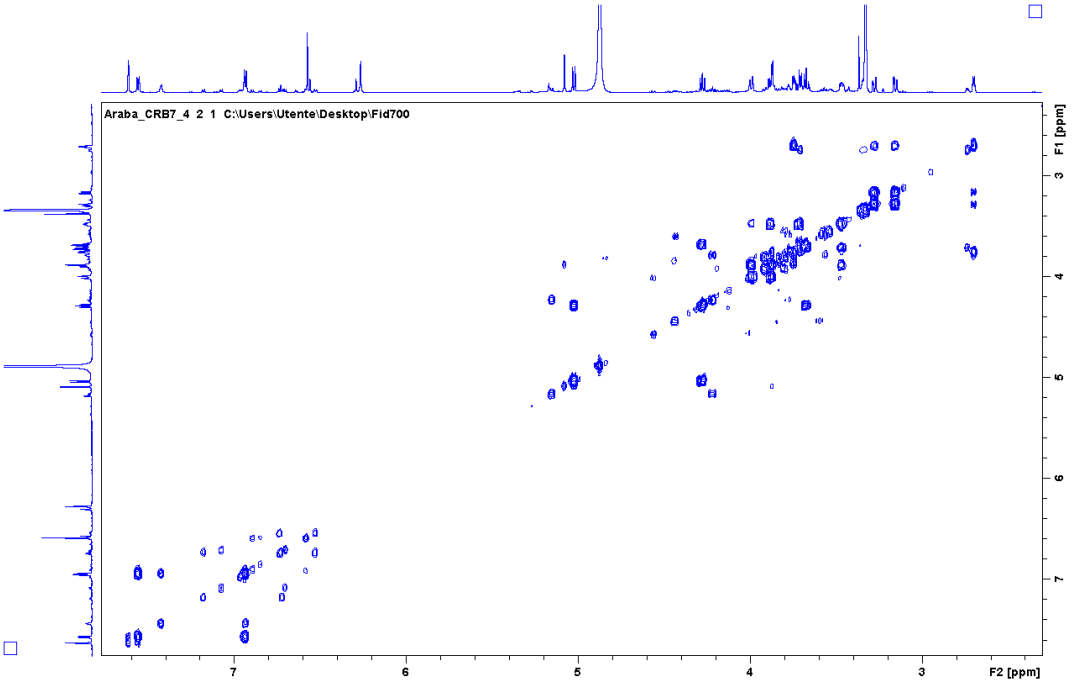

Figure 6.21: 2D NMR COSY in CD_3OD of compound **4**

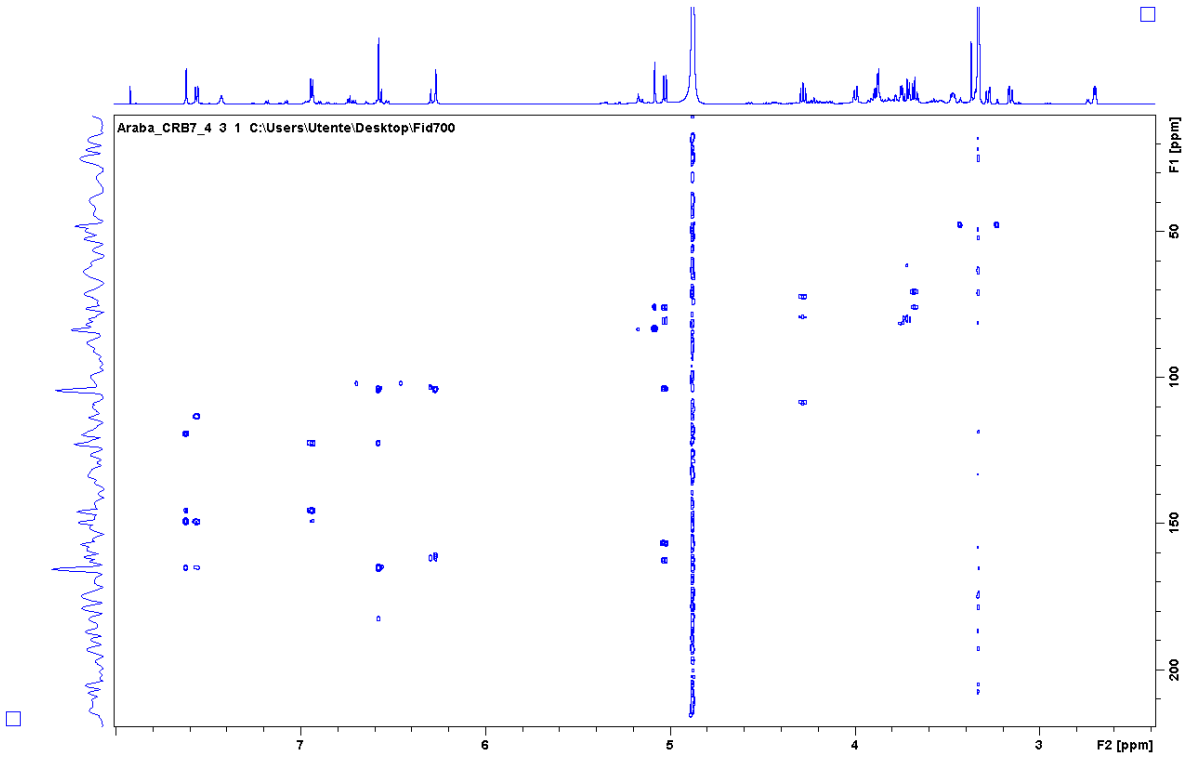

Figure 6.22: 2D NMR HMBC in CD_3OD of compound **4**

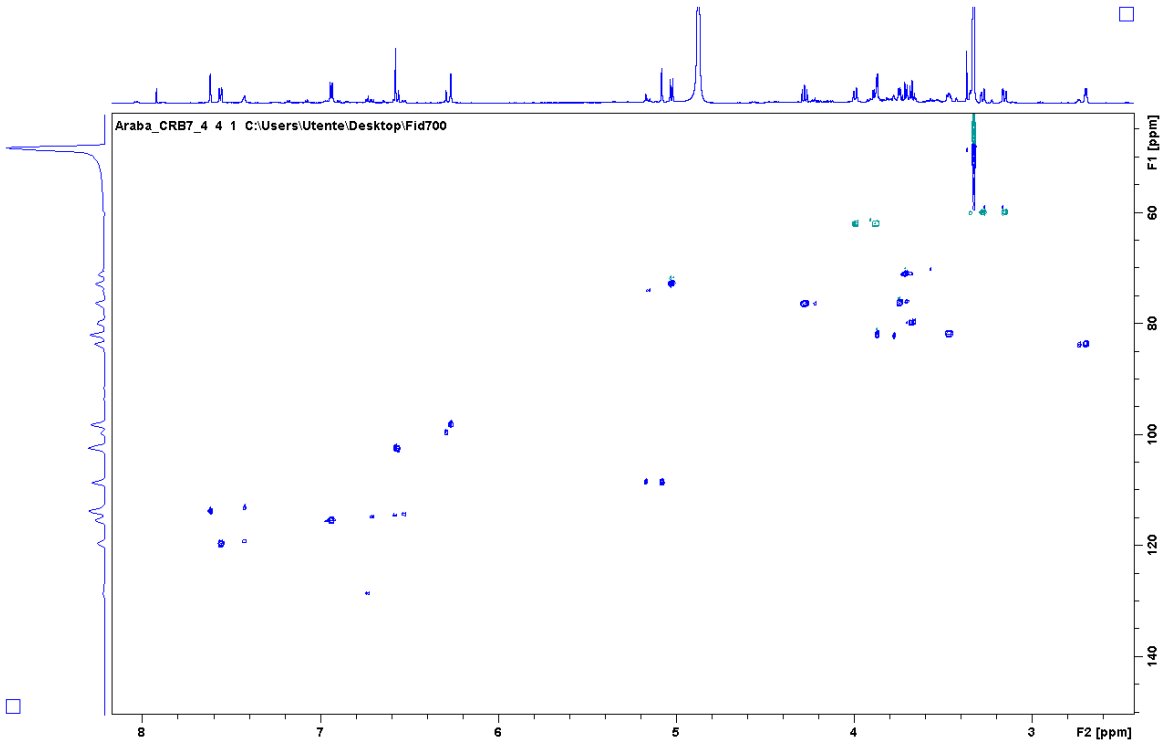

Figure 6.23: 2D NMR HSQC in CD_3OD of compound **4**

6.2. Spectral data for CHAPTER 4

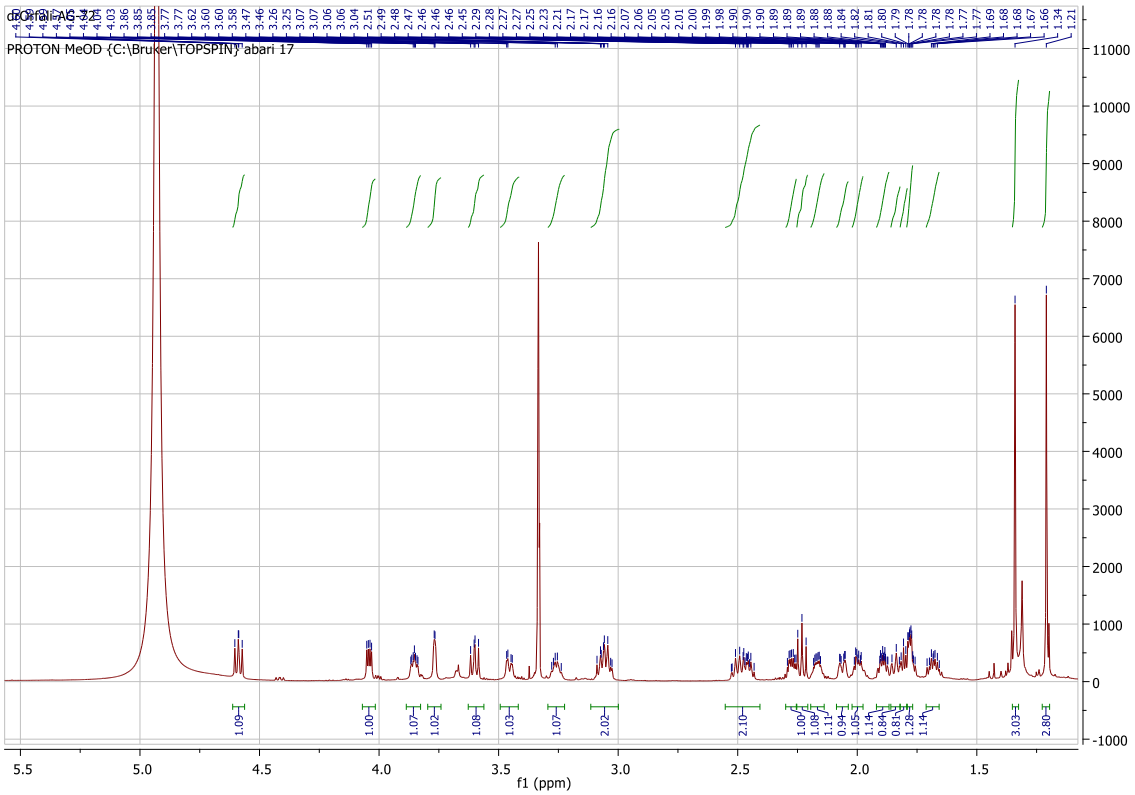

Figure 6.24: ^{1}H NMR Spectra of Compound **1** in CD_3OD.

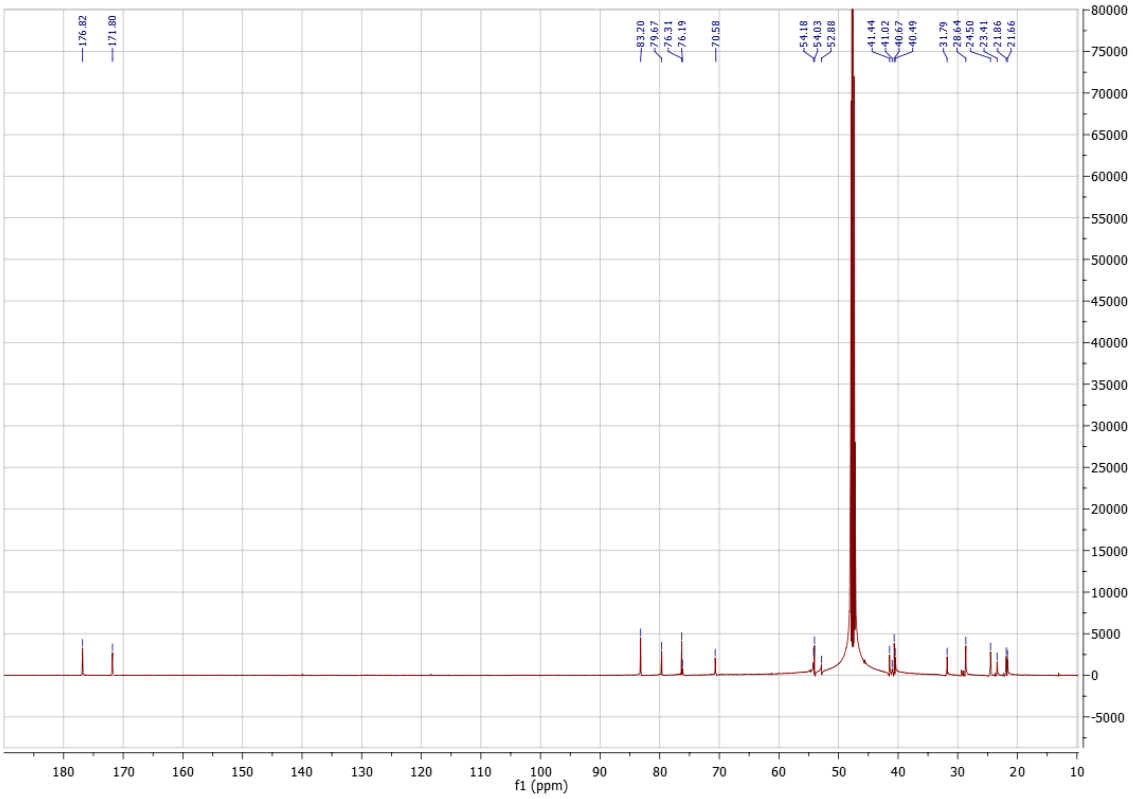

Figure 6.25: ^{13}C NMR Spectra of Compound **1** in CD_3OD.

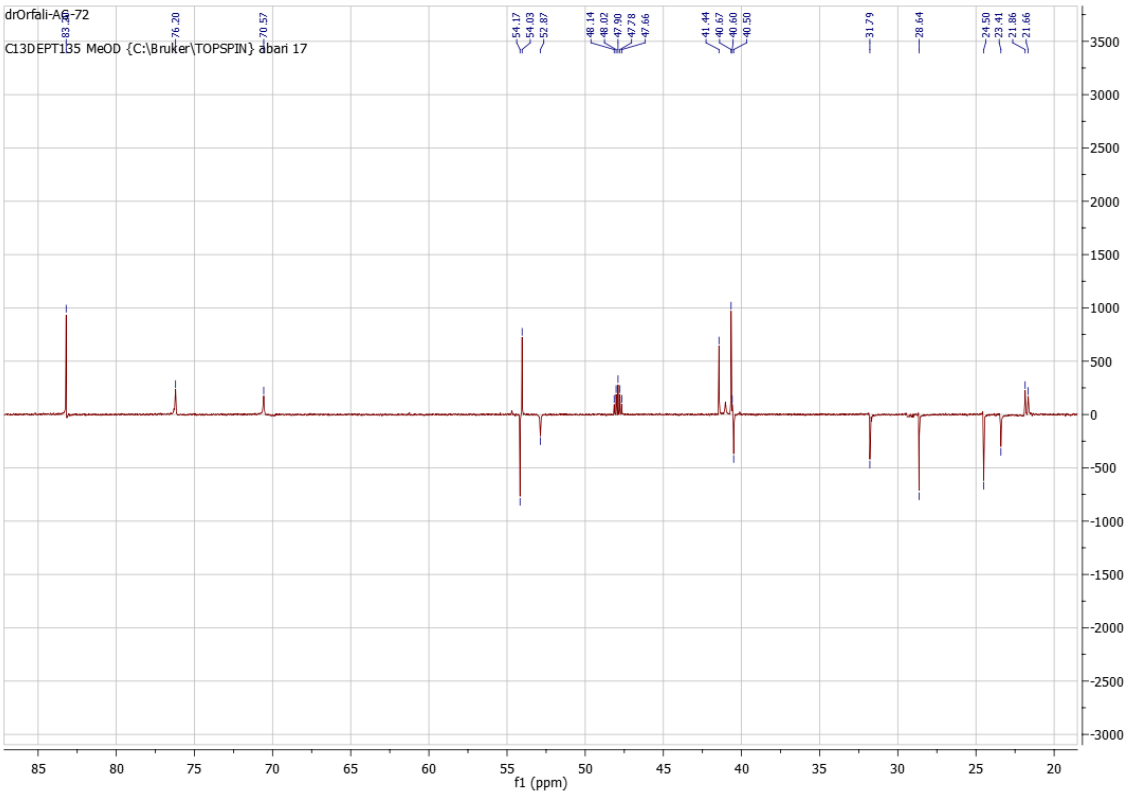

Figure 6.26: DEPT-135 NMR Spectra of Compound **1** in CD_3OD.

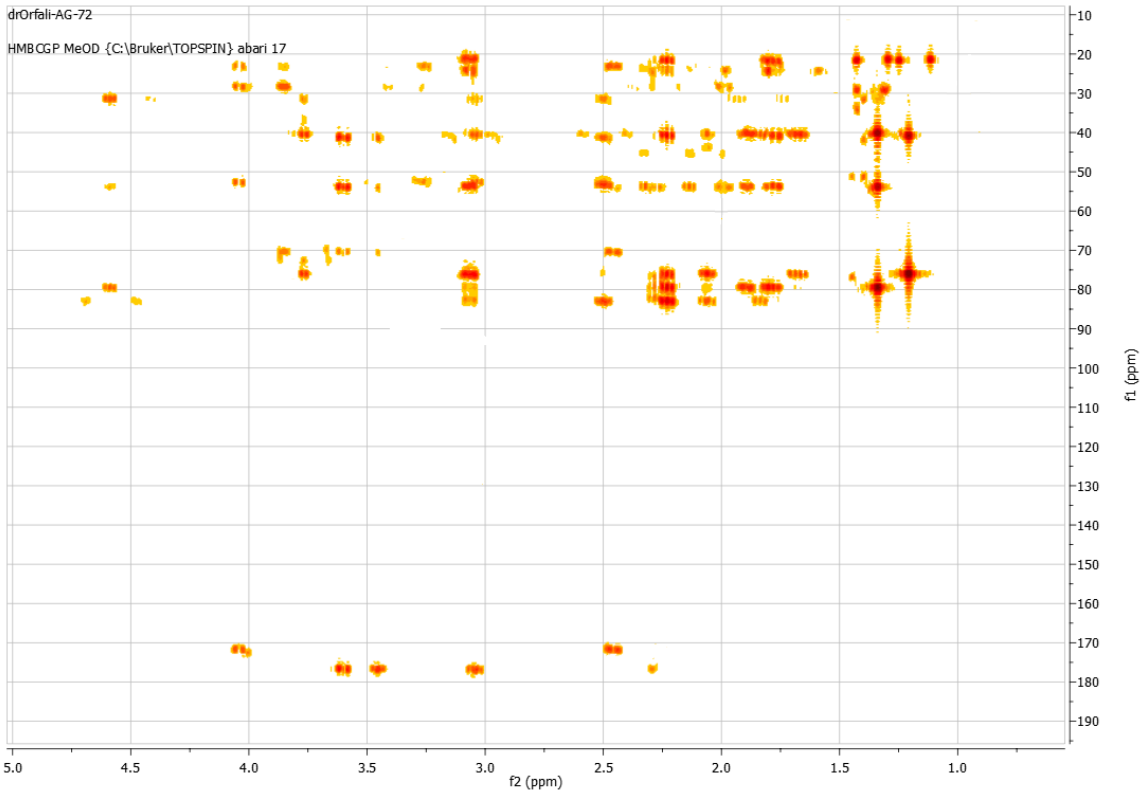

Figure 6.27: HMBC Spectra of Compound **1** in CD_3OD.

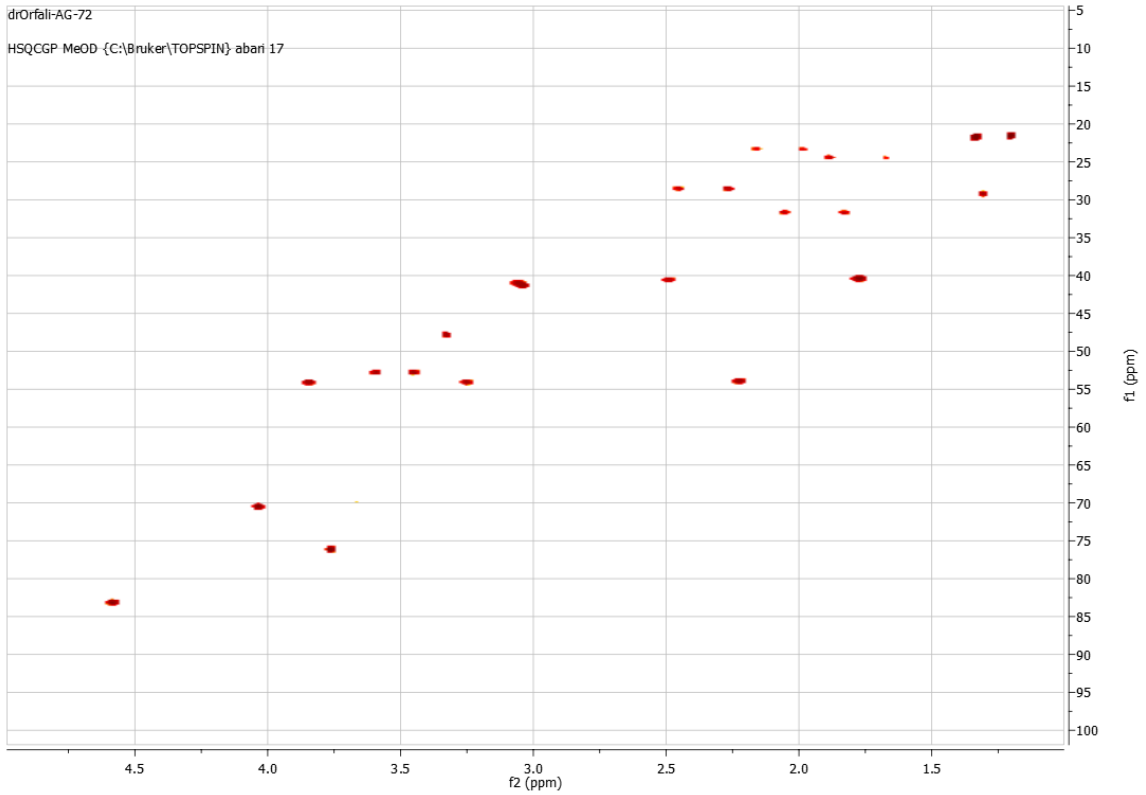

Figure 6.28: HSQC Spectra of Compound **1** in CD_3OD.

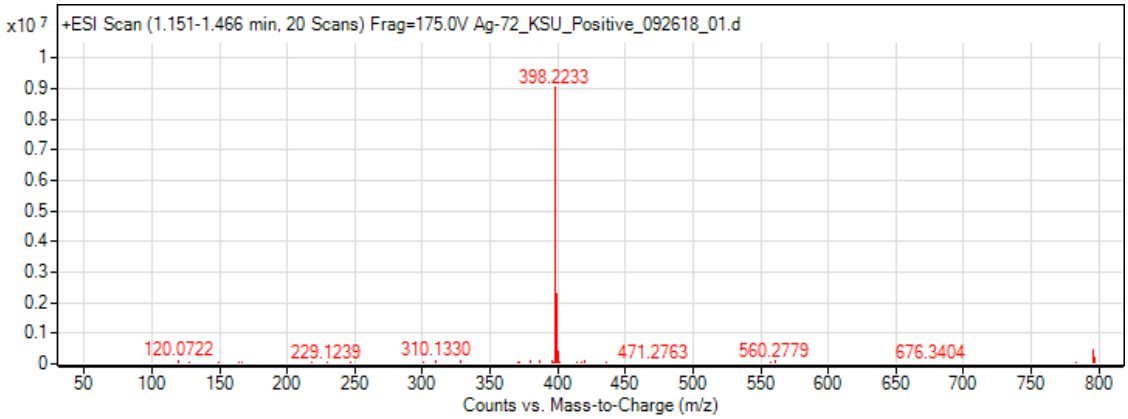

Figure 6.29: ESI Mass Spectra of Compound **1**.

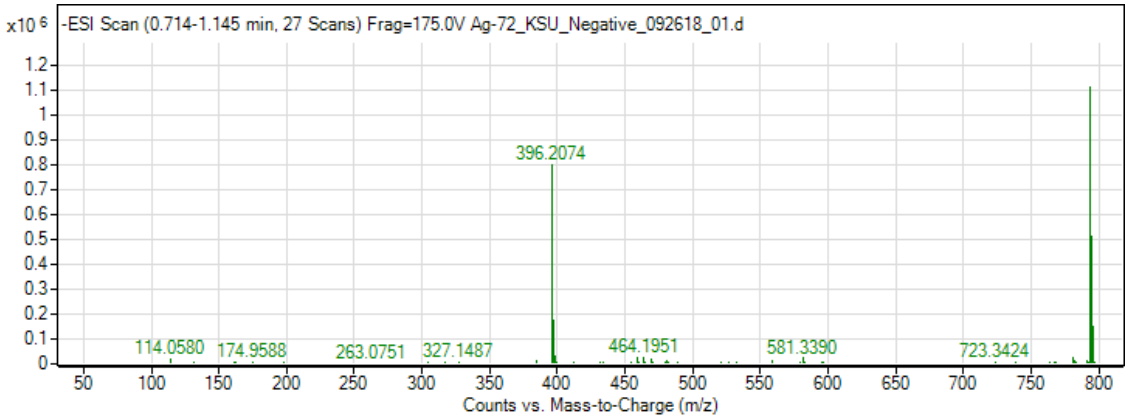

Figure 6.30: ESI Mass Spectra of Compound **1**.

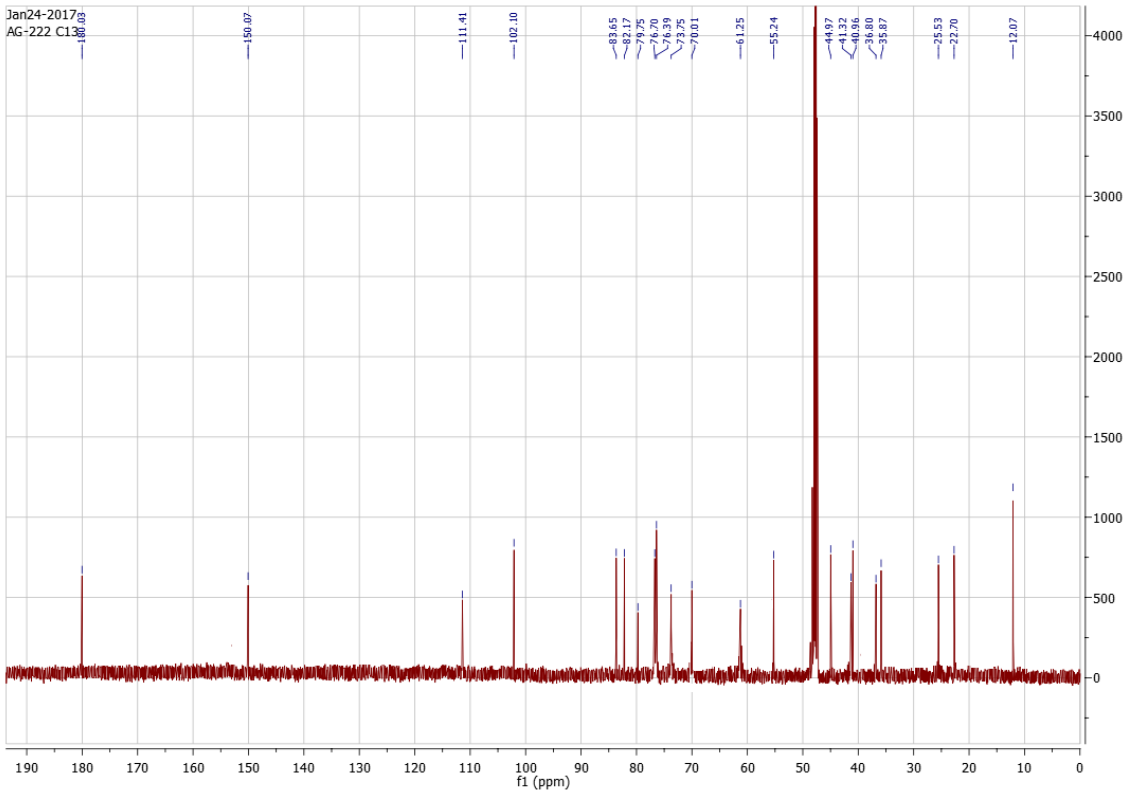

Figure 6.31: ^{13}C NMR Spectra of Compound **2** in CD_3OD.

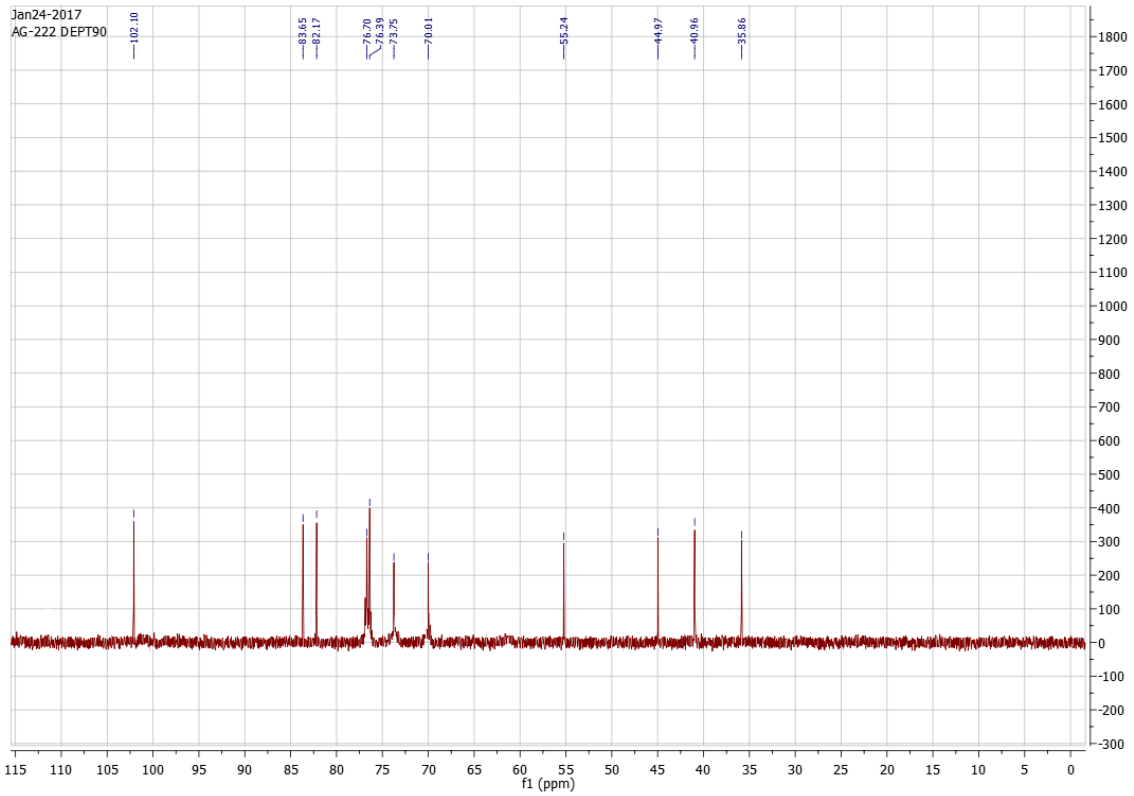

Figure 6.32: DEPT-90 NMR Spectra of Compound **2** in CD_3OD.

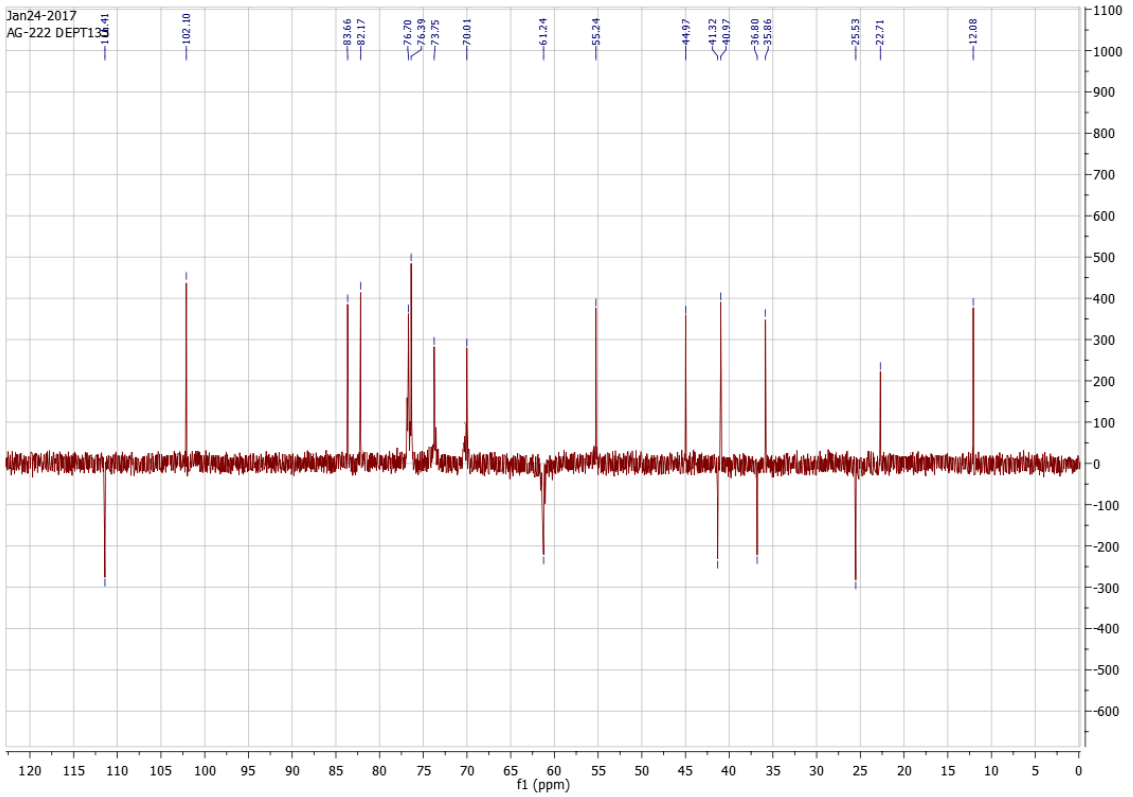

Figure 6.33: DEPT-135 NMR Spectra of Compound **2** in CD_3OD.

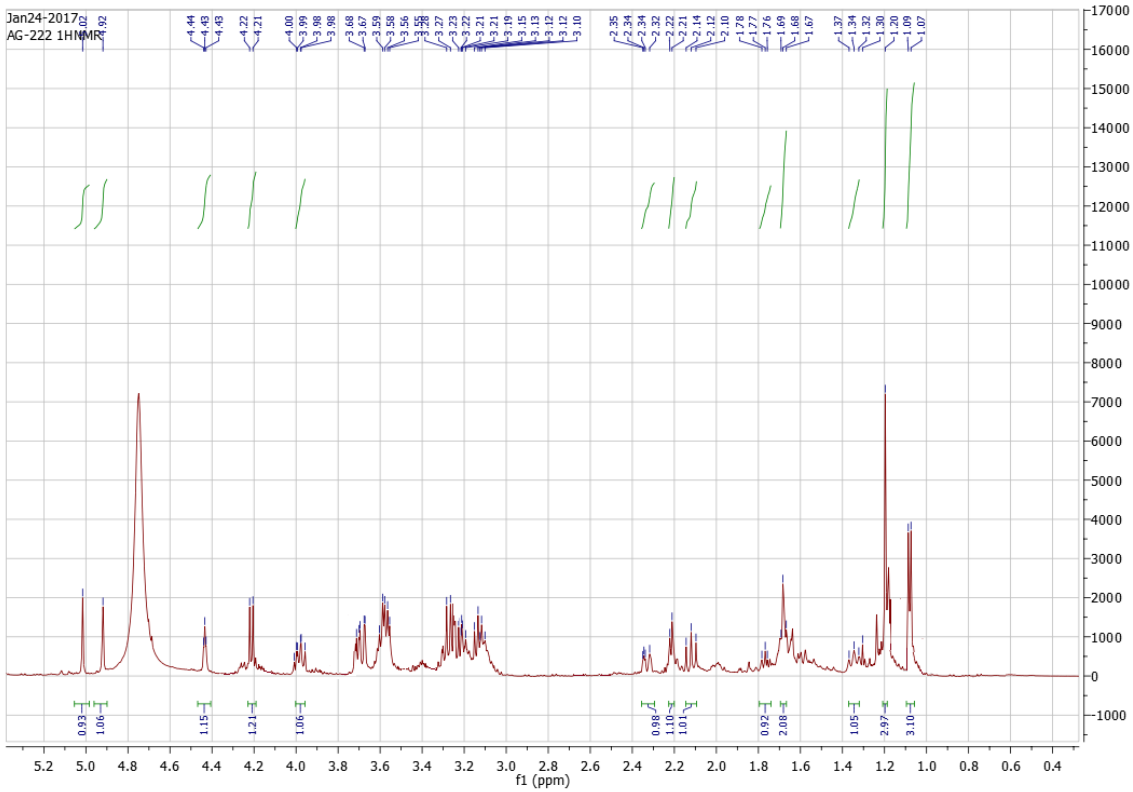

Figure 6.34: ^1H NMR Spectra of Compound **2** in CD_3OD.

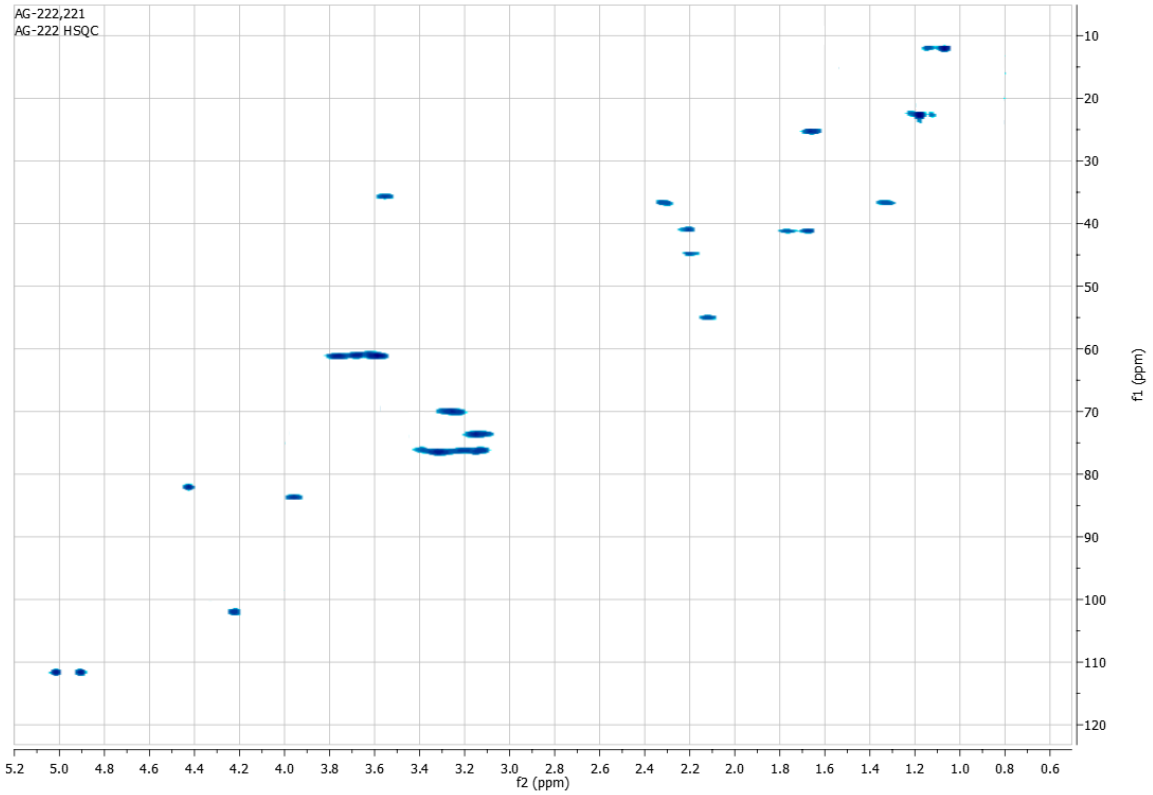

Figure 6.35: HSQC Spectra of Compound **2** in CD_3OD.

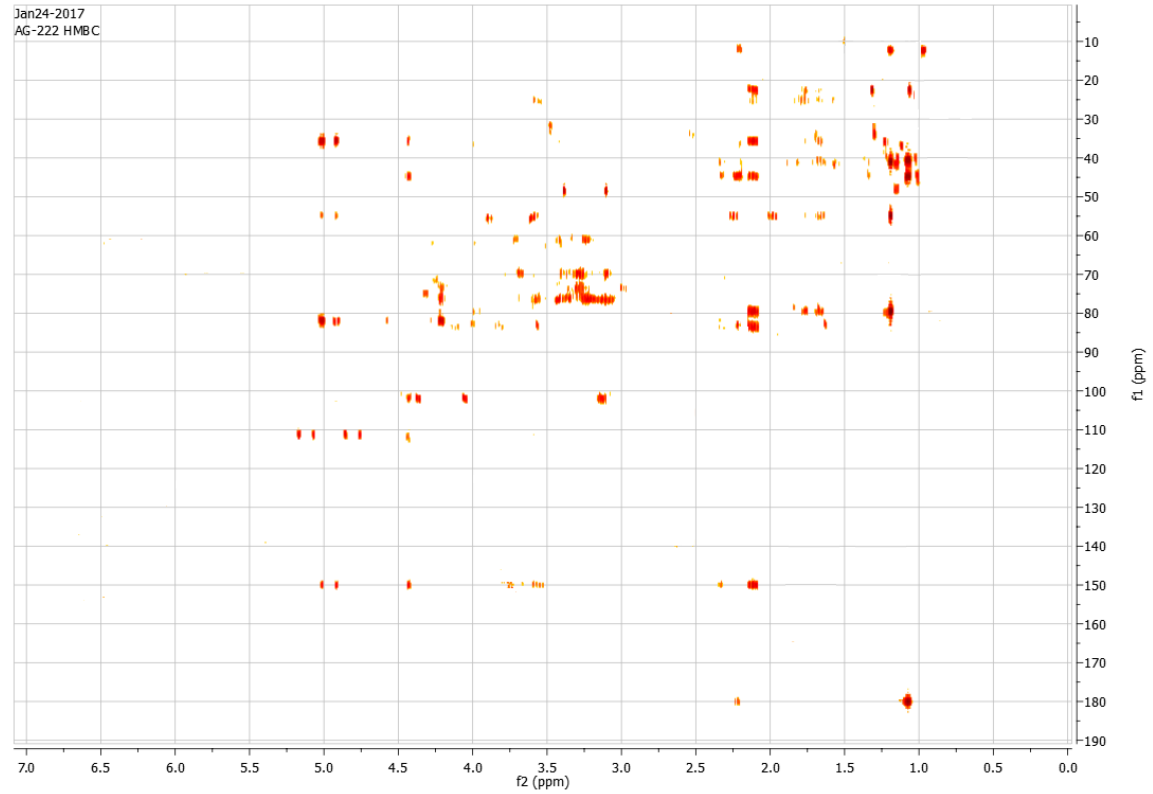

Figure 6.36: HMBC Spectra of Compound **2** in CD_3OD.

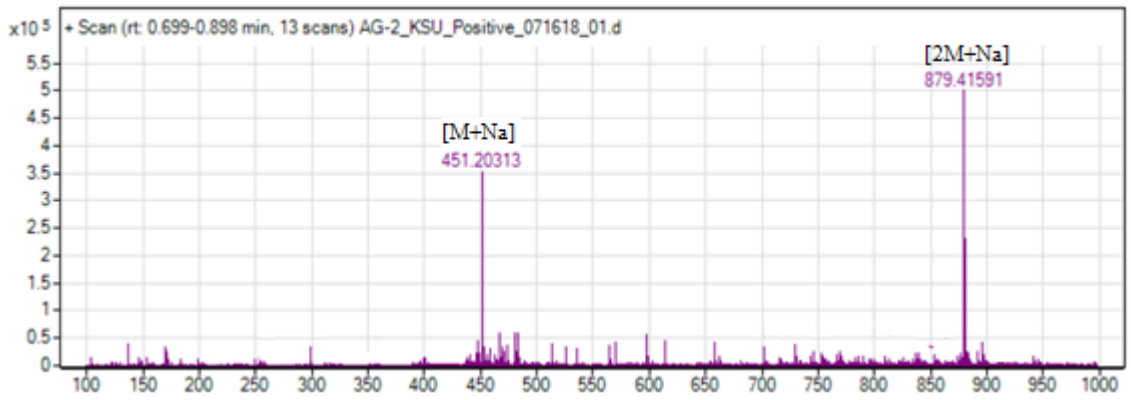

Figure 6.37: ESI Mass Spectra of Compound **2**.

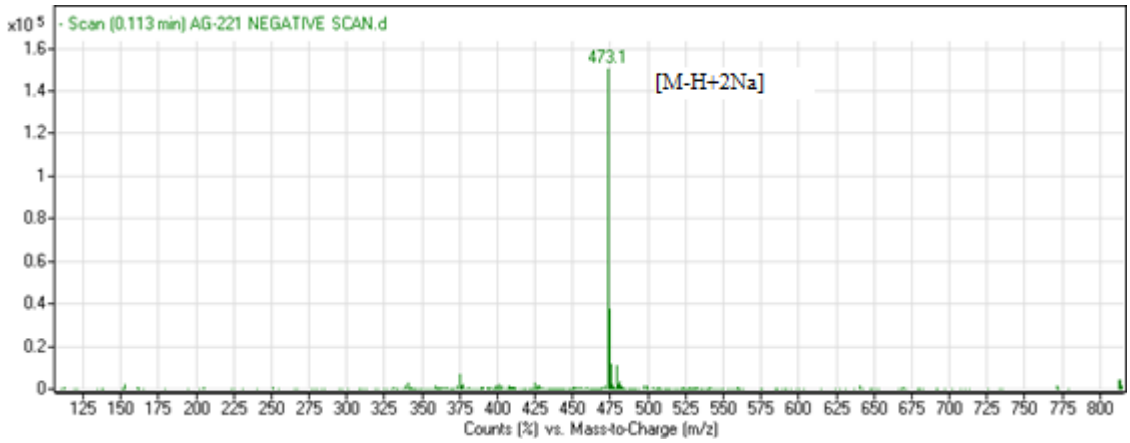

Figure 6.38: ESI Mass Spectra of Compound **2**.

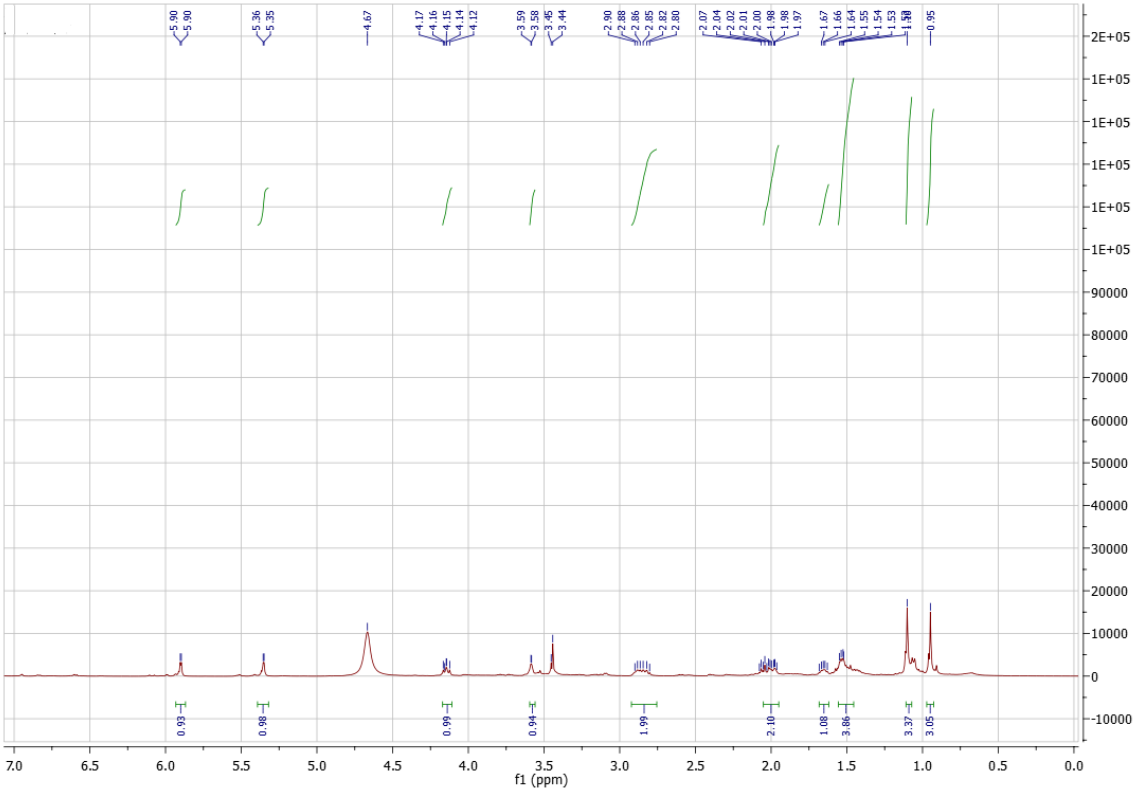

Figure 6.39: ^{1}H NMR Spectra of Compound **3** in CD_3OD.

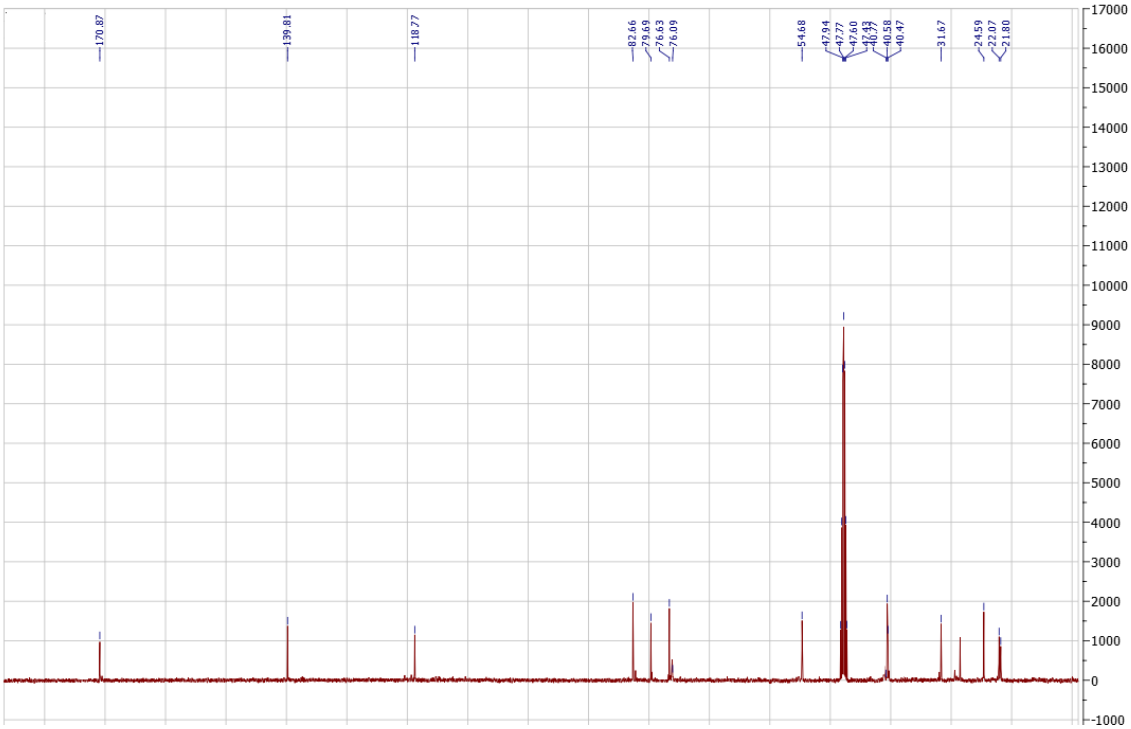

Figure 6.40: ^{13}C NMR Spectra of Compound **3** in CD_3OD.

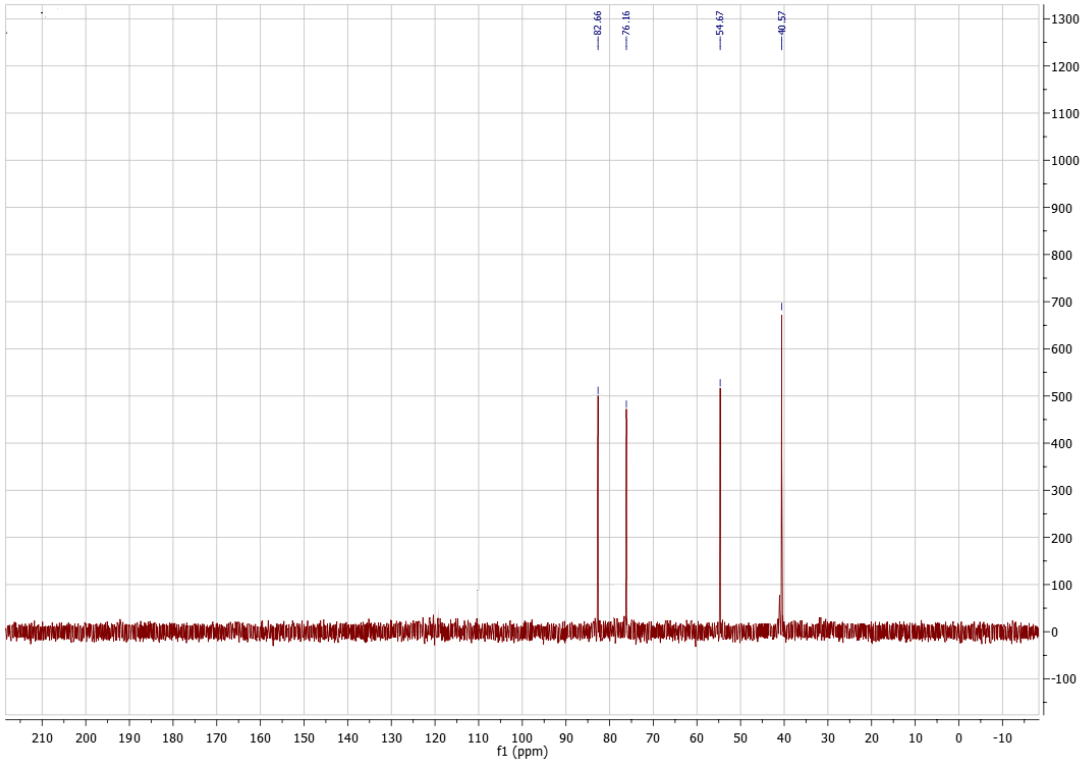

Figure 6.41: DEPT-90 NMR Spectra of Compound **3** in CD_3OD.

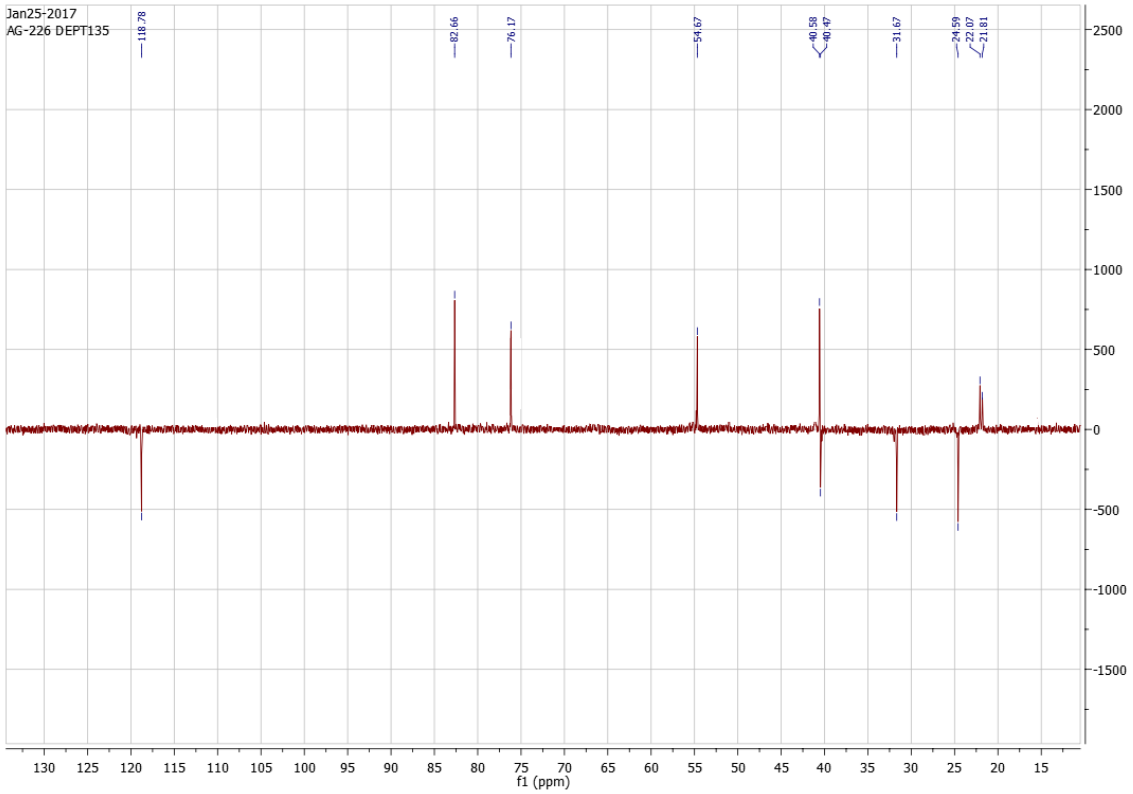

Figure 6.42: DEPT-135 NMR Spectra of Compound **3** in CD_3OD

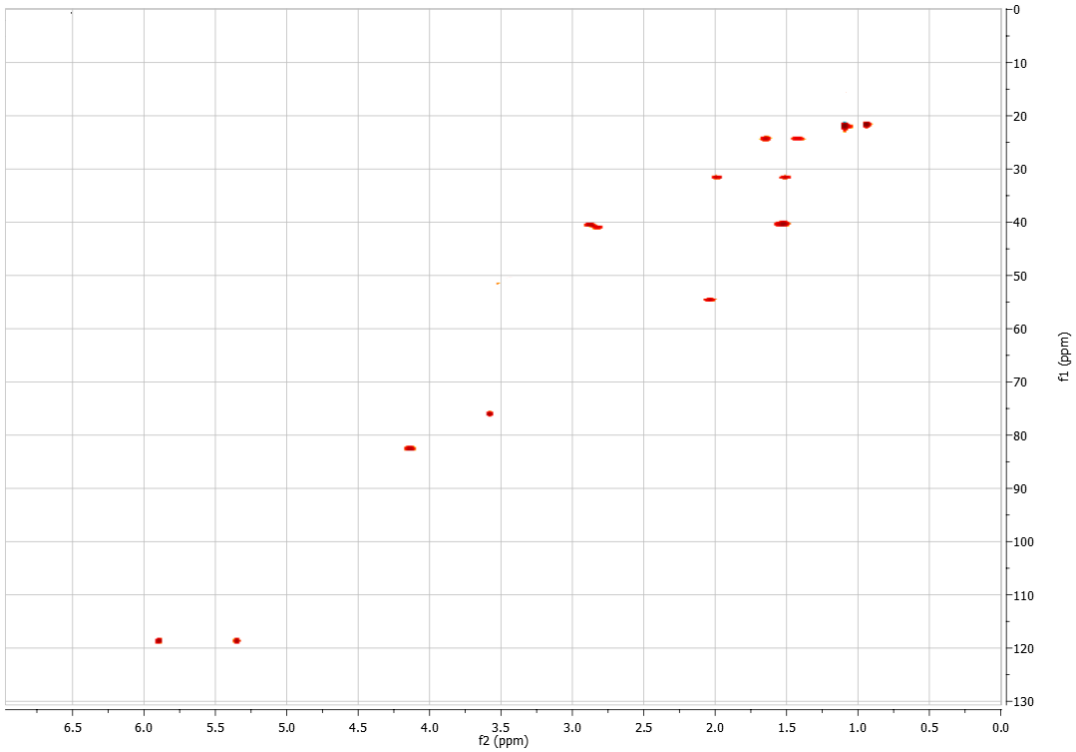

Figure 6.43: HSQC Spectra of Compound **3** in CD_3OD.

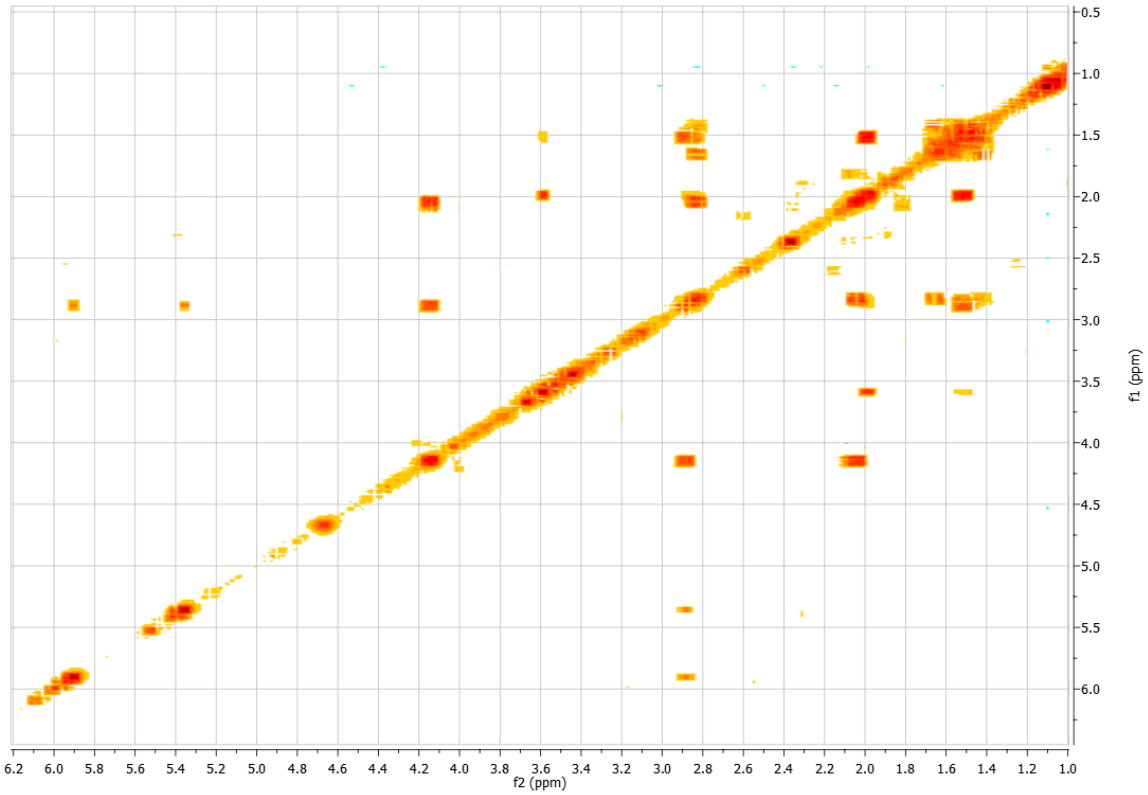

Figure 6.44: COSY Spectra of Compound **3** in CD_3OD.

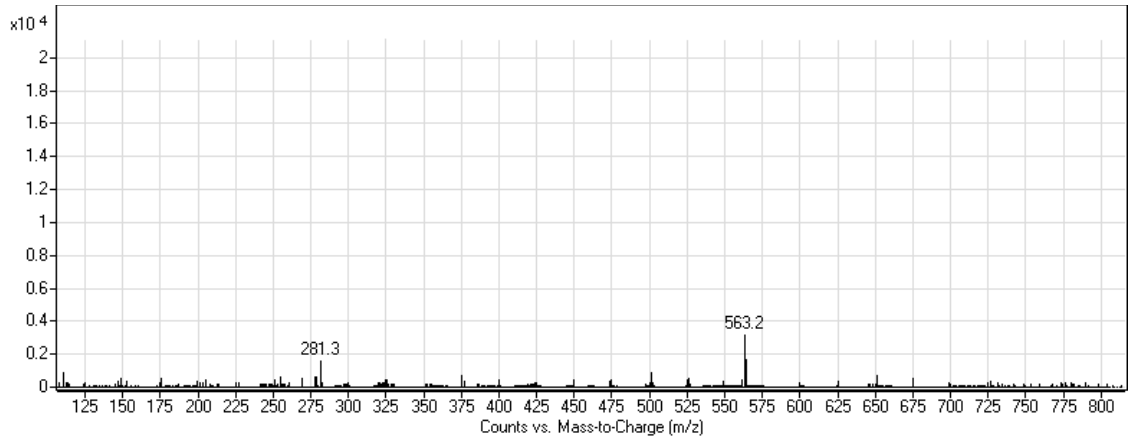

Figure 6.45: Negative ESI Mass Spectra of Compound **3**.

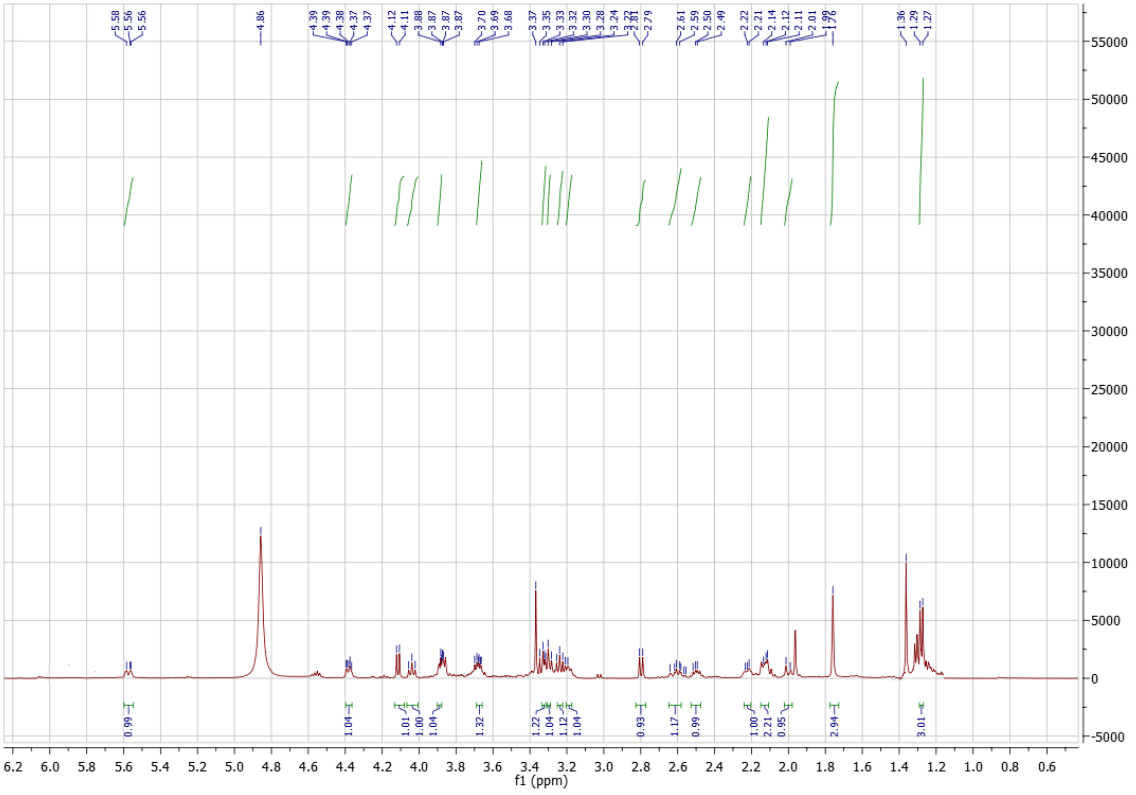

Figure 6.46: ^{1}H NMR Spectra of Compound **4** in CD_3OD.

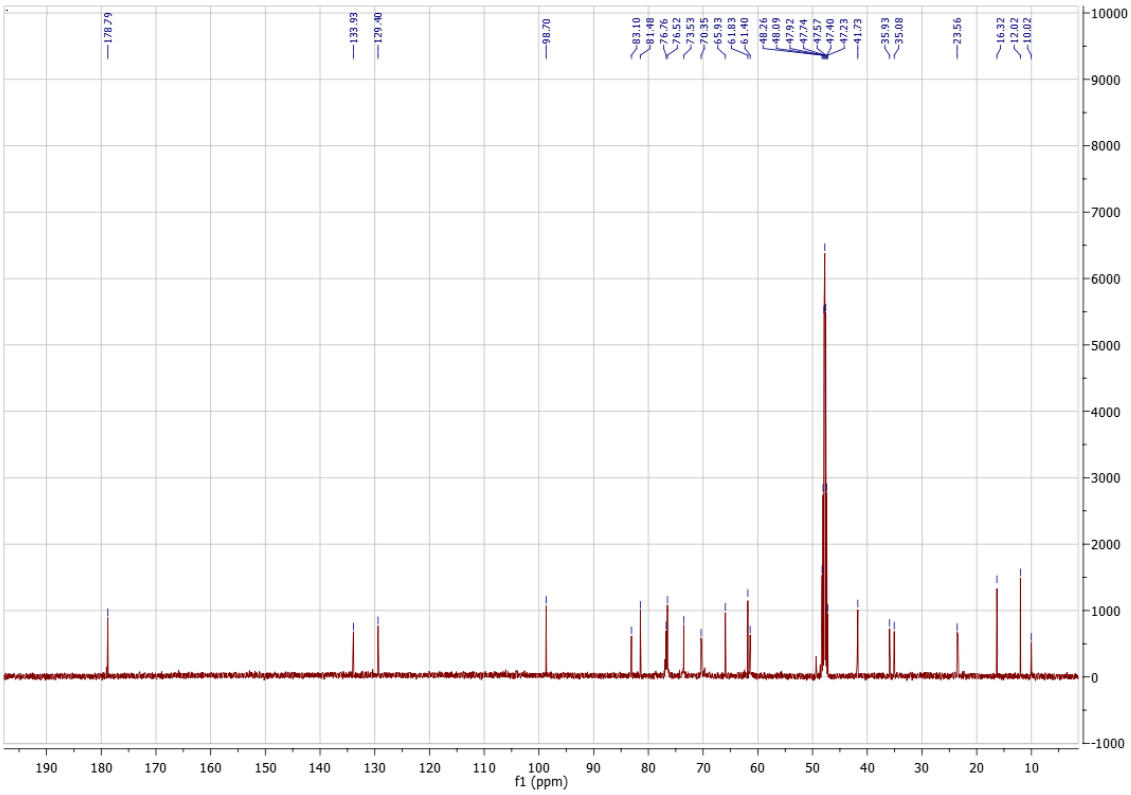

Figure 6.47: ^{13}C NMR Spectra of Compound **4** in CD_3OD.

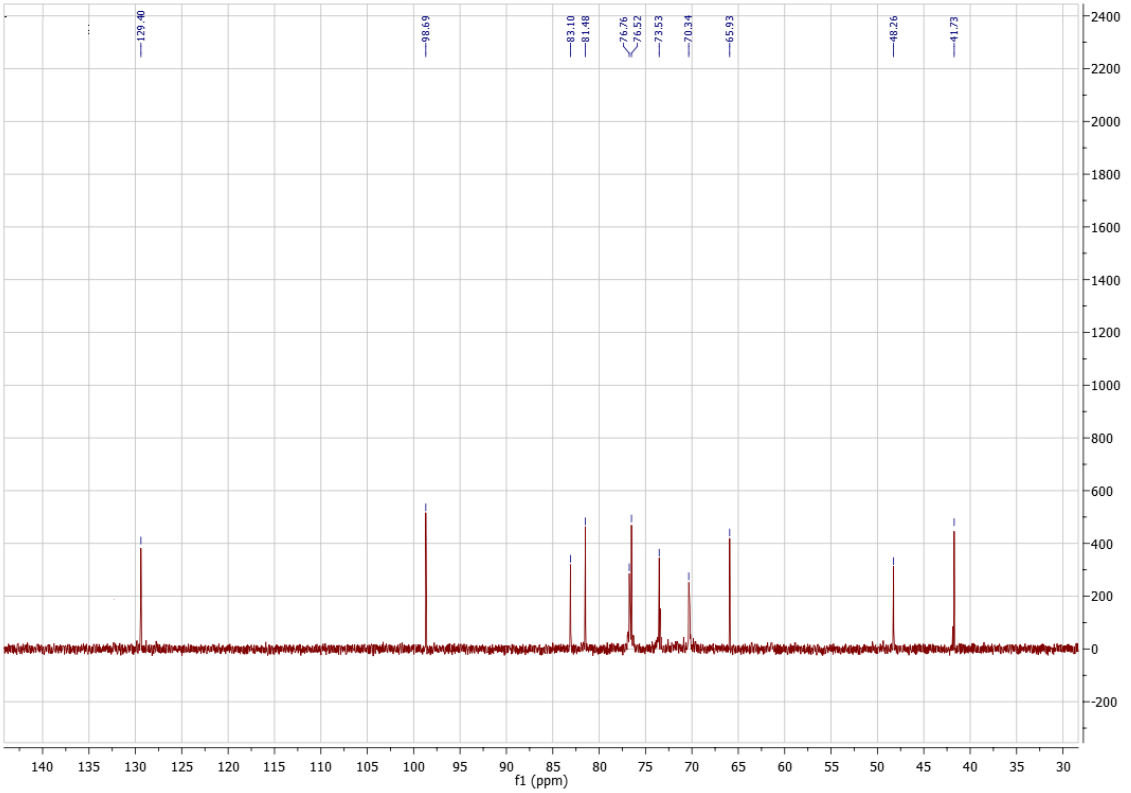

Figure 6.48: DEPT-90 NMR Spectra of Compound **4** in CD_3OD.

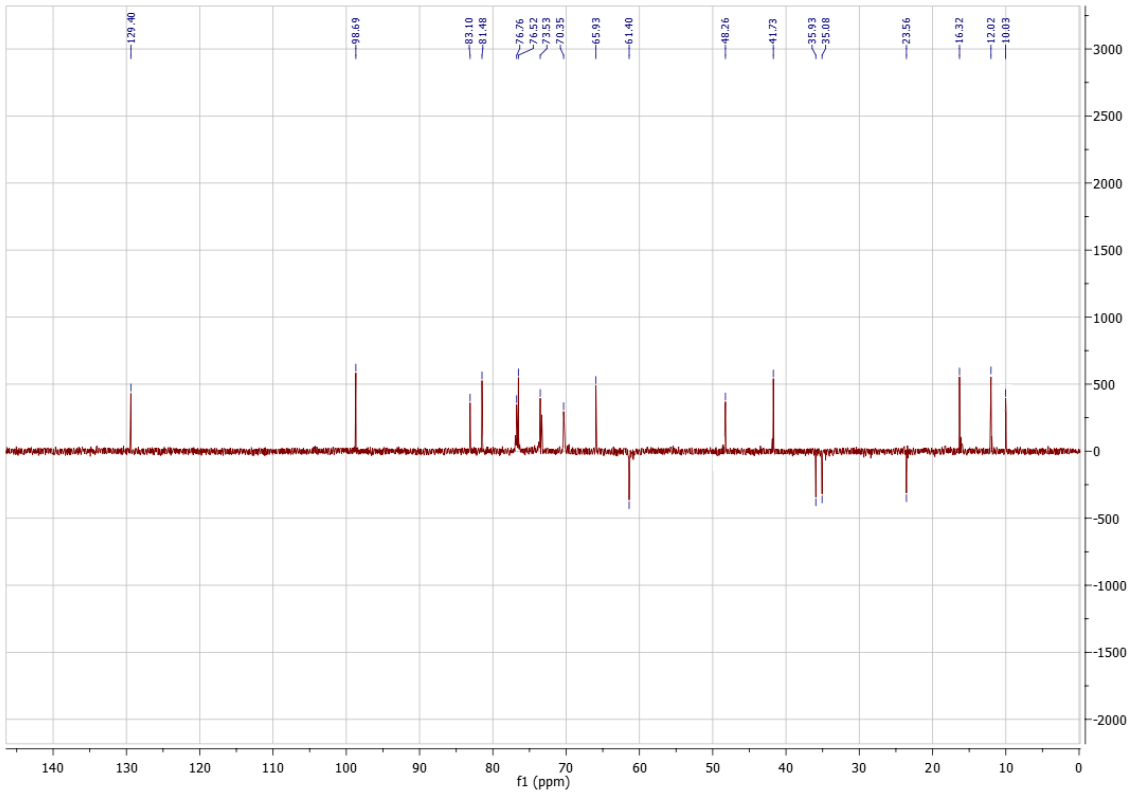

Figure 6.49: DEPT-135 NMR Spectra of Compound **4** in CD_3OD.

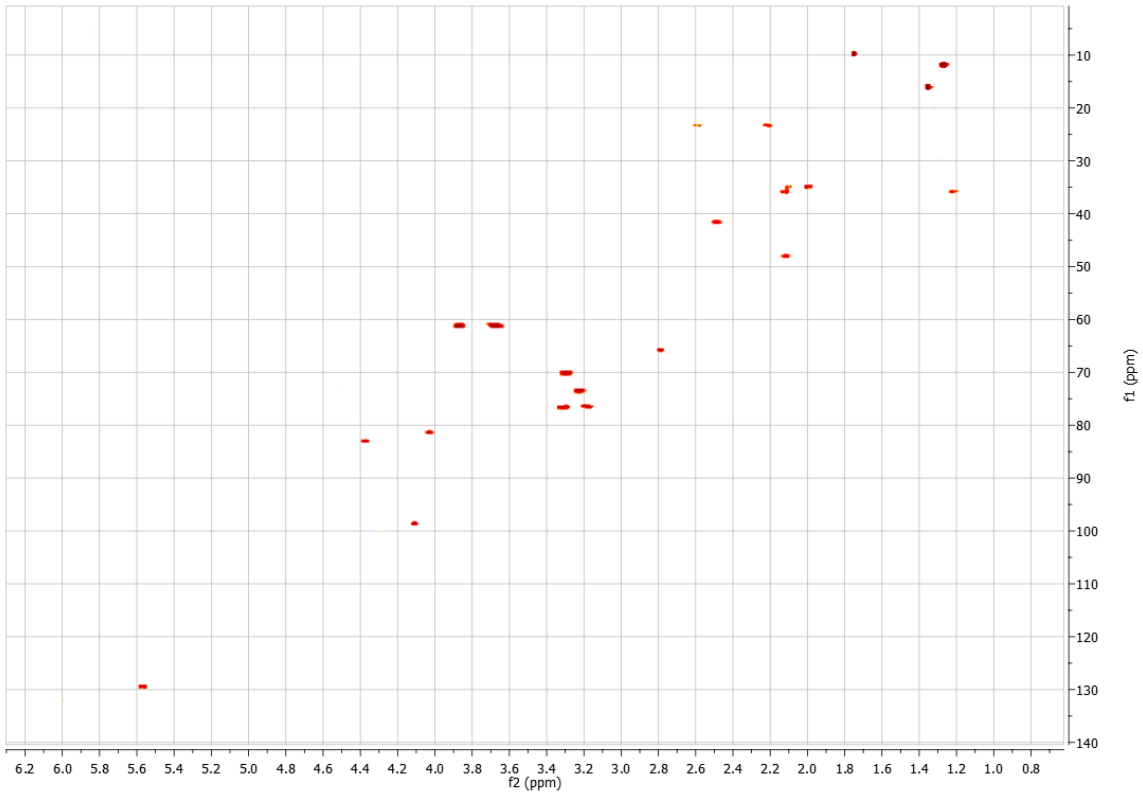

Figure 6.50: HSQC Spectra of Compound **4** in CD_3OD.

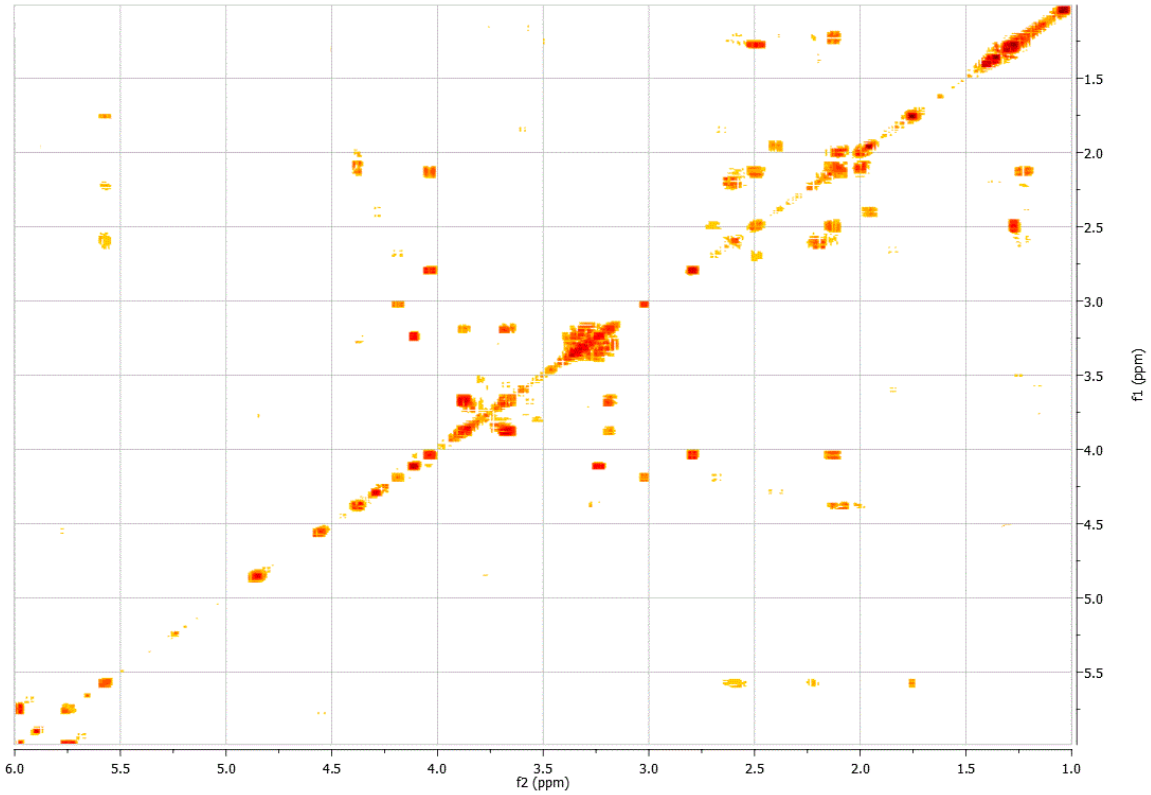

Figure 6.51: COSY Spectra of Compound **2** in CD_3OD.

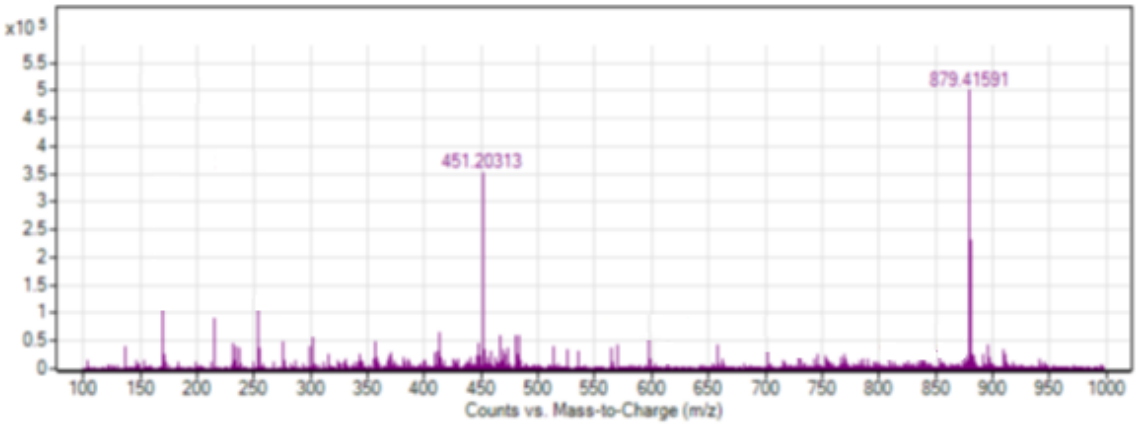

Figure 6.52: ESI Mass Spectra of Compound **4**.

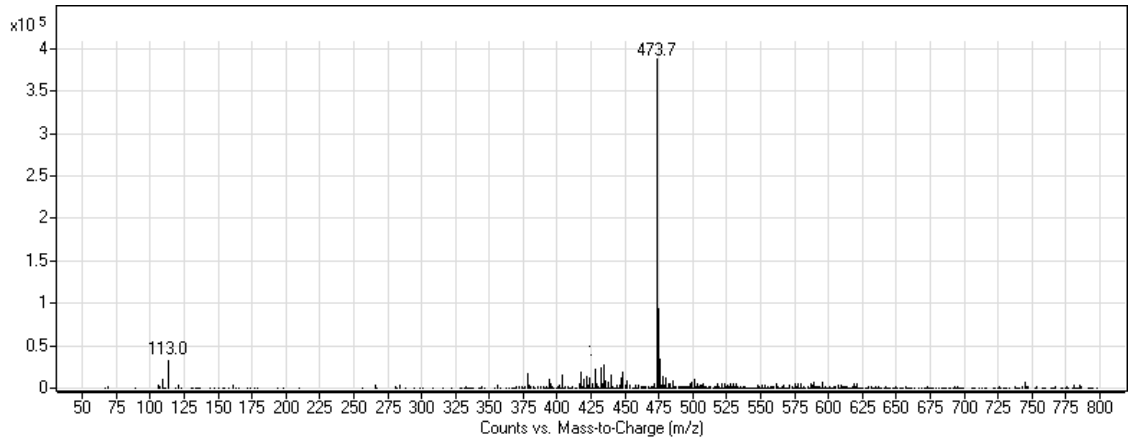

Figure 6.53: Negative ESI Mass Spectra of Compound **4**.